Technische Universität München
TUM School of Life Sciences

Deciphering the SUB-QKY signaling complex and the role of QKY in cell wall signaling

Xia Chen

Vollständiger Abdruck der von der TUM School of Life Sciences der Technischen Universität München zur Erlangung einer

Doktorin der Naturwissenschaften (Dr. rer. nat.)

genehmigten Dissertation.

Vorsitz: Prof. Dr. Ralph Hückelhoven

Prüfer der Dissertation:

1. Prof. Dr. Kay H. Schneitz
2. Priv.-Doz. Dr. Ulrich Hammes

Die Dissertation wurde am 30.03.2023 bei der Technischen Universität München eingereicht und durch die TUM School of Life Sciences am 14.07.2023 angenommen.

I. Table of contents

Table of contents

Table of contents

Table of contents

II. List of figures

List of figures

III. List of tables

IV. Summary

Intercellular communication plays a central role in organogenesis. Tissue morphogenesis in *Arabidopsis thaliana* requires signaling mediated by the atypical receptor kinase (RK) SUB and the multiple C2 domains and transmembrane region protein (MCTP) QKY.

STRUBBELIG (SUB)/QUIRKY (QKY) signal transduction represents one of the first examples of a functional link between RK- and Plasmodesmata (PD)-associated intercellular signaling. In the current model, QKY and SUB interact at PD to mediate downstream SUB signal transduction to promote tissue morphogenesis. SUB is constitutively internalized and QKY is required to stabilize SUB at the cell surface. But it is still unclear how QKY stabilizes SUB at the cell surface, and what the architecture of SUB/QKY complex is in vivo. The multiple C2 domain represent key structural features of QKY proteins and raise questions regarding their relative functional importance. Therefore, it is very important to systematically analyze the correlation between the structure and function of QKY and the architecture of SUB/QKY complex in vivo.

In this work, I focused on the vivo structure-function analysis of QKY, combining the role of its phosphorylation and its interaction with SUB using a mix of genetics, cell biology, and fluorescence microspectrometry, including FRET-FLIM. I analyzed the structural features of the SUB/QKY complex. The results indicate that the N-terminal C2A-B region of QKY is essential for the interaction with SUB in vivo, and this interaction is required to maintain SUB levels at the cell surface. Fluorescence anisotropy analysis revealed that QKY promotes the formation of SUB homo-oligomers in vivo, and QKY also undergoes SUB-independent homomerization in vivo.

Immunoprecipitation-based mass spectrometry data showed that QKY was

phosphorylated at S218, S262, S305 and S1075 in a SUB-independent fashion in vivo. I systematically analyzed the functional relevance of QKY phosphorylation in vivo. Combined results from genetics, Y2H assays, confocal microscopy and FRET-FLIM indicated that phosphorylation of the S1075 controls the subcellular localization of QKY, whereas the P-sites S218, S262, and S305 which sit on the C2A-B linker region in N-terminal of QKY revealed a complex picture. The data showed how differential phosphorylation of QKY affects its tissue-specific function and control of the architecture of the SUB receptor complex in vivo.

In addition, studies on isoxaben-induced cell wall damage have shown that QKY plays a role in the cell wall damage response induced by cellulose biosynthesis inhibition. Quantitative real-time polymerase chain reaction experiments and ectopic lignin accumulation analysis indicated that *QKY* promotes cellular responses like ectopic lignin and also plays a role in the prevention of cell bulging in the root epidermal cells, but not required for isoxaben-induced marker gene induction.

In conclusion, my data analyzed the architectural structure of the SUB/QKY complex, and systematically analyzed the structure and functional relationship of the complex. They provide novel molecular insight into a central aspect of SUB signaling and the basis for the predicted heteromeric complex formed by the QKY-SUB interaction fragment. Finally, my results revealed a function for QKY in the cell wall damage response.

V. Zusammenfassung

Die interzelluläre Kommunikation spielt eine zentrale Rolle bei der Organogenese. Die Gewebemorphogenese in *Arabidopsis thaliana* erfordert eine Signalübertragung, die durch die atypische Rezeptoren wie Kinase (RK) SUB und die multiplen C2-Domänen und das Transmembranregionprotein (MCTP) QKY vermittelt wird.

Die STRUBBELIG (SUB)/QUIRKY (QKY)-Signaltransduktion ist eines der ersten Beispiele für eine funktionellen Verbindung zwischen RK- und Plasmodesmata (PD)-assoziierter interzellulärer Signalübertragung. Im aktuellen Modell interagieren QKY und SUB bei PD, um die nachgeschaltete SUB-Signaltransduktion zu vermitteln, um die Gewebemorphogenese zu fördern. SUB wird konstitutiv internalisiert und QKY wird benötigt, um SUB an der Zelloberfläche zu stabilisieren. Es ist jedoch noch unklar, wie QKY SUB an der Zelloberfläche stabilisiert und wie die Architektur des SUB/QKY-Komplexes in vivo aussieht. Die multiplen C2-Domänen repräsentieren Schlüsselstrukturmerkmale von QKY-Proteinen und werfen Fragen hinsichtlich ihrer relativen funktionellen Bedeutung auf. Daher ist es sehr wichtig, die Korrelation zwischen der Struktur und Funktion von QKY und der Architektur des SUB/QKY-Komplexes in vivo systematisch zu analysieren.

In dieser Arbeit konzentrierte ich mich auf die vivo-Struktur-Funktionsanalyse von QKY, wobei ich die Rolle seiner Phosphorylierung und seiner Wechselwirkung mit SUB unter Verwendung einer Mischung aus Genetik, Zellbiologie und Fluoreszenzmikrospektrometrie, einschließlich FRET-FLIM, kombinierte. Ich habe die strukturellen Merkmale des SUB/QKY-Komplexes analysiert. Die Ergebnisse zeigen, dass die N-terminale C2A-B-Region von QKY für die Wechselwirkung mit SUB in vivo wesentlich ist und diese Wechselwirkung erforderlich ist, um die SUB-Konzentrationen an der Zelloberfläche aufrechtzuerhalten. Die Fluoreszenzanisotropieanalyse zeigte, dass QKY die Bildung von SUB-Homo-

Oligomeren in vivo fördert und QKY auch in vivo eine SUB-unabhängige Homomerisierung durchmacht.

Auf Immunpräzipitation basierende Massenspektrometriedaten zeigten, dass QKY an S218, S262, S305 und S1075 in einer SUB-unabhängigen Weise in vivo phosphoryliert wurde. Ich habe die funktionelle Relevanz der QKY-Phosphorylierung in vivo systematisch analysiert. Kombinierte Ergebnisse aus Genetik, Y2H-Assays, konfokaler Mikroskopie und FRET-FLIM zeigten, dass die Phosphorylierung von S1075 die subzelluläre Lokalisierung von QKY kontrolliert, während die P-Stellen S218, S262 und S305, die auf der C2A-B-Linkerregion in N-Terminal von QKY ergab ein komplexes Bild. Die Daten zeigten, wie die differentielle Phosphorylierung von QKY seine gewebespezifische Funktion und Kontrolle der Architektur des SUB-Rezeptorkomplexes in vivo beeinflusst.

Darüber hinaus haben Studien zu Isoxaben-induzierten Zellwandschäden gezeigt, dass QKY eine Rolle bei der Zellwandschädigungsantwort spielt, die durch die Hemmung der Zellulosebiosynthese induziert wird. Quantitative Echtzeit-Polymerase-Kettenreaktionsexperimente und ektopische Ligninakkumulationsanalysen zeigten, dass QKY zelluläre Reaktionen wie ektopisches Lignin fördert und auch eine Rolle bei der Verhinderung von Zellwulst in den Wurzelepidermiszellen spielt, aber nicht für die Isoxaben-induzierte Markergen-Induktion erforderlich ist.

Zusammenfassend analysierten meine Daten die architektonische Struktur des SUB/QKY-Komplexes und analysierten systematisch die Struktur und funktionalen Beziehungen des Komplexes. Sie liefern neue molekulare Einblicke in einen zentralen Aspekt der SUB-Signalgebung und die Grundlage für den vorhergesagten heteromeren Komplex, der durch das QKY-SUB-Interaktionsfragment gebildet wird. Schließlich zeigten meine Ergebnisse eine Funktion für QKY in der Antwort auf Zellwandschäden.

1 Introduction

Intercellular communication is a prerequisite for coordinating both development and environmental responses across diverse cell types in multicellular organisms. This communication has to be tightly regulated to ensure that the cell fate is appropriately specified for each cell. During evolution, the two primary groups of multicellular eukaryotes, plants and animals, have developed various mechanisms for effective intercellular communication according to their different developmental strategies (Gaillochet and Lohmann, 2015; Bloemendal and Kück, 2013).

1.1 Cell-to-cell communication during plant development

Unlike most animals, plants employ a pattern of post-embryonic development driven by the continuous activity of pluripotent stem cells. Therefore, plants are able to continuously initiate new organs throughout their whole life (Dinneny and Benfey, 2008; Birnbaum and Alvarado, 2008). This property makes cell-to-cell communication particularly important in plants. As immobile organisms, plants depend on cell-to-cell communication to coordinate growth and development with environmental conditions. This requires that cells interacting with the environment must appropriately and timely perceive and transduce environmental cues to other cells and organs. The importance and complexity of cell-to-cell communication is given greater weight because of the presence of cellulosic-rich cell walls that encase all plant cells. Consequently, such communication occurs through transporters or receptor-ligand interactions, but plants have also evolved cytoplasmic bridges called plasmodesmata (PD) that connect adjacent cells (Burch-Smith and Zambryski, 2012; Ehlers and Kollmann, 2001).

1.1.1 Plasmodesmata-mediated cell-to-cell communication in plants

PD are developed across the cell walls to enable cytoplasmic connection and

molecular trafficking between neighboring cells. PD channels are structurally defined as plasma membrane (PM)-lined channels. The PM between adjacent cells delineates the outer boundary of the channel, while the axial center of the PD, called the desmotubule (DT), is composed of compressed endoplasmic reticulum (ER). The region between the PM and the DT is known as the cytoplasmic sleeve, which provides a major path for small molecules to diffuse through PD (Blackman and Overall, 2001; Roberts and Oparka, 2003) (Figure 1). Additional evidence describes the additional transport occurs through the lumen of the DT or along the lipid bilayers of the DT (Guenoune-Gelbart et al., 2008; Cantrill et al., 1999).

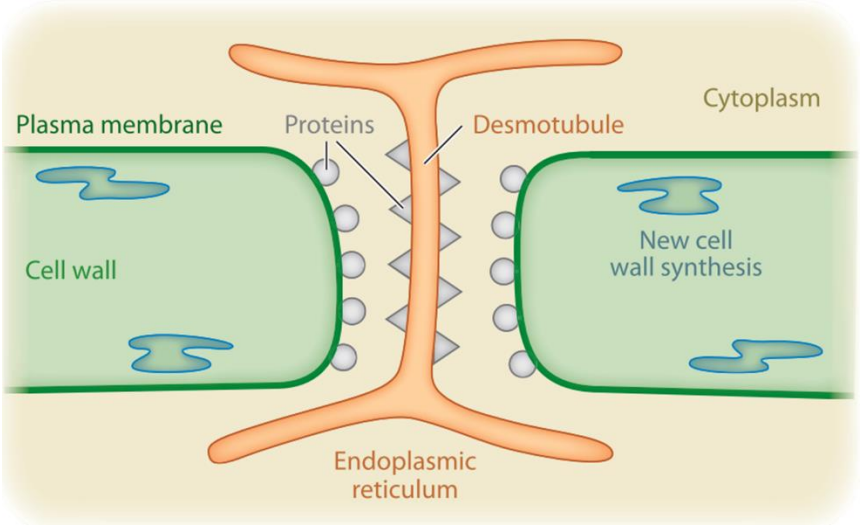

Figure 1 Schematic diagram of the structure of a single plasmodesmata.

The plasmodesma crosses the cell wall between two adjacent plant cells. The cytoplasm is continuous between the two cells and forms the plasmodesmal channel. The endoplasmic reticulum in the axial center is called the desmotubule of the plasmodesma. The plasma membrane forms the outer limit of the plasmodesmal channel. (Adopted from Burch-Smith and Zambryski, 2012).

PD can exist in different states like closed, open or dilated depending on their permeability to prevent or allow the movement of molecular during plant growth and development (Yadav et al., 2014; Zambryski and Crawford, 2000). In addition, sometimes the targeted trafficking of macromolecules requires the interaction of proteins with PD or associated protein to increase the size exclusion limit (SEL) of PD

for their movement (Xu et al., 2012; Kirk and Benitez-Alfonso, 2022; Kim et al., 2002). The SEL is known as the upper size limit of the molecules that can move through PD. Callose plays an important role in regulating the symplastic communication through PD in various developmental processes. It can be reversibly deposited at PD to regulate the movement of molecules by controlling the SEL of PD (Iglesias and Meins, 2000; Chen and Kim, 2009).

Many proteins have been identified to localize at PD, indicating that may have specific functions in the regulation and structure of PD (Faulkner et al., 2013; Stahl et al., 2013; Faulkner et al., 2009; Jo et al., 2011). Interestingly, more and more receptor kinase and receptor proteins have been found to specifically localize and function on PD. For example, the *Arabidopsis* receptor-like kinase FLAGELLIN SENSING 2 (FLS2), which targets PM and PD, mediates the reduction of molecular flux through PD in cell-to-cell diffusion (Faulkner et al., 2013). In addition, the receptor kinase STRUBBELIG (SUB) interact with the C2-domain protein QUIRKY (QKY) at PD to mediate the tissue morphogenesis in *Arabidopsis thaliana* (Vaddepalli et al., 2014).

1.1.2 Receptor kinase and cell-to-cell communication

Receptor kinases (RKs) are a large family of transmembrane proteins located on the cell surface. They normally possess the activity of protein kinases and regulate the downstream signaling through phosphorylation or dephosphorylation events (Heiss et al., 2006; Aifa et al., 2006).

Plant RKs are structurally similar in evolution, and generally they include an extracellular ligand-binding domain, a transmembrane region, a juxtamembrane domain and a serine/threonine kinase domain. The N-terminal extracellular domain defines the ligand specificity, and RKs are usually classified according to this domain. More than 20 different extracellular domains have been identified in plant RKs,

including leucine-rich repeat (LRR) domains, LysM domains, the *Catharanthus roseus* RK1-like (CrRLK1L) domains, self-incompatibility (S) domains, epidermal growth factor repeats and lectin domains (Cock et al., 2002; Shiu and Bleecker, 2001). The large diversity of extracellular domains in plant RKs implies that they need to evolve rapidly to adapt the cellular environment and to perceive a wide variety of signals.

In *Arabidopsis*, there are more than 600 plant RKs, which play important roles in various biological processes (Shiu et al., 2004). Some of RKs have been identified as being involved in perception of pathogenic microbes. For instance, the *Arabidopsis* FLS2 and the elongation factor-Tu (EF-Tu) receptor (EFR) recognize the conserved 22 amino acids of bacterial flagellin (flg22) and conserved N-terminal epitope elf18 of bacterial EF-Tu, respectively, thereby activating the pattern recognition receptor triggered immunity (Kunze et al., 2016; Gómez-Gómez and Boller, 2000). And some RKs have been described to be involved in cell/organ communication, plant development and abiotic stress response. For example, BRASSINOSTEROID-INSENSITIVE 1 (BRI1) can perceive and transmit the brassinosteroids (BRs) signal to control a variety of plant development processes (Clause and Sasse, 1998). The CLAVATA1 (CLV1) plays a central role in the homeostasis of shoot apical meristem (Clark, 1997). FERONIA (FER), one member of CrRLK1L subfamily, plays a key role in ABA signal transduction and controls the salt stress response by activating *ABA Insensitive 2* (*ABI2*) (Yu et al., 2012).

1.1.3 Plant root development, morphogenesis and cell-to-cell communication

Due to its highly organized structure, the *Arabidopsis thaliana* root is one of the most tractable systems for studying intercellular communication during plant development. *Arabidopsis* root views as a concentric cylinder. In the middle of the cylinder is the vascular bundle, which a part of stele, consisting of phloem and xylem. The vascular tissue is surrounded by four outer layers, from inside to outside, namely the pericycle,

endodermis, cortex and epidermis. The root tip contains the root apical meristem (RAM), there is one region called the quiescent center (QC), which consist of four to six cells with low mitotic activity. The QC is essential for maintaining the undifferentiated state of the surrounding stem cells (Dolan et al., 1993; Scheres et al., 2002) (Figure 2).

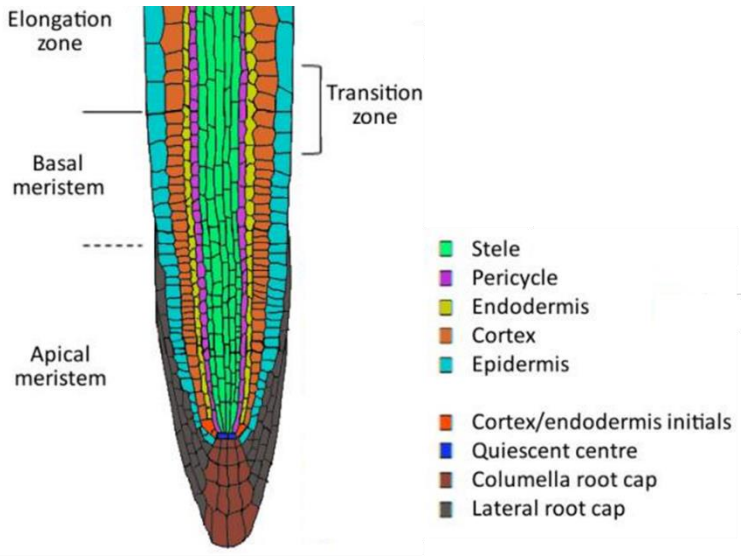

Figure 2 Organization of the Arabidopsis root.

Longitudinal section through the root showing apical-basal polarity. Distinct developmental zones are formed along the growing root. (Modified from Smet et al., 2015).

The Arabidopsis root epidermis is a canonical model system for studying the cell fate specificity based on positional information, as it composed of two types of cells, hair cells (trichoblasts) and non-hair cells (atrichoblasts). Root hair cells and non-hair cells are arranged in a distinct position-dependent pattern. Trichoblasts develop root hairs and located above the junction of two underlying cortical cells, while atrichoblasts remain hairless and located outside a single cortical cells. In general, trichoblasts are shorter and less vacuolated than atrichoblasts (Balcerowicz et al., 2015; Grierson et al., 2014; Guimil and Dunand, 2006).

Many genes and transcription factors have been identified that regulate the fate of cells in the Arabidopsis root epidermis. Non-hair cell types are specified by a transcriptional complex including the R2R3 MYB-type transcription factor WEREWOLF (WER), the basic helix-loop-helix (bHLH) protein GLABRA3 (GL3) or ENHANCER OF GLABRA3 (EGL3), and the WD repeat protein TRANSPARENT TESTA GLABRA1 (TTG1) (Salazar-Henao et al., 2016; Grebe, 2012). This complex acts in non-hair cells to promote the expression of the homeodomain transcription factor GLABRA2 (GL2), which blocks the hair pathway and specifies the fate of non-hair cells. TTG/GL3/EGL3/WER also directly promotes the expression of *CAPRICE* (*CPC*) gene in non-hair cells, which encodes an R3 single MYB-type transcription factor. Interestingly, the *CPC* gene is transcribed predominantly in non-hair cells, but specifies hair cell fate by moving to the adjacent hair cells to repress the expression of *WER* and *GL2* in hair cells (Kurata et al., 2005; Ryu et al., 2005). In addition, the leucine-rich repeat receptor-like kinase SCRAMBLED (SCM) and the multiple C2 domain and transmembrane region protein QUIRKY (QKY) have also been reported to be required for proper cell-type patterning (Song et al., 2019; Kwak et al., 2005; Fulton et al., 2009). QKY facilitates the transfer of CPC protein from non-hair cells to adjacent hair cells by stabilizing the preferential accumulation of SCM protein in hair cells, thereby inhibiting WER function and specifying the hair cell fate (Song et al., 2019, 2011).

1.2 The role of STRUBBELIG in intercellular communication

Intercellular communication during plant development and morphogenesis in *Arabidopsis thaliana* also relies on STRUBBELIG (SUB)-mediated signaling. SUB was first identified based on the phenotype of ovule defect (Chevalier et al., 2005; Schneitz et al., 1997). It is a member of the small *STRUBBELIG RECEPTOR FAMILY (SRF)/LRRV* gene family (Eyüboglu et al., 2007). SUB, also known as SCRAMBLED (SCM), is required for the proper cell type patterning in *Arabidopsis* root epidermis (Kwak et al., 2005).

1.2.1 STRUBBELIG is an atypical leucine-rich repeat RK

SUB is a leucine-rich repeat transmembrane receptor kinase (LRR-RK). It is predicted to encode 768 amino acids (aa) and has a molecular weight of 84.5 kDa. The SUB protein is predicted to contain a 24-aa signal peptide (SP), a SUB domain which conserved between the LRRV/SRF members, six LRRs, a proline-rich region (PRR), a transmembrane domain (TM), an intracellular juxtamembrane (JM) and a carboxy-terminally-located kinase domain (KD) (Vaddepalli et al., 2011) (Figure 3).

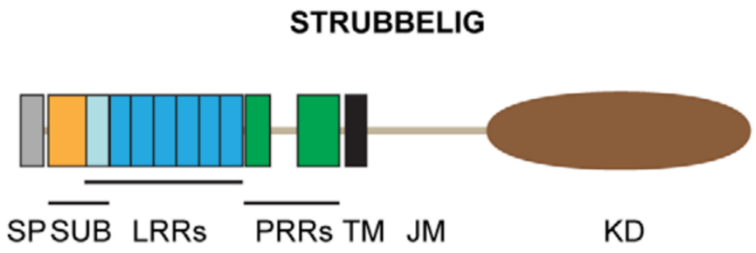

Figure 3 Overview of the domain architecture of SUB.

Abbreviations: SP, signal peptide; SUB, SUB-domain; LRR, leucine-rich repeat; PRR, proline-rich repeat; TM, transmembrane domain; JM, juxtamembrane domain; KD, kinase domain. (Adopted from Vaddepalli et al., 2011).

SUB has been shown to be an atypical receptor kinase as the kinase domain of SUB lacks enzymatic phosphotransfer activity. Biochemical assays using bacterially expressed fusion proteins showed that autophosphorylation or transphosphorylation of general substrates such as myelin basic protein could not be detected in the presence of SUB kinase domain. Genetic analysis showed that mutations in conserved amino acid residues known to interfere with the kinase activity of typical kinases did not affect the function of complementation *sub* to wild-type (Chevalier et al., 2005). Interestingly, the phenotypic *sub-4* and *sub-19* alleles hint at the importance of the kinase domain for SUB function (Vaddepalli et al., 2011). Thus, SUB protein may represent an atypical

RK as the activity of kinase domain is not essential for in vivo SUB function, but the presence of kinase domain still is indispensable for its function.

1.2.2 SUB regulates tissue morphogenesis in *Arabidopsis*

SUB is important for the control of tissue morphogenesis and plant architecture, it is involved in several developmental processes, including the floral morphogenesis, ovule integument outgrowth, leaf and silique development (Chevalier et al., 2005; Lin et al., 2012). Loss-of-function mutations in SUB result in defects in ovule integument initiation and outgrowth. The irregular growth lead to ovules with exposed inner integuments that are surrounded by outer integument tissue with “gaps” (Chevalier et al., 2005). In addition, plants lacking SUB activity also exhibit characteristic defects such as misshaped floral organs, short and twisted stems, and twisted siliques (Figure 4) (Vaddepalli et al., 2011; Fulton et al., 2009). Lin et al., 2012 reported that *sub* mutants displayed temperature-sensitive leaf development defects. The *sub-2* mutant displayed impaired blade development, asymmetric leaf shape and altered venation patterning under high ambient temperature (30℃), but these defects were less pronounced at normal growth temperature (22℃) (Lin et al., 2012).

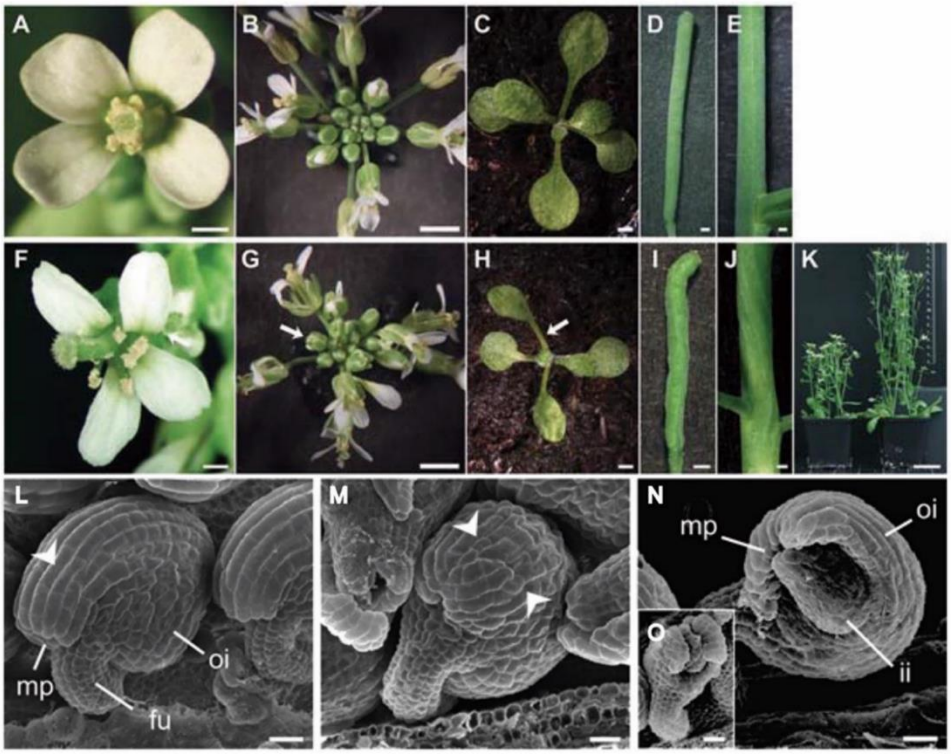

Figure 4 Phenotype comparison of the overall above-ground morphology of Ler and *sub-1*.

(A-E) Wild-type Ler. (F-K) *sub-1*. (A, F) An open stage 13 flower from a 30-day old plant. Note the misorientation of petals due to twisting in the basal end of the petal structure (arrows). (F) Petals can also show small notches. (B, G) Top view of a 30-day inflorescence. (G) Flower phyllotaxis is irregular. Arrows mark prematurely opened flower buds. (C, H) Top view of a 12- day rosette. (H) Leaf petioles can be twisted (arrow). (D, I) Morphology of mature siliques. (E, J) A lateral view of a section of stems from a 30-day plant. (K) Plant height *sub-1* (left) in comparison to Ler (right). (L-N) Scanning electron micrographs of stage 4 ovules. (L) Wild-type Ler. The arrow marks one of the elongated cells of the distal outer integument. (M) *sub-1*. A mild phenotype is shown. Note the irregular size and shape of cells at the distal outer integument (arrow heads, compare to (L)). (N, O) *sub-1*. Strong phenotypes are depicted. Note the half-formed outer integument. (O) shows an example where the outer integument shows several gaps. Scale bars: (A, D, E, F, I, J) 0.5 mm, (B, C, G, H) 2 mm, (K) 3 cm, (L, M, N, O) 20 µm. (Adopted from Fulton et al., 2009).

Furthermore, SCM/SUB is required for cells to establish an appropriate cell-type pattern in the developing root epidermis. SUB preferentially accumulates in root hair cells through an autoregulatory feedback loop, and is proposed to repress the expression of *WER* in hair cells to define the cell fates (Figure 5) (Kwak et al., 2005; Kwak and Schiefelbein, 2008).

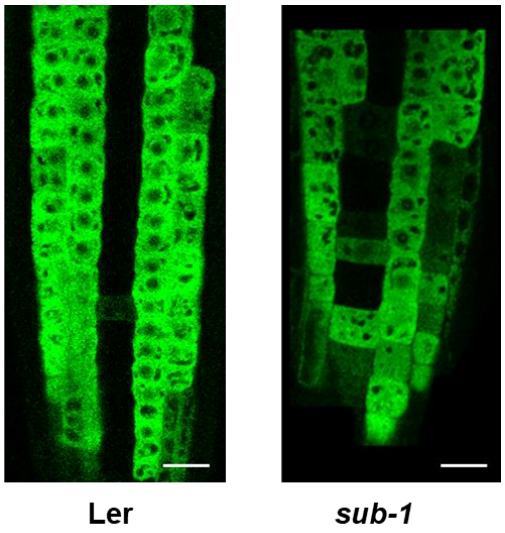

Figure 5 Comparison of the root hair patterning morphology of Ler and *sub-1*.

Expression of *pGL2::GUS* reporter gene during root development. The *sub-1* mutation disturbs the normal file-specific *GL2* expression pattern. Scale bar, 20 μm.

1.2.3 Subcellular and intracellular localization of SUB

The signal of SUB-enhanced green fluorescent protein (EGFP) reporter has been observed to localize on plasma membrane (PM) in *Arabidopsis* using the conventional confocal microscopy (Yadav et al., 2008; Kwak and Schiefelbein, 2008). Interestingly, using a confocal microscope equipped with high sensitivity detectors (HSD), the punctate signal at the circumference of cells of SUB-EGFP can be detected. These spots colocalized with signals derived from aniline blue, which a standard stain for callose associated with PD (Figure 6) (Vaddepalli et al., 2014). This indicate that SUB not only localizes to the PM but also enriched at PD.

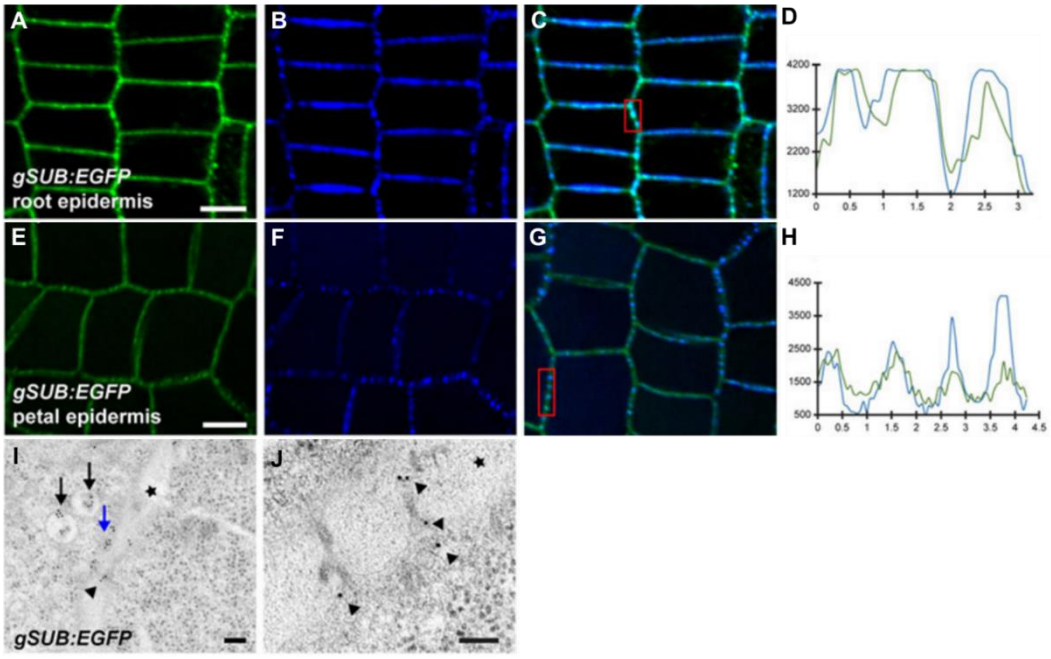

Figure 6 Subcellular localization of SUB.

(A-C, E-G) Confocal micrographs of *sub-1* gSUB:EGFP stained with Aniline Blue. (A, E) GFP signal. (B, F) Aniline Blue signal. (C, G) Overlay of aniline blue and GFP channels. (D, H) Intensity profiles measured along a line connecting the dots highlighted by the red rectangle in C, G, respectively. The x-axis marks the distance in μm. The y-axis denotes arbitrary intensity units. (I, J) Immunogold electron micrographs. The reporters are indicated. Sub-epidermal cortical cells in the flank of the root just behind the meristem of 7-day seedlings are depicted. Arrowheads indicate signals at plasmodesmata. The asterisk indicates the cell wall. (I) Signal can also be seen at multivesicular bodies (black arrows) and plasma membrane (blue arrow). (J) Signal is detected at plasmodesmata. Scale bars: (A, B, C, E, F, G) 5 μm, (I, J) 0.1 μm. (Modified from Vaddepalli et al., 2014).

SUB also can be found in internal compartments (Vaddepalli et al., 2011; Wang et al., 2016). Various mutant SUB variants are retained in the endoplasmic reticulum (ER) and degraded by endoplasmic reticulum-associated degradation (ERAD) (Vaddepalli et al., 2011). A misfolded variant of SUB extracellular domain, SUBEX-C57Y, is retained in the ER, and degraded in a glycan-dependent manner in plants (Hüttner et al., 2014). Wang et al., 2016 showed that ovules of a mutant of *HAPLESS13*, *hap 13-1*, preferentially accumulate signal from a functional SUB-EGFP reporter in the cytoplasm, rather than the PM. It was recently shown that the intracellular domain of SUB is degraded with ubiquitination, and the mechanism of clathrin-mediated endocytosis

(CME) contribute to internalization of SUB (Gao et al., 2019; Song et al., 2019).

1.2.4 Novel components in SUB signaling pathway

Using forward genetics approach three genes were identified to potentially function in SUB-dependent processes, *DETORQEO* (*DOQ*), *QUIRKY* (*QKY*) and *ZERZAUST* (*ZET*) (Fulton et al., 2009). Plants with a defect in these genes show *sub*-like phenotype and corresponding defects in outer integument development, floral organ shape, stem twisting and root hair patterning. *SUB*, *DOQ*, *QKY* and *ZET* contribute to the *STRUBBELIG-LIKE MUTANT* (*SLM*) class of genes (Fulton et al., 2009). *DOQ*, also named *ANGUSTIFOLIA* (*AN*), is a gene described to affect trichome branching, leaf morphology and silique shape (Tsuge et al., 1996; Folkers et al., 1997). *DOQ* has also been showed directly interact with SUB to mediate SUB-dependent signaling (Bai et al., 2013). *ZET* encodes a putative β-1.3 glucanase to involve in the control of cell wall organization (Vaddepalli et al., 2017). Molecular identification of *QKY* by map-based cloning predicted to encode a putative transmembrane protein carrying four C2 domains, and QKY may function in membrane trafficking in Ca^{2+}-dependent fashion (Fulton et al., 2009). Thus, *DOQ*, *ZET* and *QKY* are involved in *SUB*-dependent organogenesis and elucidate the mechanisms of signaling through the atypical receptor-like kinase SUB (Fulton et al., 2009).

1.3 *QUIRKY*, a component of SUB signaling complex at plasmodesmata

1.3.1 Functional overview of QUIRKY in plant development

Three mutant alleles of *QUIRKY* (*QKY*) were isolated by forward genetic approach, *qky-7*, *qky-8* and *qky-9*. All alleles are likely to be nulls and did not noticeably differ in their respective phenotypes (Fulton et al., 2009). *QKY* is a *SLM* class gene and contribute to *SUB*-dependent organogenesis. Plants lacking QKY showed the similar

phenotype with lacking of SUB. *qky-8* mutant showed the *sub*-like phenotype, including aberrant floral phyllotaxis, twisted leaf, twisted siliques and stems, shorter plant height and defective outer integument. *qky-9* mutant also showed the cellular defects in root hair patterning and floral meristems (Fulton et al., 2009). The *qky-7*, *qky-8* and *qky-9* alleles were predicted to introduce stop codons leading to shorter proteins and cause a complete loss of QKY function (Figure 7) (Fulton et al., 2009).

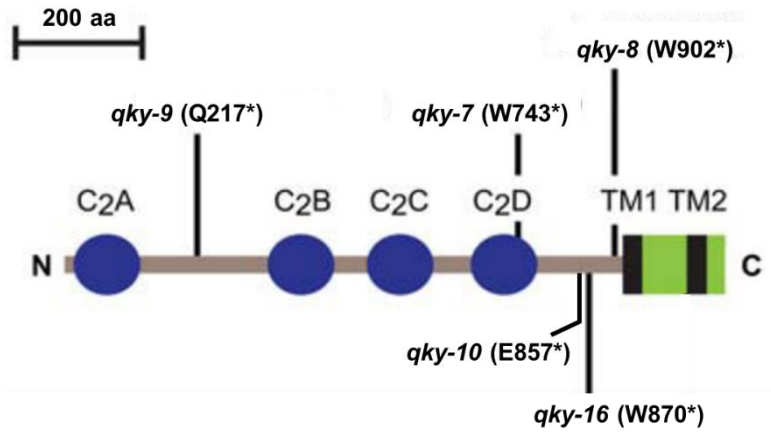

Figure 7 Predicted domain topology of the QKY protein and *qky* alleles.

The sequence and numbering of the C2 domains, and the altered C-termini of the mutant protein variants, are given. Stars mark the premature stops in the predicted mutant proteins. The green box denotes the plant phosphoribosyl- transferase C-terminal region (PRT_C). Abbreviations: aa, amino acids; N, amino terminus; C, carboxy terminus; TM, transmembrane domain. (Modified from Fulton et al., 2009).

The *qky* mutant alleles isolated by γ-ray-mutagenesis and T-DNA insertion, *qky-10* to *qky-15*, all displayed a similar phenotype as previously described, with shorter and irregularly twisted siliques containing fewer seeds than wild-type and slightly aberrant floral phyllotaxis (Trehin et al., 2013). QKY physically interacts with PAL OF QUIRKY (POQ), with SUB together, to be a macromolecular complex, to regulate the global shape of the gynoecium by changing the cell growth anisotropy (Trehin et al., 2013). SYNTAXIN OF PLANTS 121 (SYP121), a PM-resident syntaxin-like Q-SNARE (soluble N-ethylmaleimide-sensitive factor protein attachment protein

receptor), interacts with QKY, coordinately mediate FLOWERING LOCUS T (FT) movement to the PM through the endosomal trafficking pathway and are required for FT export from companion cells to sieve elements (Liu et al., 2019). Furthermore, genetic evidence indicates that QKY and its maize homolog Carbohydrate Partitioning Defective33 (cpd33) play a role in sugar export from leaves and thus carbohydrate partitioning (Tran et al., 2019).

A new allele of *QKY*, *qky-16*, has been isolated by a genetic approach. In *qky-16*, the position-dependent expression pattern of *WER*, *CPC* and *EGL3*, which are regulate the fate of root epidermal cells, was disrupted, causing the expression of these genes at each position (Song et al., 2019). The accumulation of QKY in the H-position cells was greater than the N-position cells of the root epidermis. QKY stabilizes SCM by preventing the internalization and vacuolar degradation triggered by SCM ubiquitination. QKY and SCM complex facilitates the effective trafficking of CPC in root epidermis and accumulation into H-position cells, helping to establish the cell-type pattern of root epidermis (Song et al., 2019; Gao et al., 2019).

1.3.2 QKY is a member of the MCTP family

QKY contains no introns and encodes a transmembrane protein of 1081 amino acids with a calculated molecular mass of 121.4 kDa. QKY protein contains four C2 domains in N-terminal and a plant-specific phosphoribosyltransferase C-terminal domain (TMR) which embedded two transmembrane regions (Fulton et al., 2009). According to the PFAM database the TMR domain often appears together with calcium-ion dependent C2 domains (Mistry et al., 2021). Some related domain topology are found in several proteins present in different organisms, including *Caenorhabditis elegans*, *Drosophila melanogaster*, humans, Arabidopsis, rice and moss, collectively referred to as multiple C2 domain and transmembrane region proteins (MCTPs) (Shin et al., 2005; Liu et al., 2018; Fulton et al., 2009). MCTPs is a family of evolutionarily conserved which contains three to four C2 domains in N-terminal and one to four transmembrane regions

in C-terminal.

QKY is the first described MCTP-class gene in plant (Fulton et al., 2009). Recently, many other MCTPs in plant have been found. The endoplasmic reticulum (ER) membrane protein, FT-INTERACTING PROTEIN 1 (FT1P1), is one member of the MCTPs family, interacts with FLOWERING LOCUS T (FT) in companion cells and mediates its transport to induce flowering (Song et al., 2017; Liu et al., 2012). 16 members of MCTPs in *Arabidopsis* have been identified by bioinformation analysis. They are classified into five clades through phylogenetic analysis based on multiple sequence alignment (Figure 8) (Liu et al., 2018). Although there are many members of MCTPs found in the plant lineage, it is unknown how the biological function and information on most plant MCTPs. The multiple C2 domains represent the key structural features of MCTPs, which have been suggested to either additively or individually act to mediate protein function (Cho and Stahelin, 2006; Marty et al., 2013), but how these domains play roles in mediating MCTPs function in plants still remains unknown.

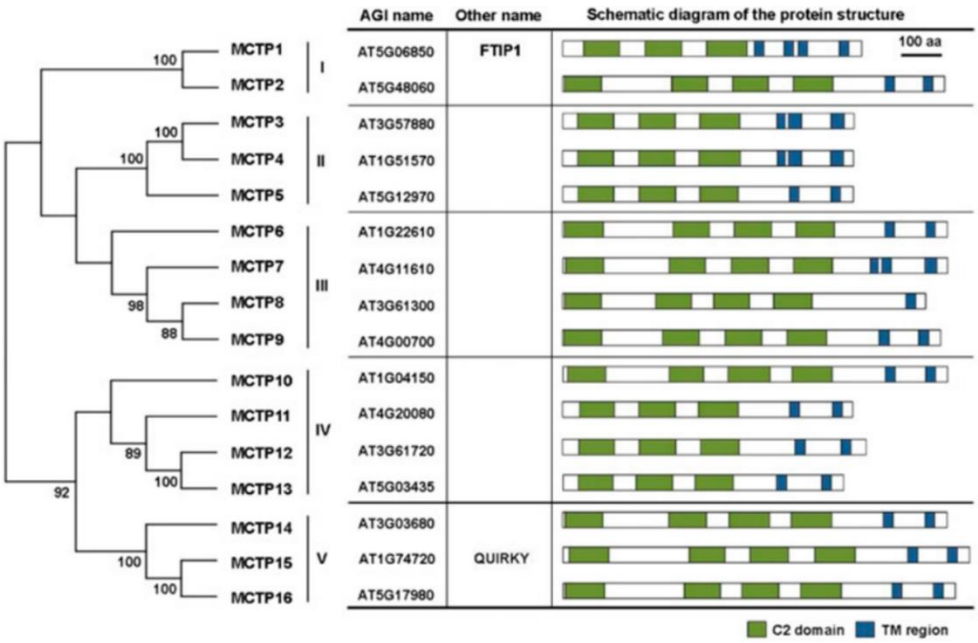

Figure 8 Classification of MCTP family proteins in Arabidopsis.

Five groups of MCTP proteins are defined based on phylogenetic analysis of Arabidopsis MCTPs shown on the left. For each MCTP, the Arabidopsis Genome Initiative (AGI) gene number, other name, and schematic diagram of major motifs are indicated in the table on the right. The prediction of protein motifs is based on SMART (http://smart.embl-heidelberg.de). C2 domains and transmembrane (TM) regions are labeled as green and blue boxes, respectively. aa, Amino acids. (Modified from Liu et al., 2018).

C2 domains are autonomously folding modules and often form Ca^{2+}-dependent phospholipid complexes, however, some exceptions are known that do not bind Ca^{2+} or phospholipids or both (Rizo and Sudhof, 1998). The *Arabidopsis* phospholipid binding Synaptotagmin 1 (SYT1), a plant ortholog of the mammal extended synaptotagmins (E-Syts) and enriched in ER-PM membrane contact sites to regulate the communication in response to abiotic stress, is functioned by Ca^{2+}-dependent and Ca^{2+}-independent phospholipid binding (Li et al., 2006; Pérez-Sancho et al., 2015; Lee et al., 2019; Benavente et al., 2021). Comparison of QKY C2 domain structure with related C2 domains suggests a role in Ca^{2+}-dependent signaling, but the Ca^{2+} binding capacity needs to be tested to further understand the biochemical nature of QKY.

1.3.3 QKY localize to PD and interact with SUB

Vaddepalli et al. 2014 claimed that a punctate pattern around the circumference of cells was observed in a reporter which fused EGFP to the N terminal of QKY under the control of the UBIQUITIN 10 (UBQ10) promoter (EGFP:QKY). In addition, they investigated the colocalization of EGFP:QKY and aniline blue (AB) which a stain for callose associated with PD, determined that 89% of EGFP:QKY spots overlapped with AB punctae in root epidermis cells. Furthermore, they confirmed that EGFP:QKY is localized at PD by immunogold electron microscopy (Figure 9) (Bell and Oparka, 2011; Vaddepalli et al., 2014).

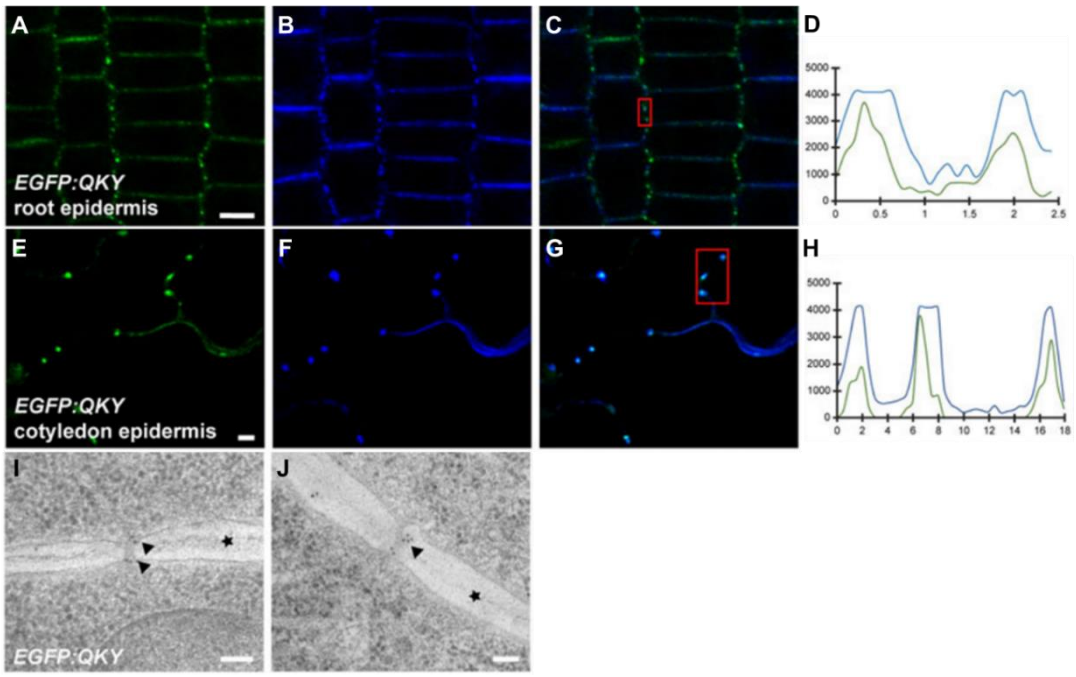

Figure 9 Subcellular localization of QKY.

(A-C, E-G) Confocal micrographs of *qky-8* EGFP:QKY stained with Aniline Blue. (A, E) GFP signal. (B, F) Aniline Blue signal. (C, G) Overlay of Aniline Blue and GFP channels. (D, H) Intensity profiles measured along a line connecting the dots highlighted by the red rectangle in C, G, respectively. The x-axis marks the distance in µm. The y-axis denotes arbitrary intensity units. (I-J) Immunogold electron micrographs. The reporters are indicated. Subepidermal cortical cells in the flank of the root just behind the meristem of 7-day seedlings are depicted. Arrowheads indicate signals at plasmodesmata. The asterisk indicates the cell wall. (I) Signal is seen at the neck region of a plasmodesma. (J) Signal is detected in a more central region of a plasmodesma. Scale bars: (A, B, C, E, F, G) 5 µm, (I, J) 0.1 µm. (Modified from Vaddepalli et al., 2014).

In the light of the PM and PD localization of SUB, it led to the speculation that QKY and SUB colocalize to the same PD. On further analysis it has been revealed that QKY can interact with the intracellular domain (ICD) of SUB in yeast two-hybrid (Y2H) assay. Moreover, the Förster Resonance Energy Transfer - Fluorescence Lifetime Imaging Microscopy (FRET-FLIM) assays further supported SUB:EGFP can interact physically with mCherry:QKY at PD in planta (Vaddepalli et al., 2014).

1.3.4 QKY and SUB act on a common downstream target genetically

Subcellular localization analysis in SUB:EGFP *qky-8* transgenic plants indicated that QKY is not required for localizing SUB:EGFP to the PM or PD. Phenotypic observation in SUB:EGFP *qky-8* transgenic plants exhibited that SUB mildly but reproducibly reduces the *qky-8* mutant phenotype. In T2 lines of SUB:EGFP *qky-8*, although the *qky-8* phenotype was never fully rescued, only 5/42 lines showed no rescue. In the other hand, SUB does not affect the subcellular localization of QKY and the EGFP:QKY transgene did not rescue the *sub-1* phenotype. Taken together, these genetic results imply that *QKY* acts upstream of *SUB* or that *QKY* and *SUB* act in parallel on a common downstream target (Vaddepalli et al., 2014).

1.4 The role of cell wall signaling in plant morphogenesis

1.4.1 The plant cell wall and cell wall integrity signaling

The plant cell wall is a highly complex structure and plays the important role throughout the plant lifecycle. The cell wall provides a pathological and environmental barrier to stress, maintains the structural integrity of the cell, and also provides the flexibility to support cell division. During plant growth and development, cell wall integrity needs to be continuously monitored and maintained to cope with various

challenges. (Hamann, 2012; Wolf et al., 2012).

In general, plant cell walls are composed of three layers: a middle lamina, a primary cell wall, and a secondary cell wall. The middle lamina is deposited during cytokinesis, and binds the primary cell walls of two neighboring plant cells together. The primary cell wall is a thin and flexible layer (0.1-1 μm) that provides basic structural support, protects the cell and mediates cell-to-cell interactions. When the cell has stopped growing and dividing, a thicker secondary cell wall is deposited between the primary wall and plasma membrane, to provide plants with mechanical properties that allow plants to withstand upright growth (Houston et al., 2016). The major components of cell wall are polysaccharides, such as cellulose, hemicellulose, pectin and non-cellulosic polysaccharides. Moreover, the cell wall also contains phenolic compounds such as lignin and a large number of different cell-wall-bound proteins (Lampugnani et al., 2018).

Morphogenesis in higher plants is tightly controlled by the cell wall to facilitate cell division, selective cell expansion and differentiation. The cell wall counteracts turgor-driven growth, that might have an impact on morphogenesis (Mirabet et al., 2011; Cosgrove, 2016). Cell wall fragments released by pathogen-derived lytic enzymes can act as danger signals and elicit plant immunity responses (Boller and Felix, 2009). To achieve proper growth and ensure cell wall defense against external challenges, plant cells must be able to monitor cell wall integrity (CWI) and activate downstream responses when appropriate. The CWI signaling mechanism would sense any physicochemical changes occurring in the cell wall and elicit a corresponding compensatory and protective cellular response (Wolf, 2017; Vaahtera et al., 2019).

1.4.2 Isoxaben-induced cellulose biosynthesis inhibition and cell wall damage

Little is known about the molecular mechanisms involved in monitoring cell wall

status and controlling developmental and stress responses. So far, only a few cell surface signaling factors have been implicated in CWI monitoring (Voxeur and Höfte, 2016; Franck et al., 2018; Wolf, 2017). For example, members of *Catharanthus roseus* receptor-like kinase 1-like (CrRLK1L) family are implied in CWI signaling (Nissen et al., 2016). THESEUS1 (THE1), one member of the CrRLK1 family, is required for the altered expression levels of several stress-response genes upon cell wall damage (CWD) (Hématy et al., 2007). There is evidence indicates that a cell wall sensing mechanism depending on a complex between FERONA (FER) and extracellular leucine-rich repeat extensins (LRXs) negatively regulates vacuolar size. In addition, FER is also required to prevent cell bursting upon exposure of root cells to salt to maintain cell wall integrity (Feng et al., 2018; Dünser et al., 2019).

Plant cells also respond to changes to cellulose levels in the cell wall. Recently, impairing cellulose biosynthesis has become a popular method to study CWI signaling. Cellulose is the main load-bearing element of the cell wall and is synthesized by cellulose synthase (CESA) complexes at the plasma membrane (Somerville, 2006). The effect of reduced cellulose production on plant growth and development can be studied by analyzing mutants with defects in genes encoding CESA subunits involved in primary cell wall biosynthesis (Fagard et al., 2000; Ellis et al., 2002; Caño-Delgado et al., 2003). Alternatively, various pharmacological agents can be applied to specifically inhibit cellulose biosynthesis and similar responses could be observed.

The herbicide isoxaben is a specifically well-characterized inhibitor of cellulose biosynthesis that acts by affecting the CESA complex (Lefebvre et al., 1987; Heim et al., 1990). Isoxaben resistance mutants *ixr1-1* and *ixr2-1* carry mutations encoding CESA3 and CESA6 subunits, respectively, and isoxaben-induced cell wall perturbation could not be observed in *ixr1-1* and *ixr2-1* (Scheible et al., 2013; Desprez et al., 2017; Fagard et al., 2016). Isoxaben can induce the rapid disappearance of YFP:CESA6 from PM into intracellular vesicle, thereby disrupting the CESA complex (Paredez et al.,

2006). The reaction of culture-grown seedlings to isoxaben-induced cellulose biosynthesis inhibition (CBI) represents a universal study of the stress response to CWD (Hamann et al., 2009; Hamann, 2015; Wormit et al., 2012a; Engelsdorf et al., 2018). Treatment with isoxaben causes a reduction in microfibril formation in the cell wall, resulting in cell swelling or bursting (Engelsdorf et al., 2018). CBI also results in the upregulation of stress response genes, the production of reactive oxygen species (ROS), the accumulation of phytohormones such as jasmonic acid (JA) and salicylic acid (SA), the deposition of ectopic lignin and callose, and finally plant growth arrest (Ellis et al., 2002; Caño-Delgado et al., 2003; M. Fagard et al., 2000; Hamann et al., 2009). These responses are sensitive to osmotic support and can be attenuated with the addition of sorbitol (Hamann et al., 2009; Engelsdorf et al., 2018).

1.4.3 The role of SUB signaling in cell wall integrity

Current data suggest that SUB signaling is also involved in cell wall biology. Whole-genome transcriptomics analysis revealed that many genes responsive to SUB-mediated signal transduction relate to cell wall remodeling (Fulton et al., 2009). Moreover, Fourier-transform infrared spectroscopy (FTIR) analysis on cell wall preparations from *sub-1*, *qky-8* and *zet-2*, showed notable and near-identical deviations from wild-type, revealing that *SUB*, *QKY* and *ZET* directly or indirectly influence cell wall composition in an overlapping fashion (Vaddepalli et al., 2017). This is also consistent with the fact that *SUB*, *QKY* and *ZET* are genes of the *SLM* class (Fulton et al., 2009). Thus, *SUB* and *QKY* may also relate to cell wall biology.

1.5 Fluorescence resonance energy transfer (FRET) applications in plant systems

The transfer of energy from one fluorescent molecule to another one that is close physical proximity can cause fluorescence quenching. This transfer of energy is known as fluorescence resonance energy transfer (FRET). In microscopy, the term “resolution”

is the minimum distance to distinguish two different points as separate entities by the microscope camera. If two points are closer than resolution, then they blur together and unable to distinguish them in the microscope image. The resolution of a microscope is linked to the numerical aperture (NA) of the optical components as well as the wavelength of light which is used to examine a specimen. The normal light microscope has a maximum resolution of around 200 nm. With the progress of technology, the exploitation of FRET can increase the spatial resolution of the fluorescence microscope to below 10 nm (Figure 10). The dramatic leap in resolution makes FRET an important tool for scientists studying co-localization and protein-protein interaction events in biological samples at the molecular level of living cells (Bücherl et al., 2014).

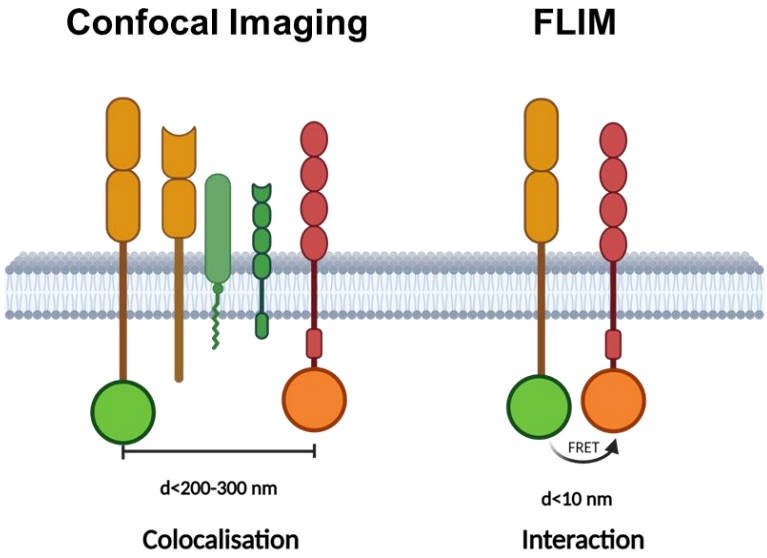

Figure 10 Comparison of the spatial resolution of confocal microscopy and fluorescence lifetime imaging microscopy.

For studying the oligomerisation of proteins, donor FLIM is a suitable method to detect FRET between fluorescently tagged fusion proteins. Since FRET can only occur in the range of protein dimensions, the physical interaction of the two appropriately labeled proteins can be deduced.

FRET takes place when the excited-state energy of a fluorescent donor is transferred to the fluorescent acceptor in a non-radiative manner. There are three conditions for FRET to occur: 1. the distance of donor and acceptor is less than 10 nm, 2. the donor emission band and acceptor absorption band have a spectral overlap, 3. the donor's

emission and the acceptor's absorption transition dipole moments are not perpendicularly oriented (Lakowicz, 2006). Essentially, FRET can be measured between different (hetero-FRET) or identical (homo-FRET) fluorophores. Hetero-FRET results in quenching of the donor emission and this in turn in a reduction of the donor's lifetime. Fluorescence lifetime imaging microscopy (FLIM) has turned out to be a reliable way to measure hetero-FRET.

1.4.1 FRET-FLIM is applied to visualize protein interaction in living plant cells

FLIM is a technique that produces images based on fluorescence lifetime differences of the fluorescent molecules in the sample. The fluorescence lifetime (τ) is defined as the average time of a fluorophore resides in the excited state before returning to the ground state. It is strongly affected by the properties of the local environment, but not affected by fluorophore concentration (Lakowicz, 2006). Normally, the fluorescence lifetime needs to be analyzed according to the data obtained by different FLIM measurement principles. A common approach used for measuring the fluorescence lifetime is time domain FLIM based on time correlated single photon counting (TCSPC). In time domain FLIM, using TCSPC, a picosecond pulsed laser excitation is used and the temporal profile of the fluorescence decay is measured in real time (Becker et al., 2004).

FLIM is widely used in the study of biological processes. A combination of FLIM with FRET allows for protein interaction studies in live cells. For example, Bücherl et al. used FRET-FLIM technology to demonstrate the interaction between BRI1 and SERK3 membrane receptor proteins during brassinosteroid signaling in 5-day-old seedlings of *Arabidopsis* (Bücherl et al., 2013). Stahl et al. demonstrated the interaction of CLV1 and ACR4 in *N. benthamiana* leaves (Stahl et al., 2013). Recently, PIN2, MEL1 and PID have been demonstrated by FRET-FLIM in transiently transformed protoplasts and in root epidermal cells in *Arabidopsis*, to directly interact with each

other within one multiprotein complex to regulate plant development (Glanc et al., 2021).

1.4.2 Fluorescence anisotropy imaging is used to quantify protein clustering

Homo-FRET, the FRET that occurs between identical fluorophores, cannot be imaged using standard hetero-FRET methodologies as the spectral properties of two molecules are the same and the excitation energy is reversibly transferred between fluorophores. Homo-FRET does not change the donor's lifetime because the reduction in the lifetime of the directly excited donor is fully compensated by the additional emission of the indirectly excited "donor". Thus, FLIM is not applicable to measure homo-FRET. Fortunately, homo-FRET can be quantified using its effect on the fluorescence anisotropy (FA), since homo-FRET predominantly takes place between differently oriented fluorophores and causes a depolarization of the emission. Accordingly, homo-FRET can be imaged using fluorescence anisotropy imaging methods and is often employed to investigate clustering of identical proteins (Lakowicz, 2006).

Excitation with polarized light results in photoselection of fluorophores according to their orientation relative to the direction of the polarized excitation. When the emission transition dipole moment is parallel to the absorption transition dipole moment, there are no process resulting in depolarization, the FA will be maximal and amount to 0.4. In principle, the measured FA is often lower due to the rotation and energy transfer of the excited molecules. Rotation leads to a broadening of orientation distribution of the fluorophores, when the intensities of emission parallel to and perpendicular to the excitation polarization direction are the same, the emission is completely depolarized and the anisotropy is zero. Energy transfer also decrease the FA since the measured FA is the average of the individual anisotropy of "directly excited fluorophores" and "fluorophores indirectly excited after energy transfer" that are not polarized by the

excitation light (Bader et al., 2011). In such instances, free cytosolic GFP was measured to have a FA value of 0.332. For comparison, the FA value of GFP fusion to the receptor kinase ACR4 at the PM revealed as 0.300 and 0.263 at PD. This indicates the increased clustering of ACR4:GFP at PD (Stahl et al., 2013).

1.6 Objectives

SUB/QKY signal transduction represents one of the first examples of a functional link between RK- and PD-associated intercellular signaling. The multiple C2 domain represent key structural features of QKY proteins and raise questions regarding their relative functional importance. However, it is unclear how multiple C2 domains play roles in mediating MCTP functions in plants and the architecture of the SUB/QKY signaling complex in vivo is not understood. In this study, I wanted to examine the vivo structure-functional relationship of QKY and its interaction with SUB to address the topology of SUB/QKY complex and analyze the roles of the different domains of QKY. In addition, I was also interested to examined the role of QKY in cell wall signaling associated with growth and defense of plant.

2 Materials and Methods

2.1 Plant work, plant genetics and plant transformation

Arabidopsis thaliana (L.) Heynh. var. Columbia (Col-0) and var. Landsberg (*erecta* mutant) (L*er*) were used as wild-type strains. Plants were grown essentially as described previously (Fulton et al., 2009). The mutant alleles *sub-1* (L*er*), *qky-9* (L*er*) and *sub-9* (Col) have been described previously (Chevalier et al., 2005; Fulton et al., 2009; Vaddepalli et al., 2011). The *qky-17* (L*er*) allele was generated using a CRISPR/Cas9 system in which the egg cell-specific promoter pEC1.2 controls Cas9 expression (Wang et al., 2015b). Two single-guide RNAs (sgRNA), sgRNA1 (5'-ACTCGGATCCTCCGCCGTCG-3') and sgRNA2 (5'-TTACGACGAGCTCGATATCG-3) were employed. sgRNA1 binds to the region +20 to +39, while sgRNA2 binds to the region +237 to +256 of the *QKY* coding sequence. The sgRNAs were designed according to the guidelines outlined in (Xie et al., 2014). The *qky-17* mutant carries a frameshift mutation at position 36 relative to the *QKY* start AUG, which was verified by sequencing. The resulting predicted short QKY protein comprises 60 amino acids. The first 12 amino acids correspond to QKY, while amino acids 13-60 represent an aberrant amino acid sequence. The lines carrying pSUB::gSUB:EGFP (SSE, in *sub-1*, L*er*, *sub-9*), pUBQ10::gSUB:mCherry (USM, in Col), pUBQ10::EGFP:QKY (UEQ, in *sub-1*, L*er*), pUBQ10::mCherry:QKY (UMQ, in L*er*) have been previously reported (Chaudhary et al., 2020; Vaddepalli et al., 2014, 2011). The reporter lines Q4, Lti6a:GFP, Lti6b:2xmCherry, TMO7:1xGFP, and TMO7:3xGFP have been described previously (Noack et al., 2022; Cutler et al., 2000; Schlereth et al., 2010). The reporter constructs pGL2::GUS:GFP and pQKY::mCherry:QKY have been described earlier (Gao et al., 2019; Vaddepalli et al., 2014).

Wild-type, *sub-1* and *qky-9* plants were transformed with different constructs using

Agrobacterium strain GV3101/pMP90 (Koncz and Schell, 1986) and the floral dip method (Clough and Bent, 1998). Transgenic T1 plants were selected on either kanamycin (50 µg/ml) or hygromycin (20 µg/ml) plates and transferred to soil for further inspection. Plate-grown seedlings were grown in long-day conditions (16 h light/8 h dark) on half-strength Murashige and Skook (1/2 MS) agar plates supplemented with 1% sucrose. Before sowing seeds on 1/2 MS, they were surface sterilized in 3.5% (V/V) sodium hypochlorite (NaOCl) plus 0.1% (V/V) Triton X-100 for 10min on a rotator to prevent bacterial and fungal growth on plates. Seeds were washed three times with ddH2O and stratified for 4d at 4°C prior to incubation. Dry seeds were sown on soil (Patzer Einheitserde, extra- gesiebt, Typ T, Patzer GmbH & Co. KG, Sinntal-Jossa, Germany) situated above a layer of perlite, stratified for 4 days at 4°C and then placed in a long day cycle (16 hrs light) using Philips SON-T Plus 400 Watt fluorescent bulbs. The light intensity was 120-150 µmol/m2sec. The plants were kept under a lid for 7-8 days to increase humidity (50-60%) and support equal germination. All the crossed materials used in this study were F1 seeds.

2.2 Recombinant DNA work

For DNA and RNA work, standard molecular biology techniques were used. DNA and RNA used for cloning were extracted from *Arabidopsis thaliana* using the NucleoSpin Plant II kit (Macherey-Nagel GmbH und Co. KG) and the NucleoSpin RNA plant kit (Macherey-Nagel GmbH und Co. KG). RNA was used as a template, mRNA was reverse transcribed into cDNA using the RevertAid 1st strand cDNA synthesis kit (Fermentas) and a poly-T primer according to the manufacturer's protocol. Cloning was performed using standard methods described in (Sambrook et al., 1989). PCR-fragments used for cloning were obtained using Q5 high-fidelity DNA polymerase (New England Biolabs, Frankfurt, Germany). Restriction enzymes and T4 DNA Ligase used for cloning were also received from NEB GmbH and used according to the manufacturer's protocols. PCR products were purified using the NucleoSpin Gel and

PCR clean- up kit (Macherey-Nagel GmbH und Co. KG) according to the manufacturer's protocol. Plasmids were isolated with the NucleoSpin Plasmid kit (Macherey- Nagel GmbH und Co. KG) according to the manufacturer's protocol. Escherichia coli strain DH10β was used for amplification of the plasmids. Bacteria were grown on corresponding selection media (Lysogeny broth). Antibiotics for bacterial selection were used at final concentrations as follows: Kanamycin 50 µg/mL; Ampicillin 100 µg/mL; Gentamycin 25 µg/mL; Spectinomycin 100 µg/mL; Tetracyclin 12.5 µg/mL; and Rifampicin 10 µg/mL.

All PCR-based constructs were sequenced by MWG-Biotech AG following the company's standards. Sequencing results were aligned with geneious software to reference sequences received from The Arabidopsis Information Resource (TAIR, https://www.arabidopsis.org/). The plasmids pCAMBIA2300 (https://cambia.org/) and pGGZ001 (Lampropoulos et al., 2013) were used as binary vectors. Details of the PCR reaction mix and steps involved in PCR using both Q5 high-fidelity DNA polymerase and Taq polymerase have been summarized in Table 1. Vectors used in this work are listed in Table 2. Detailed information for all oligonucleotides used in this study are listed in supplementary material Table S1.

Table 1 PCR reaction mix and cycler program.

Reaction mix for Q5® High-Fidelity DNA polymerase based PCR amplification

Components/reaction	Volume (µl)
5x Q5 Reaction buffer	10
2 mM dNTPs	5
10 µM Forward primer	2.5
10 µM Reverse primer	2.5
Q5 High-Fidelity DNA polymerase (2 U/µl)	0.5
Template DNA (100 ng made up to 2.5 µl)	2.5
Sterile double distilled water	to 50

PCR Cycler program for Q5 polymerase

Temperature	Time	Cycles
98 °C	30 sec	1 cycle
98 °C X °C 72 °C	15 sec 10 sec 30 sec/kb	35 cycles
72 °C	3 min	1 cycle

Reaction mix for Taq polymerase based PCR amplification

Components/reaction	Volume (µl)
10x Standard Taq Reaction buffer	2.5
2 mM dNTPs	2.5
10 µM Forward primer	0.5
10 µM Reverse primer	0.5
Taq polymerase (5 U/µl)	0.125
Template DNA (100 ng made up to 1 µl)	1
Sterile double distilled water	17.875

PCR Cycler program for Taq polymerase Temperature

Temperature	Time	Cycles
95 °C	2 min	1 cycle
95 °C X °C 72 °C	20 sec 20 sec 1 min/kb	35 cycles
72 °C	5 min	1 cycle

Table 2 Plasmid vectors used in this study.

Name	Purpose	Description
pGADT7	Yeast two-hybrid interaction test	Express a protein of interest fused to a GAL4 activation domain
pGBKT7	Yeast two-hybrid interaction test	Express a protein fused to GAL4 DNA binding domain
pGGA000	GG entry vector	Entry vector for promoter region of interest
pGGB003	GG entry with N-decoy	Entry vector carrying N-decoy in case no D-tag is needed
pGGC000	GG entry vector	Entry vector for CDS of interest
pGGD001	GG entry vector with linker-GFP	Entry vector carrying GFP as C-tag
pGGE009	GG entry with tUBQ	Entry vector carrying terminator of UBQ10
pGGF005	GG entry with Hygromycin-R	Entry vector carrying Hygromycin resistance for plant selection
pGGZ001	GG destination vector	Destination vector, binary vector for plant transformation
pCambia2300	Binary vector for plant transformation	

2.3 Arabidopsis genomic DNA extraction and genotyping PCR

DNA was extracted from a small piece of leaf tissue of diameter ~ less than 1 cm. Leaf disk was freeze in liquid nitrogen and grinded to a fine powder (Qiagen grinder or pestle). The powdered tissue was suspended in 500 µl gDNA extraction buffer and incubated for 15 min at 65°C using a thermo mixer at 1000 rpm after brief vortexing. 300 µl chloroform was added and mixed thoroughly by inverting Eppendorf tubes. The mixture was centrifuged for 10 min at 13000 rpm. 400 µl of the supernatant was transferred into a new tube (make sure to avoid any interphase junk). 280 µl of

isopropanol was added to the supernatant (70% vol of supernatant), mixed by inversion, incubated 5 min at room temperature and centrifuged for 15 min at 12000 rpm. The pellet was washed with 1 ml ice cold 70% ethanol, dried completely and resuspended in 50 µl 5 mM Tris-Hcl PH 5.8 or ddH2O. The entire preparation was stored at 4 °C until use. PCR-based genotyping was performed with the following primer combinations: *sub-1*: sub-1_NdeI_F, sub-1_NdeI_R; *qky-9*: qky-9_XbaI_F, qky-9_XbaI_R; Primer sequences are listed in Table S1.

2.4 RNA extraction from plant material and cDNA synthesis Total

Total RNA was isolated from the 7-day-old seedlings using the kit according to the instructions given in the manufacturer's manual. Purified total RNA in RNase- free water were quantified and analyzed for purity using the NanoPhotometer P330 (Implen GmbH). Non-denaturing agarose gel electrophoresis was performed to examine the quality and integrity of RNA (Rio et al., 2010). Isolated RNA was stored at -80 °C until use. First-strand cDNA synthesis was performed using the RevertAid 1st strand cDNA synthesis kit (#1622, Thermo Scientific) accordingly. Details of the reaction mix and steps involved in the cDNA synthesis have been summarized in Table3.

Table 3 Reaction mix and steps involved in cDNA synthesis.

Reaction mix for the cDNA synthesis

Components per reaction	Volume (µl)
5x Reaction Buffer	4
RiboLock RNase Inhibitor (20 U/µl)	1
10 mM dNTP Mix	2
RevertAid M-MuLV RT (200 U/µl)	1
Oligo (dT)18 primer	1
Template RNA	1 µg
Nuclease-free water	to 20µl

Steps for cDNA synthesis

Step	Temperature (°C)	Incubation time (min)
Step 1	42	60
Step 2	70	5
Step 3	4	forever

2.5 PCR-Based Gene Expression Analysis

Floral tissue for quantitative real-time PCR (qPCR) was harvested from plants grown under long day conditions. With minor changes, tissue collection, RNA extraction, quality control and cDNA synthesis were performed as described above. qPCR and analysis was done essentially as previously described (Enugutti et al., 2012). For detection of QKY expression by qPCR primers QKY_RT_Fnew/QKY_RT_Rnew were employed.

2.6 Generation of various reporter constructs

2.6.1 Generation of pSUB::SUB:GFP constructs

The pSUB::gSUB:GFP (SSG) construct was assembled using the GreenGate system (Lampropoulos et al., 2013). The sequences of pSUB and gSUB were amplified as previously described (Yadav et al., 2008; Vaddepalli et al., 2011). Other sequences, including GFP and the plant resistance modules, were available from the GreenGate vectors. The pSUB::gSUB:GFP was assembled into the intermediate vectors and then combined into the pGGZ0001 destination vector with a standard GreenGate reaction.

2.6.2 Generation of pQKY::mCherry:QKYdel constructs

The pCambia2300-based progressive N-terminal deletions of QKY carrying EGFP

driven by the UBQ10 promoter (pUBQ10::mCherry:QKYdel) were described previously (Vaddepalli et al., 2014). To generate the deletion constructs of QKY fused to mCherry driven by the endogenous QKY promoter (pQKY::mCherry:QKYdel), the fragment of pQKY::mCherry was digested with KpnI/SpeI from plasmid pQKY::mCherry:QKY, and subcloned into the KpnI/SpeI digested pUBQ::mCherry:QKYdel.

2.6.3 Generation of pQKY::mCherry:QKY phosphorylation site mutant constructs

The pCAMBIA2300-based pQKY::mCherry:QKY (QMQ) construct was described previously (Vaddepalli et al., 2014). The pQKY::mCherry:QKY phosphorylation site mutant plasmid was obtained using the Q5 site directed mutagenesis kit (NEB, #E0554S) according to the manufacturers recommendation and primers as follow: QMQS218A: Q5SDM S218A_F, Q5SDM S218A/E_R; QMQS218E: Q5SDM S218E_F, Q5SDM S218A/E_R; QMQS262A: Q5SDM S262A_F and Q5SDM S262A_R; QMQS262E: Q5SDM S262E_F, Q5SDM S2262E_R; QMQS305A: Q5SDM S305A_F, Q5SDM S305A/E_R; QMQS305E: Q5SDM S305E_F, Q5SDM S305A/E_R; QMQS1075A: Q5SDM S1075A_F, Q5SDM S1075A_R; QMQS1075E: Q5SDM S1075E_F, Q5SDM S1075E_R. Primers were designed with NEBaseChanger™ tool (https://nebasechanger.neb.com/).

2.6.4 Construction of yeast two-hybrid vector

The backbone vectors for the yeast two-hybrid (Y2H) analysis were pGADT7 AD (AD) and pGBKT7 BD (BD). The pGBKT7 plasmids containing either the SUB extracellular (ECD) or intracellular (ICD) domain were described previously (Bai et al., 2013). The construct pGADT7-QKYC2A-D is equivalent to a previously described construct pGADT7-QKYΔPRT_C (Vaddepalli et al., 2014). For the generation of

pGADT7-SUB carrying ECD or ICD, the fragment of pGBKT7-SUB carrying the ECD or ICD was digested by NdeI/XmaI and subcloned into the NdeI/XmaI-digested pGADT7. Similarly, in order to generate pGBKT7-QKYC2A-D, the fragment of pGADT7-QKYC2A-D was digested by NdeI/XmaI and subcloned into pGBKT7 digested with NdeI/XmaI.

In order to generate the pGADT7 carrying the various truncated fragments of QKY, the different truncated fragments of QKY were amplified from L*er* cDNA with the following primers: NdeI/QKY(-TM)_F and QKY(C2A-B)/XmaI_R for the fragment of C2A-B, QKY(C2C-D)/NdeI_F and QKY(-TM)/XmaI_R for the fragment of C2C-D, NdeI/QKY(-TM)_F and C2ALinker_XmaI_R for the fragment of C2AL, NdeI/QKY(-TM)_F and C2A_XmaI_R for the fragment of C2A, C2ALinker_NdeI_F and C2ALinker_XmaI_R for the fragment of L. Fragments were digested by NdeI/XmaI and subcloned into the NdeI/XmaI digested pGADT7. All clones were verified by sequencing. Primers are listed in Table S1.

In order to generate the pGADT7 carrying the various phosphosites mutants of QKYC2A-D, the pGADT7-QKYC2A-D phosphorylation site mutant plasmid was obtained using the Q5 site directed mutagenesis kit (NEB, #E0554S) according to the manufacturers recommendation and primers as follow: QMQS218A: Q5SDM S218A_F, Q5SDM S218A/E_R; QMQS218E: Q5SDM S218E_F, Q5SDM S218A/E_R; QMQS262A: Q5SDM S262A_F and Q5SDM S262A_R; QMQS262E: Q5SDM S262E_F, Q5SDM S2262E_R; QMQS305A: Q5SDM S305A_F, Q5SDM S305A/E_R; QMQS305E: Q5SDM S305E_F, Q5SDM S305A/E_R. All constructs were verified by sequencing.

2.7 Yeast two-hybrid assay

The Matchmaker yeast two-hybrid system (Takara Bio Europe, Saint-Germain-en-

Laye, France) was employed and experimental procedures followed the manufacturer's recommendations. In order to assess possible interactions in yeast, the different combinations of pGBKT7 and pGADT7 plasmids were co-transformed into the yeast strain AH109. Transformants were selected on synthetic complete (SC) medium lacking leucine and tryptophan (-LW) at 30°C for 3 days. To examine yeast two-hybrid interactions, the transformants were grown on solid SC medium lacking leucine and tryptophan (SC-LW) or leucine, tryptophan and histidine (-LWH). Standard -LWH growth medium was supplemented with 2.5 mM 3-amino-1,2,4-triazole (3-AT) to minimize false positive signals. Yeast were grown for 3 days at 30°C.

2.8 Confocal laser scanning microscopy (CLSM)

For the quantitative analysis of pGL2::GUS:GFP-expressing cells in the root epidermis, 6-days-old seedlings of different genotypes carrying the pGL2::GUS:GFP reporter were counterstained with 5 μg/ml propidium iodide and examined using a FV3000 confocal laser scanning microscope (Olympus Europe, Hamburg, Germany). A high sensitivity detector (HSD) and a 60x water immersion objective (NA 1.2) were employed. Scan speed was set at 4.0 μs/pixel (image size 1024x1024 pixels), line average at 2, and the digital zoom at 1. GFP was excited using a 488 nm diode laser (2% intensity) and emission was detected at 500 to 540 nm. Propidium iodide was excited using a 561 nm diode laser (1% intensity) and emission detected at 584-653 nm.

To assess pQKY::mCherry:QKY (QMQ) subcellular localization, confocal microscopy was performed on root epidermal cells of 6-days-old seedlings using an Olympus FV1000 confocal microscope and on epidermal cells of several stage 13 floral organs using an Olympus FV3000 confocal microscope. High sensitivity detectors (HSDs) and a 60x water immersion objective (NA 1.2) were employed in both microscopes. Scan speed was set at 4.0 μs/pixel (image size 1024x1024 pixels) and line average at 2. The mCherry fluorescence excitation was performed with a 561 nm diode

laser (5% intensity) and detected at 584-653 nm.

For the colocalization of mCherry:QKY with the ER marker Q4, 6-days-old seedling roots were imaged using an Olympus FV3000 confocal microscope equipped with HSD detectors. In some instances, the seedlings of the ER marker Q4 were counterstained with 4 µM FM4-64 (Molecular Probes) for 5 minutes. A 60x water immersion objective (NA 1.2) was employed. Scan speed was set at 2.0 µs/pixel (image size 1024x1024 pixels), line average at 2, and the digital zoom at 2. The mCherry fluorescence and the FM4-64 stain were excited using a 561 nm diode laser (7% intensity for mCherry and 2% intensity for FM4-64) and emission was detected at 584-653 nm. GFP was excited using a 488 nm diode laser (1% intensity) and emission was detected at 500-540 nm.

To observe the subcellular localization of QMQ mutant variants, the root epidermal cells of 6-days-old seedlings were imaged using an Olympus FV3000 confocal microscope equipped with a HSD and a 60x water immersion objective (NA1.2). Scan speed was set at 4.0 µs/pixel (image size 1024x1024 pixels) and the digital zoom at 4. The mCherry fluorescence excitation was performed with a 561 nm diode laser (7% intensity) and detected at 584-653 nm. Images were adjusted for color and contrast using ImageJ/Fiji software (Schindelin et al., 2012).

Root cell bulging were imaged with an Olympus FV1000 setup using an inverted IX81 stand and FluoView software (FV10-ASW version 01.04.00.09) (Olympus Europa GmbH, Hamburg, Germany) equipped with a 10x objective (NA 0.3). For assessing cell bulging a projection of a 5 µm z-stack encompassing seven individual optical sections was used.

For the quantification of SUB-GFP accumulation at the PM, epidermal cells of root meristems of 6-days-old seedlings in the corresponding plant line were imaged using an Olympus FV3000 microscope equipped with a HSD and a 60x water immersion

objective (NA 1.2) at digital zoom 4. Scan speed was at 4.0 µs/pixel (image size 1024x1024 pixels) and line average at 2. GFP was excited using a 488 nm diode laser (1% intensity) and emission was detected at 500 to 540 nm. For the direct comparisons of fluorescence intensities, laser, pinhole, and gain settings of the confocal microscope were kept identical when capturing the images in different QKY mutant backgrounds. The mean gray values of GFP fluorescence signal intensity at the PM were measured in 5-10 cells from each image by creating a region of interest covering the PM area using ImageJ/Fiji.

2.9 Phenotyping floral organ and siliques

Floral organs were imaged using a Leica SAPO stereo microscope equipped with a digital MC 170 HD camera (Leica Microsystems GmbH, Wetzlar, Germany). Silique micrographs were obtained using an Olympus SZX12 stereomicroscope equipped with a XC CCD camera and Cell Sense Dimension software. Whole plant pictures were taken with a Nikon COOLPIX B500 digital camera (NIKON CORP.). Images were manipulations such as brightness and contrast, were carried out using ImageJ/Fiji and Adobe Photoshop CS6 software (Adobe System Inc.).

2.10 Observation of ovule morphology and root epidermal cell pattern

Ovule morphology was investigated using an Olympus BX61 upright microscope. For the analysis of root epidermal cell patterning, 6-days-old seedlings were imaged using an Olympus BX61 upright microscope equipped with an XM10 monochrome camera (Olympus Europe, Hamburg, Germany). The number of H-position and N-position cells in at least ten seedlings were scored and the relative ratio of H-position with hair and N-position without hair were deduced.

2.11 Three dimensional ovule imaging using CLSM and MorphoGraphX

Clearing and imaging of ovules was performed as reported previously (Tofanelli et al., 2019). Carpel were obtained from appropriate flower buds and dissected before suspending in fixative 4% paraformaldehyde (PFA) in 1×PBS pH7.3 for one to two hours at room temperature with gentle agitation or overnight at 40C. The fixed tissues were washed twice for 1 min in 1 x PBS. Then the tissues were transferred to ClearSee solution at room temperature with gentle agitation for overnight or more. Cleared ovules were stained with (0.1 %) SCRI Renaissance 2200 (SR2200) stain (Musielak et al., 2015) in 1x PBS for 30 min. Subsequently, the ovules were transferred to ClearSee solution for another 30 min before imaging (Ursache et al., 2018). Ovules were mounted on slides and dissected from the carpel wall. For imaging, a Leica TCS SP8 X microscope with 63 x glycerol objective was used. SR2200 was excited with a 405-nm laser line and emission recorded between 415 and 476 nm (405/415–476). The confocal images of the ovules were used to construct a 3D image with MorphoGraphX 2.0 (de Reuille et al., 2015).

2.12 FRET-FLIM measurement

FRET-FLIM was performed using an Olympus FV3000 microscope equipped with a time-correlated single photon counting (TCSPC) device (LSM upgrade kit, PicoQuant, Berlin, Germany). Root epidermal cells of 5-days-old seedlings co-expressing SUB:GFP and mCherry:QKY were imaged with a 60x water immersion objective (NA 1.2) at digital zoom 4. Scan speed was 4.0 µs/pixel (image size 512x512 pixels). The FLIM filter cube DIC560 for GFP/RFP was employed. GFP fluorescence lifetimes were measured with two photon-counting PMA hybrid 40 detectors and a pulsed 485 nm diode laser (LDH-D-C-485, PicoQuant) using a laser pulse rate of 40 MHz. For each image, a minimum of 300 photons per pixel were acquired with a TCSPC resolution of 25.0 ps (image size 512x512 pixels). Results were analyzed using SymPhoTime 64

software 2.7 (PicoQuant) using n-exponential reconvolution and an internally calculated instrument response function (IRF). The lifetime fitting model parameter as 1 was defined (n=1). The analysis results with a correctional factor ($\chi 2$) between 0.9 and 1.9 were accepted. Intensity-weighted average lifetime (τ Av Int) of membrane ROIs was taken as the final value for each FLIM image.

2.13 Fluorescence anisotropy measurement

Steady-state fluorescence anisotropy was performed and analyzed as reported previously (Chaudhary et al., 2021; Chaudhary and Schneitz, 2022). Note that if one has to work with weak reporter expression and therefore around the minimum number of detected photons required for a meaningful result (on average 15 photons per pixel of a ROI detected in the channel belonging to the perpendicular detector of the PicoQuant system (channel 1 in the SymPhoTime 64 software 2.7), maximum scan time of 5 min), the actual calculated anisotropy value is also influenced to some extent by the number of photons collected. In such a scenario, a lower number of photons leads to a low FA value, and a higher number of photons leads to a higher FA value.

2.14 Immunoprecipitation and western blot analysis

Five hundred milligrams of 9-days-old transgenic seedlings carrying EGFP:QKY reporter driven by UBQ10 promoter (pUBQ::EGFP:QKY) in Ler, qky-8 or sub-1 background were lysed using a TissueLyser II (Qiagen) and homogenized in 1 ml lysis buffer A [50 mM Tris-Cl pH 7.5, 150 mM NaCl, 0.5 mM ethylenediaminetetraacetic acid (EDTA), 1% Triton X-100, 0.1 mM phenylmethylsulfonyl fluoride (PMSF), protease inhibitor cocktail (cOmpleteTM), phosphatase inhibitor cocktail (cell signaling technology), 10% glycerol]. Sonicate the homogenate for 5 pulse under 50% power by Ultrasonic homogenizer (Sonopuls, Bandelin). Cell lysate was mildly agitated for 15 min on ice and centrifuged for 15 min at 8000 rpm at 4 ℃. Then supernatant was incubated with GFP-Trap magnetic agarose (MA) beads (ChromoTek) for 4 h at 4 °C.

Beads were concentrated using a magnetic separation rack. Samples were washed four times in buffer B [50 mM Tris-Cl pH 7.5, 150 mM NaCl, 0.1 mM PMSF, protease inhibitor cocktail (cOmpleteTM), phosphatase inhibitor cocktail (cell signaling technology), 10% glycerol]. Bound proteins were eluted from beads by heating the samples in 40 µl 2× Laemmli buffer (Bio-Rad) for 15 min at 70 ℃. 30 µl of eluted samples were used for subsequent immunoprecipitation-based mass spectrometry analysis. 10 µl of eluted Samples were separated by SDS-12% PAGE and analysed by immunoblotting according to standard protocol to test the quality of immunoprecipitated proteins. For immunoblotting, primary antibody was rat monoclonal anti-GFP antibody 3H9 (ChromoTek), and secondary antibody was obtained from Agrisera: goat anti-rat IgG antibody (AS10 1187).

2.15 Drug treatment

Isoxaben (ISX) and epigallocatechin gallate (EGCG) were obtained from Sigma-Aldrich and used from stock solutions in DMSO (ISX: 100 µM; EGCG: 1 mM). FM4-64 was purchased from Molecular Probes (2 mM stock solution in water). For FM4-64 staining seedlings were incubated in 4 µM FM4-64 in liquid 1/2 MS medium for 5 minutes prior to imaging.

2.16 Lignin staining and imaging

Staining for lignin (phloroglucinol) was performed as described previously (Van der Does et al., 2017). Images of seedlings exhibiting phloroglucinol staining were taken on a Leica MZ16 stereomicroscope equipped with a Leica DFC320 digital camera. Phloroglucinol staining was quantified on micrographs using ImageJ software (Rueden et al., 2017).

2.17 Bioinformatics

Protein domain searches were conducted using the PFAM database. Bioinformatic analysis was mainly performed using geneious software. Alignments were generated with geneious software using a ClustalW algorithm with BLOSUM62 matrix. Sequencing results were analyzed in geneious software using the map to reference tool with geneious mapper and highest sensitivity.

2.18 Statistical analysis

Statistical analysis was performed with PRISM 9.4.0 software (GraphPad Software, San Diego, CA, USA). All statistical tests and P-values are described in the respective figure legends.

3 Results

3.1 Analysis of SUB/QKY complex architecture

3.1.1 The isolated C2A domain of QKY does not have a function

Previous genetic tools used to study QKY function in *Arabidopsis* were mainly *qky-8*, *qky-10*, *qky-16*, etc. (Figure 7) (Fulton et al., 2009; Song et al., 2019; Trehin et al., 2013). Although these mutations were reported as likely to be nulls, the N-terminal C2A-D domain still remained. Given that the multiple C2 domains represent key structural features of QKY protein, and my study focused on the analysis of structural and functional relevance of QKY, it was necessary to produce a cleaner mutational background to be used as a genetic tool in this study.

Using the CRISPR/Cas9 editing technology, I generated a new null allele of *QKY*, *qky-17*, in which all C2 domains have been deleted. Sequence analysis predicted that *qky-17* allele carries a frameshift mutation at position 36 relative to the *QKY* start AUG, and introduced a stop codon at position 178. The short protein comprises 12 amino acids correspond to QKY, while amino acids 13-60 represent an aberrant amino acid sequence (Figure 11A). Morphological observation of flower, silique, ovule and root hair pattern revealed that *qky-17* displayed QKY loss-of-function phenotypes, such as asymmetric floral organs, short and twisted siliques, defects in integument initiation and outgrowth in ovule, and irregular root hair pattern, indicating that *qky-17* is a putative null allele (Figure 11B-M).

Our laboratory previously reported that the *qky-9* allele carries a nonsense mutation at position 649. The short protein in *qky-9* contains 217 amino acids corresponding to QKY, and the C2A domain is retained (Fulton et al., 2009). Morphological observation of *qky-9* revealed that the identical phenotypes as *qky-17*, indicating that the C2A

domain of QKY potentially present in cells of *qky-9* does not has residual function or act in a dominant-negative fashion (Figure 11B-M). Thus, *qky-9* represents a putative null alleles as well.

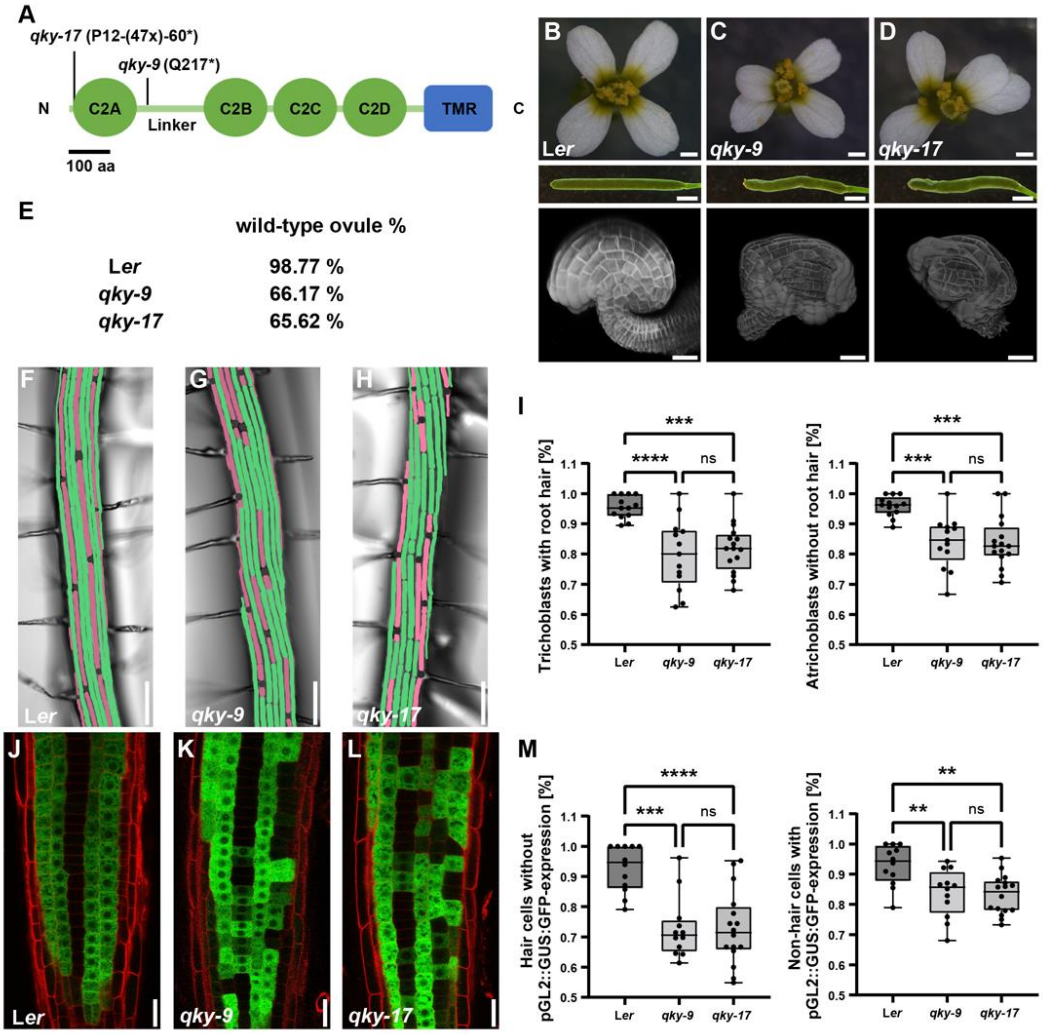

Figure 11 Phenotypic comparison of L*er*, *qky-9* and *qky-17*.

(A) Cartoon depicting the structure of QKY protein. The four C2 domains in the N-terminal and the transmembrane region (TMR) in C-terminal are indicated. The positions of the *qky-9* and *qky-17* mutations are also shown. (B-D) Floral organ morphology of L*er*, *qky-9*, *qky-17*. Upper panel: stage 13 flower, middle panel: stage 15 silique, bottom panel: stage 3-V ovule. Ovule images made by Tejasvinee Mody. (E) The proportion of ovules with wild-type appearance in L*er*, *qky-9* and *qky-17*, respectively. For each genotype, 7 to 10 different carpels from at least two different plants were analysed (430≤n≤458). (F-H) Micrographs showed epidermal root hair cell patterning in 7-days-old seedlings of L*er* (F), *qky-9* (G) and *qky-17* (H). (I) Quantification of results shown in (F-H). The percentage of H position hair cells with root hairs (left panel) and that of N position hair cells without root hairs (right panel) are shown, respectively. 13≤n≤16, each data point represents the percentage

in per different root, which was calculated by at least 15 cells of each cell type. ***P<0.001, ****P<0.0001, ns: not significant. One-way ANOVA with Tukey's multiple comparison test. Experiments were repeated at least two times with similar results. (J-L) Expression pattern of the pGL2::GUS:GFP reporter in L*er* (J), *qky-9* (K) and *qky-17* (L). (M) Quantification of the results shown in (J-L). The percentage of H position hair cells without expressing the pGL2::GUS:GFP reporter (left panel) and that of N position hair cells expressing the pGL2::GUS:GFP reporter (right panel) are shown, respectively. 12≤n≤16, each data point represents the percentage in per different root, which was calculated by at least 15 cells of each cell type. **P<0.01, ***P<0.001, ****P<0.0001, ns: not significant. One-way ANOVA with Tukey's multiple comparison test. Experiments were repeated at least two times with similar results. Note that *qky-9* and the putative null allele *qky-17* show identical phenotypes, indicating that the C2A domain of QKY potentially present in cells of *qky-9* does not have residual function or act in a dominant-negative fashion. Thus, *qky-9* represents a putative null allele as well. Scale bars: (B-D) flowers: 400 µm, siliques: 2mm, ovules: 20 µm. (F-H) 100 µm, (J-L) 20 µm.

3.1.2 QKY localizes to the ER and to PD

A previous study involving stable transgenic *Arabidopsis* plants carrying a functional reporter indicated a PD localization for QKY (Vaddepalli et al., 2014). Transient expression studies in *Nicotiana benthamiana* leaves frequently suggested ER localization of MCTP proteins, but also indicated a number of different subcellular associations, depending on the family member (Hu et al., 2021; Liu et al., 2019; Brault et al., 2019; Tran et al., 2019; Liu et al., 2018). In particular, they suggested that QKY is localized to ER, intracellular vesicles, PM, and cytoplasm. In order to further address this issue, I generated new stable transgenic *qky-9* plants carrying an N-terminal translational fusion of mCherry to QKY reporter driven by its endogenous promoter (pQKY::mCherry:QKY, QMQ), and reinvestigated the subcellular localization of QKY in its native context in *Arabidopsis* cells. First, I analyzed the phenotype of 17 independent transformant lines (Table 4). I found that QMQ robustly rescued the floral tissue and root hair patterning defects of *qky-9* (Table 4, Table 5, Figure 12). This data demonstrates the functionality of the QMQ reporter.

Table 4 Phenotypes of *qky-9* lines homozygous for different QKYdel variants.

Genotype	Phenotype[a]	Percentage of independent homozygous T3 lines[b]
QMQ *qky-9*	WT	15/17
delC2A *qky-9*	*qky*	10/10
delC2AL *qky-9*	*qky*	12/12
delC2A-B *qky-9*	*qky*	11/11
delC2A-C *qky-9*	*qky*	6/6
delC2A-D *qky-9*	*qky*	9/9

[a]Phenotype was scored based on the morphology of flowers, siliques, and stems.

[b]Number of independent transgenic lines with corresponding phenotype / total number of independent transgenic lines scored.

Table 5 Integument defects of L*er*, *qky-9, qky-9* QMQ, and different *qky-9* QMQdel lines.

Genotype	N ovules scored[a]	% defective ovules[b]
L*er*	324	3.40
qky-9	428	36.92
QMQ *qky-9*	396	4.55
delC2A *qky-9*	371	34.23
delC2AL *qky-9*	422	33.89
delC2A-B *qky-9*	463	32.83
delC2A-C *qky-9*	367	35.15
delC2A-D *qky-9*	335	39.70

For L*er* and *qky-9*, 7 to 10 different carpels from at least two different plants were analyzed. For each *qky-9* QMQdel genotype, 7 to 10 different carpels from at least two different plants of two independent lines each were analyzed.

[a]Total number of ovules scored.

[b]Percentage of ovules with *qky*-like integument defects.

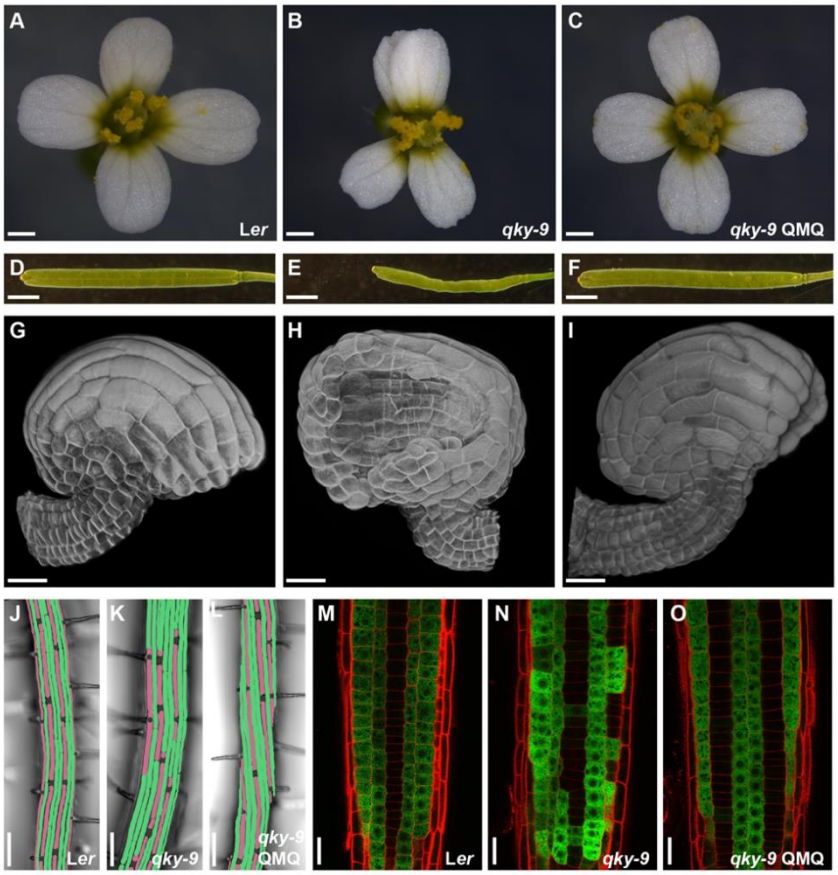

Figure 12 pQKY::mCherry:QKY rescues the *qky-9* phenotype.

pQKY::mCherry:QKY (QMQ) encodes a functional fusion protein. (A-C) Stage 13 flower morphology of Ler (A), *qky-9* (B) and QMQ *qky-9* (C). (D-F) Silique shape (stage 15) of Ler (D), *qky-9* (E) and QMQ *qky-9* (F). (G-I) Stage 3-V ovule morphology of Ler (G), *qky-9* (H) and QMQ *qky-9* (I). Ovule images made by Athul Vijayan and Rachele Tofanelli. (J-L) Micrographs showed epidermal root hair cell patterning in 7-days-old seedlings of Ler (J), *qky-9* (K) and QMQ *qky-9* (L). (M-O) Expression pattern of the pGL2::GUS:GFP reporter in Ler (M), *qky-9* (N) and QMQ *qky-9* (O). Confocal micrographs show optical sections of epidermal cells of root meristems of 7-days-old seedlings. The cell wall was counterstained with propidium iodide. Scale bars: (A-C) 0.5 mm, (D-F) 2 mm, (G-I) 20 µm, (J-L) 100 µm, (M-O) 20 µm.

Second, I analyzed the subcellular localization of QMQ reporter in live tissues by confocal laser scanning microscopy (CLSM). I detected the reporter signals in several tissues, including the root epidermis of 6-days-old seedlings and stage 13 floral organs (Figure 13) (floral stages according to previously reported (Smyth et al., 1990)). As showed in Figure 13A-C, a spotty PD-related pattern along the cell periphery and a

faint ER-like signal in the root epidermis of seedlings was observed. In addition, a similar pattern, though with a somewhat less prominent ER-like and PD-related signal, was observed in the epidermis of mature sepals, petals, and carpels (Figure 13D-L).

Finally, I performed a co-localization experiment to identify whether QKY was localized on ER. As a control, I stained lateral root cap cells of 6-days-old seedlings expressing Q4, a well-established marker for the ER (Cutler and Ehrhardt, 2002; Cutler et al., 2000), with the PM marker FM4-64 for 5 minutes, and investigated the subcellular distribution of Q4 and FM4-64-derived signals. Very little if any overlap between two signals in these cells have been detected (Figure 13M-P). Then using 6-days-old Q4 and QMQ lines crossed F1 seedlings, I analyzed the subcellular distribution of the two reporters in the same cells. As Figure 13Q-T shows, QMQ localization in lateral root cap cells exhibited a prominent ER-like pattern, and I could readily observe co-localization of Q4 and QMQ signals in these cells. The results indicated that QKY localizes to the ER and PD in *Arabidopsis* cells.

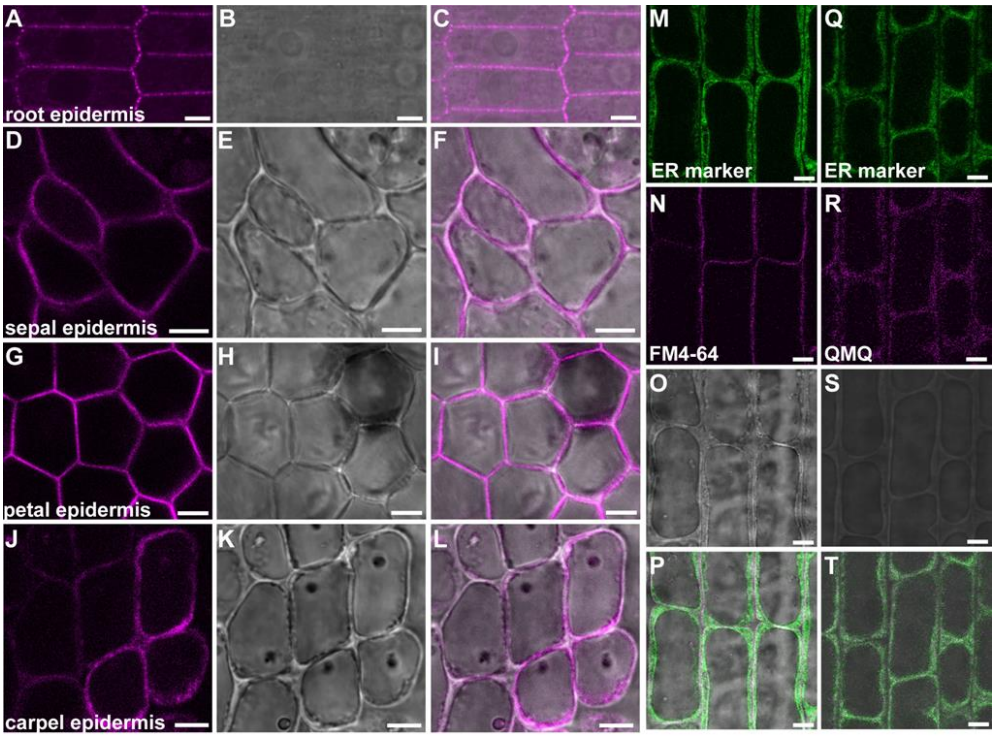

Figure13 Subcellular localization of the pQKY::mCherry:QKY reporter in different tissues of *qky-9*.

(A-C) Confocal micrographs of 6-days-old seedling roots. (A) The mCherry signal in root epidermis. (B) The micrograph of differential interference contrast (DIC) channel. (C) Merge of mCherry signal (A) with DIC channel (B). (D-L) Confocal micrographs of different part of floral organs at stage 13. (D-F) Micrographs in sepal epidermis. (G-I) Micrographs in petal epidermis. (J-L) Micrographs in carpel epidermis. (M-P) Confocal micrograph of ER-resident Q4 and the PM-stained FM4-64. (M) The GFP signal in lateral root cap cells of Q4. (N) The PM-stained FM4-64 signal. (O) The DIC channel. (P) Merge of micrograph (M), (N) and (O). (Q-T) Colocalization of Q4 and mCherry:QKY signal. (Q) Micrograph of GFP signal in lateral root cap cells of Q4. (R) Micrograph of mCherry:QKY signal. (S) Channel of DIC. (T) Merge of (Q), (R) and (S). Abbreviations: QMQ, pQKY::mCherry:QKYqky-9. Scale bars: 5 μm.

3.1.3 QKY undergoes SUB-independent homo-oligomerization

Maize MCTP CPD33 was reported to form homodimers in bimolecular fluorescence complementation (BiFC) assays in tobacco leaf cells (Tran et al., 2019). However, it was not known whether plant MCTP family members form homo-multimers in their native environment. Therefore, I investigated whether QKY forms homo-multimers. To this end, I first performed a yeast two-hybrid (Y2H) experiment in which the region

spanning the C2A to C2D domains (C2A-D) served as bait and prey. I observed yeast growth on the selective medium, indicating that this region can interact with itself (Figure 14). In addition, I generated a series of deletions within the C2A-D domain and tested their ability to interact with the C2A-D domain. The results showed that the C2A-B domain is necessary for interaction of QKY itself in yeast (Figure 14).

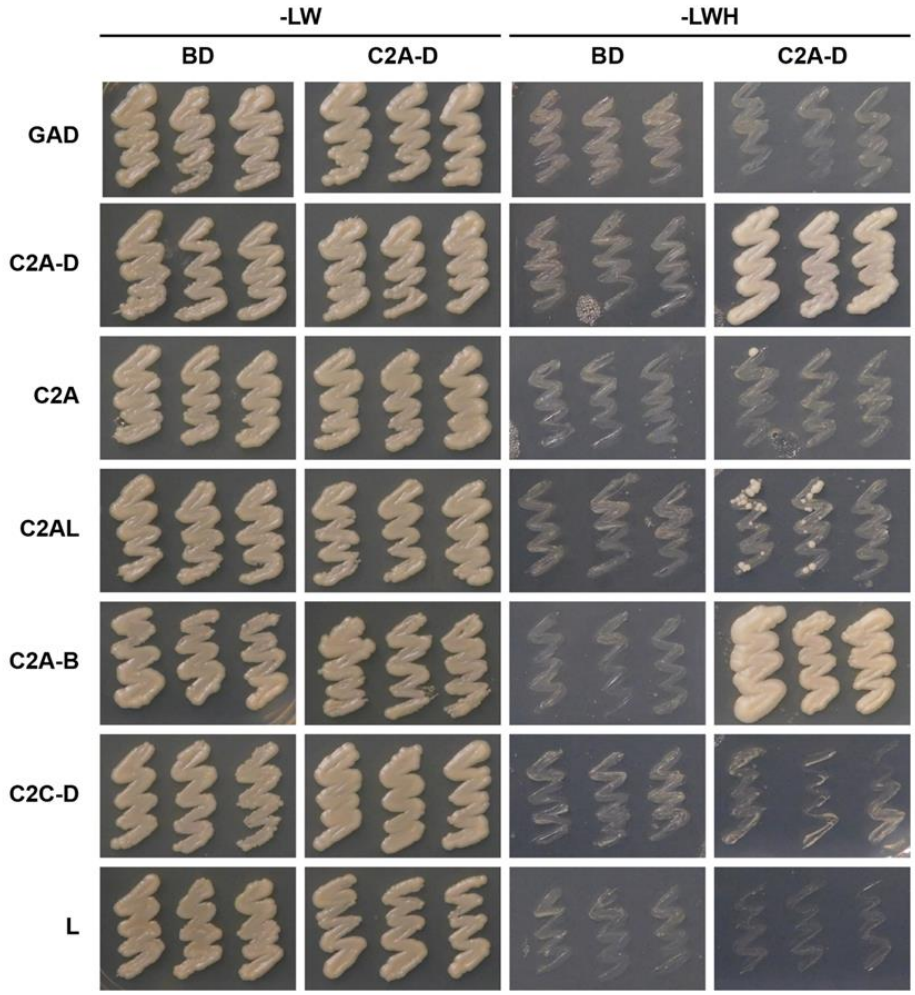

Figure 14 QKY homo-dimerizes in a yeast two-hybrid assay.

Yeast two-hybrid assay involving the QKY C2A-D domain or various deletions fused to the GAL4 activating domain (GAD) and QKY C2A-D domain fused to the GAL4 DNA-binding domain (GBD). Growth on -LW panel indicates successful transformation of both plasmids and on -LWH panel indicates presence or absence of interaction. Results from three independent transformation events are shown. The experiment was repeated twice with identical results.

Furthermore, using steady-state Förster resonance energy transfer (FRET)/fluorescence lifetime imaging microscopy (FRET/FLIM), I tested for interaction of QKY itself in root epidermal cells of 5-days-old seedlings expressing functional pUBQ10::EGFP:QKY (UEQ) or UEQ and pUBQ::mCherry:QKY (UMQ) reporters. For this analysis, I distinguished between the transverse PM, the longitudinal PM and the PD located along the longitudinal PM, since I observed stronger signals along the longitudinal cell periphery of QKY expressing cells (Figure 22). The results showed that the mean fluorescence lifetime of UEQ was significantly reduced when UMQ was present, indicating that UEQ forms homo-oligomers in *Arabidopsis* cells (Figure 15A). As a negative control, I used a line co-expressing the PM-localized p35S::Lti6a:GFP (Lti6a:GFP) (Cutler et al., 2000) and p2x35S::Lti6b:2xmCherry (Lti6a:2xmCherry) (Noack et al., 2022) reporters. I never observed significant mean fluorescence lifetime reductions for Lti6a:GFP in the prescence of Lti6b:2xmCherry (Figure 15B).

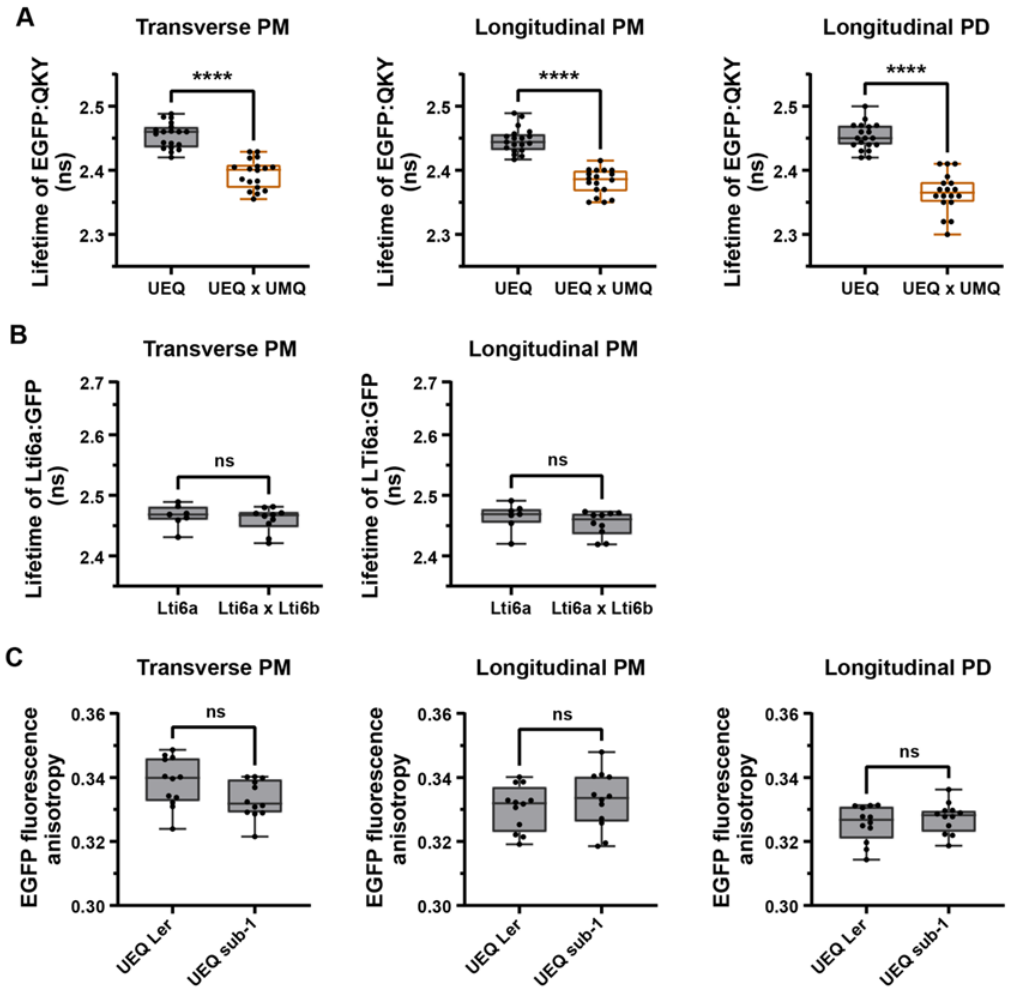

Figure 15 QKY undergoes SUB-independent homo-oligomerization in vivo.

(A) FRET-FLIM analysis in stably transgenic plants harboring EGFP:QKY or EGFP:QKY combined with mCherry:QKY at the transverse PM, longitudinal PM and longitudinal PD, respectively. Experiments were in Ler background. 18≤n≤19, each data point represents a mean of at least five cells per root. ****P<0.0001. Unpaired t test, two-tailed P-values. (B) Quantification of the Lti6a:GFP fluorescence lifetime in stably transgenic Lti6a:GFP and Lti6a:GFP/Lti6b:2xmCherry plants at the transverse and longitudinal PM, respectively. 7≤n≤10, each data point represents a mean of at least five cells per root. ns: not significant. Unpaired t test, two-tailed P-values. (C) Analysis of EGFP:QKY fluorescence anisotropy in the indicated genetic backgrounds at the transverse PM, longitudinal PM and longitudinal PD, respectively. 12≤n≤13, each data point represents a mean of at least five cells per root. ns: not significant. Unpaired t test, two-tailed P-values. Experiments were repeated at least two times with similar results. Abbreviations: CW, cell wall; DM, desmotubule; ER, endoplasmic reticulum; Lti6a, p35S::Lti6a:GFP; Lti6b, p2x35S::Lti6b:2xmCherry; PM, plasma membrane; UEQ, pUBQ10::EGFP:QKY; UMQ, pUBQ10::mCherry:QKY.

Since SUB and QKY are functionally related, I also explored whether QKY clustering was dependent on SUB using the steady-state fluorescence anisotropy (FA). FA is an important technique for quantifying homo-FRET, which is used to investigate the clustering of proteins. In general, the value of FA will decrease as homo-FRET occurs. Upon protein homo-oligomerization of GFP-based fusion proteins homo-FRET can occur resulting in a decrease in FA (Bader et al., 2011). I also confirmed this in Figure 16 in which I observed a FA of 0.35 for TMO7-1xGFP and 0.25 for TMO7-3xGFP in the nuclei of *Arabidopsis* root epidermal cells. Then I measured the FA value of UEQ in epidermal root cells of 5-days-old wild-type and *sub-1* seedlings. I did not find any significant differences in wild-type compared with *sub-1* (Figure 15C). Taken together, these results suggested that QKY undergoes SUB-independent homo-oligomerization in vivo and the interaction is mediated by C2A-B domain.

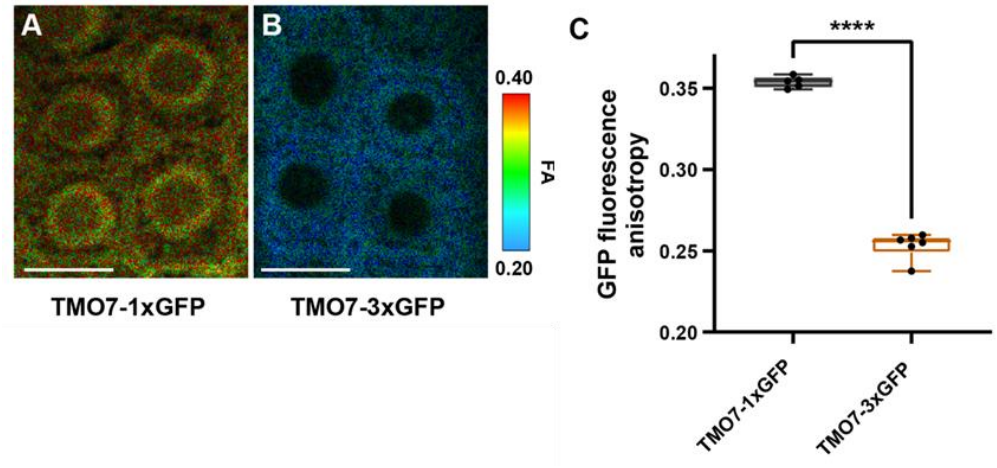

Figure 16 Fluorescence anisotropy of TMO7:1xGFP and TMO7:3xGFP in root epidermal cells.

(A-B) Images of root epidermal cells of 5-days-old seedlings carrying TMO7:1xGFP and TMO7:3xGFP, respectively. Color bar denotes the false color code for SUB:GFP fluorescence anisotropy. (C) Quantification of GFP florescence anisotropy in (A-B). Note the significant reduction of anisotropy in TMO7:3xGFP. 5≤n≤6, each data point represents a mean of at least five cells per root. ****P<0.0001. Unpaired t test, two-tailed P-values. Experiments were repeated at least two times with similar results. Scale bars: 9 μm.

3.1.4 QKY physically interacts with SUB in vivo

A previous study suggested the physical interaction of QKY and SUB at PD (Vaddepalli et al., 2014). To further confirm the interaction I generated novel lines expressing a newly generated translational fusion of SUB to GFP driven by the endogenous SUB promoter (pSUB::SUB:GFP, SSG) and the functional reporter QMQ. Phenotypic observation revealed that SSG reporter is functional as it complements the null allele *sub-1* (Figure 17). Taking advantage of an advanced microscopy set up, I performed FRET-FLIM assays in root epidermal cells of 5-days-old seedlings. As outlined above, the fluorescence lifetime of SSG at the transverse PM, longitudinal PM and longitudinal PD, respectively, was measured. From the results, I observed a significant decrease in the mean fluorescent lifetime of SSG in presence of QMQ (Figure 18). Interestingly, the lifetime of SSG in longitudinal PM showed more significantly reduced compared to the lifetime in transverse PM, revealing the subcellular polarity in SUB/QKY interaction. This is consistent with the observed polar distribution of signal intensity of SSG and QMQ. There was not significant difference in the reduction of SSG lifetime between longitudinal PM and longitudinal PD (Figure 18). As a negative control, I used a line co-expressing SSG and the Lti6b:2xmCherry reporter. The result showed there was not any significant reduction of SSG lifetime in presence of Lti6b:2xmCherry (Figure 18). Taken together, these results suggested that QKY and SUB preferentially interact at longitudinal edges of epidermal root cells in *Arabidopsis*.

Figure 17 Functionality of the pSUB::SUB:GFP (SSG) reporter.

Micrographs of stage 13-14 flowers and siliques are shown. The genotypes are indicated. Note the wild-type appearance of SSG sub-1 flowers (compare A with B and C). Scale bars: flowers, 0.5 mm; siliques, 2 mm.

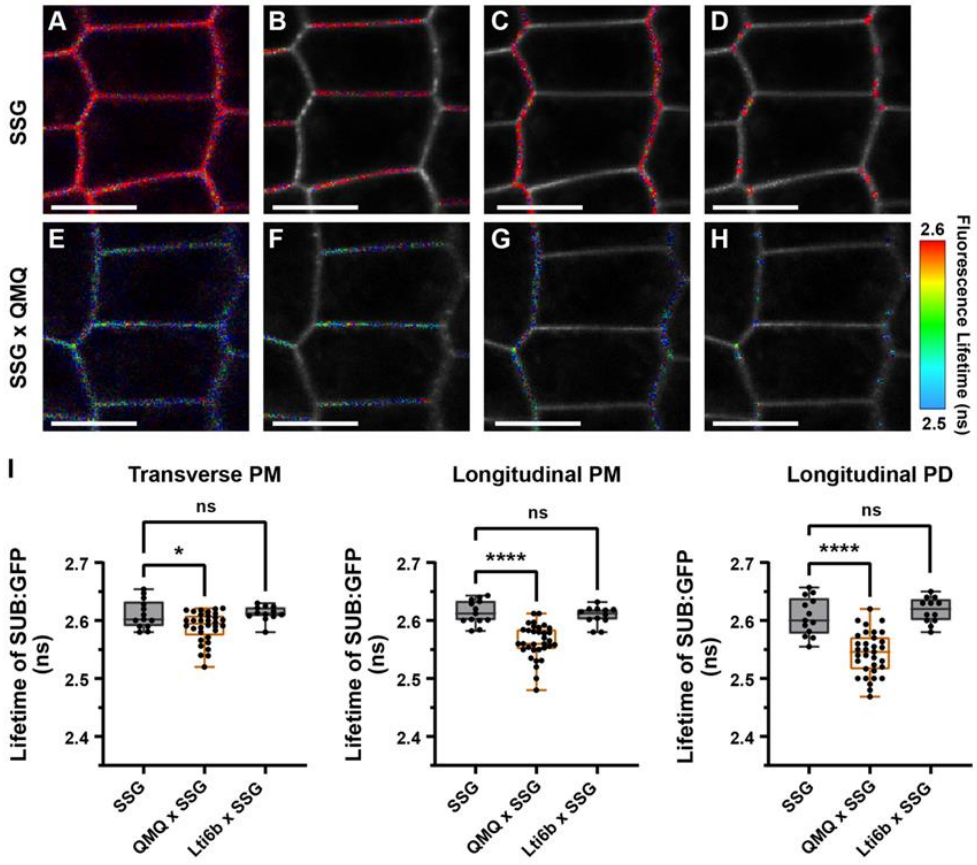

Figure 18 QKY physically interacts with SUB in vivo.

FRET-FLIM analysis in root epidermal cells of 5-days-old seedlings of stably transgenic Arabidopsis plants. (A-D) Fluorescence lifetime images of SSG transgenic plants. (A) Signal collected around the entire circumference of the cells. (B-D) Red areas indicate regions of interest used for signal collection at the transverse and longitudinal PM and at PD located at the longitudinal edges of the cells. (E-H) Fluorescence lifetime images of transgenic plants harboring SSG and QMQ. Color bar denotes the false color code for SSG fluorescence lifetime. (I) Quantification of the SSG fluorescence lifetimes in (A-H) at the transverse and longitudinal PM and the longitudinal PD, respectively. The transgenic plants carrying the SSG, or SSG and QMQ reporters were in the *qky-9* background. Note the more pronounced reduction of SSG lifetime along the longitudinal PM and longitudinal PD compared to the transverse PM. $12 \leq n \leq 33$, each data point represents a mean of at least five cells per root from two independent transgenic lines. *P<0.02, ****P<0.0001, ns: not significant. One-way ANOVA with Tukey's multiple comparison test. Experiments were repeated at least two times with similar results. Abbreviations: Lti6b, p2x35S::Lti6b:2xmCherry; QMQ, pQKY::mCherry:QKY; SSG, pSUB::gSUB:GFP. Scale bars: 8 µm.

3.1.5 The C2A-B domain of QKY is required for interaction with SUB in vivo

To fully understand the topology of QKY and SUB interaction, I further examined which domain of QKY could interact with SUB. First, the previous data from our lab suggested that the linker region (L) separating the C2A and C2B domains of QKY was sufficient for interaction with the intracellular domain (ICD) of SUB in a Y2H assay (Figure 19). In addition, I failed to detect interaction between the C2A-D domain of QKY and the extracellular domain (ECD) of SUB in Y2H assay with multiple independent repetitions (Figure 20).

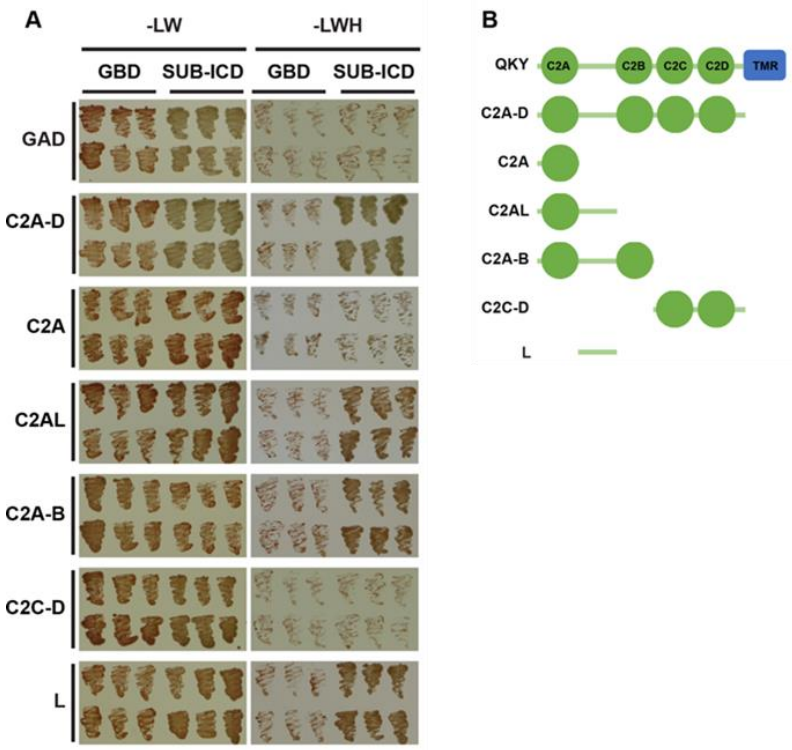

Figure 19 Mapping the SUB interaction region of QKY.

(A) Yeast two-hybrid assay involving different truncated QKY variants fused to the GAL4 activating domain (GAD) and the SUB intracellular domain (SUB-ICD) fused to the GAL4 DNA-binding domain (GBD). Growth on -LW panel indicates successful transformation of both plasmids and on -LWH panel indicates presence or absence of interaction. Data from Prasad Vaddepalli. (B) Cartoon depicting the different truncated QKY variants.

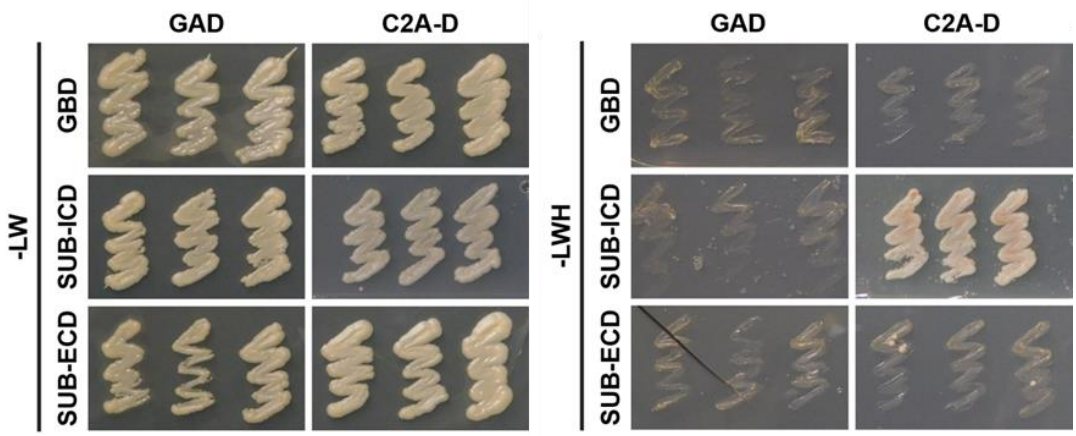

Figure 20 The ECD of SUB does not interact with the C2A-D domain of QKY in a Y2H assay.

The intracellular domain (ICD) of SUB serves as a positive control. Standard conditions (2.5 mM 3-AT) were applied. Yeast growth was stopped after 3 days. Identical results were obtained when stopping yeast growth after 7 days. The experiment was repeated twice with identical results.

In order to test if the C2A-B domain of QKY was also required for physical interaction with SUB in vivo. I generated stable transgenic *qky-9* plants carrying sequential deletions up to and including the C2D domain of QMQ variants (Figure 21A). Next, I analyzed the phenotype of plants and the ovule defects and found all the deletion variants failed to rescue the *qky-9* phenotype (Table 4, Table 5). *QKY* affects the root hair patterning growth and *qky-9* develop root hairs at discordant position in epidermis, I found all the deletion variants also could not rescue the root hair distribution of *qky-9* (Figure 21B-C). Analysis of root epidermal cell patterns in combination with the pGL2::GUS:GFP reporter expressed only in non-hair cells also showed that none of the deletion variants rescued the effect of *qky-9* on root epidermal cell patterns (Figure 21D-E). All these results indicated that all C2 domains are necessary for QKY function.

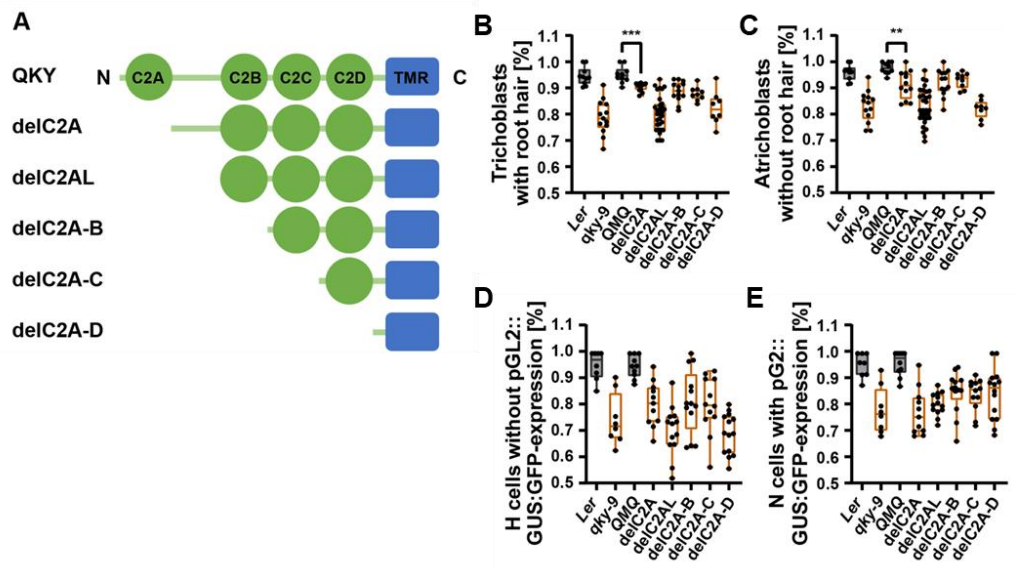

Figure 21 Specification of root epidermal cell types in *qky-9* mutants carrying progressive N-terminal deletions of the C2A-C2D domain.

(A) Cartoon depicting the different QKY mutants carrying progressive N-terminal deletions of the C2A-D domain. (B-C) The percentage of H position hair cells with root hair and that of N position hair cells without root hair in different genotypes, respectively. 8≤n≤31, each data point represents the percentage in per root from two independent lines, which was calculated by at least 15 cells of each cell type. **P<0.01, ***P<0.001. (D-E) The percentage of H position hair cells without expressing the pGL2::GUS:GFP reporter and that of N position hair cells expressing pGL2::GUS:GFP reporter in different genotypes, respectively. 8≤n≤14, each data point represents the percentage in per root from two independent lines, which was calculated by at least 15 cells of each cell type. Black boxes represent no significant differences in the data between Ler and QMQ. Orange boxes represent significant differences in the data of *qky-9* and QKY mutants compared to Ler and QMQ. Unpaired t test, two-tailed P-values. Experiments were repeated at least two times with similar results.

Second, I observed the subcellular localization of QMQ deletion variants in root epidermal cells of 6-days-old seedlings. Interestingly, in the QMQdelC2A or QMQdelC2A-B variants, the stronger PD-related signals along the longitudinal cell periphery of QMQ were not observed (Figure 22A-I). The QMQdelC2A-C and QMQdelC2A-D variants exhibited an ER-like pattern (Figure 22J-O). These results suggest that the C2A-B domain of QKY is involved in the preferential accumulation of QKY along the longitudinal periphery of epidermal root cells. And the C2C-D domain mediates PD localization, that the TMR region is required for anchoring of QKY in the ER.

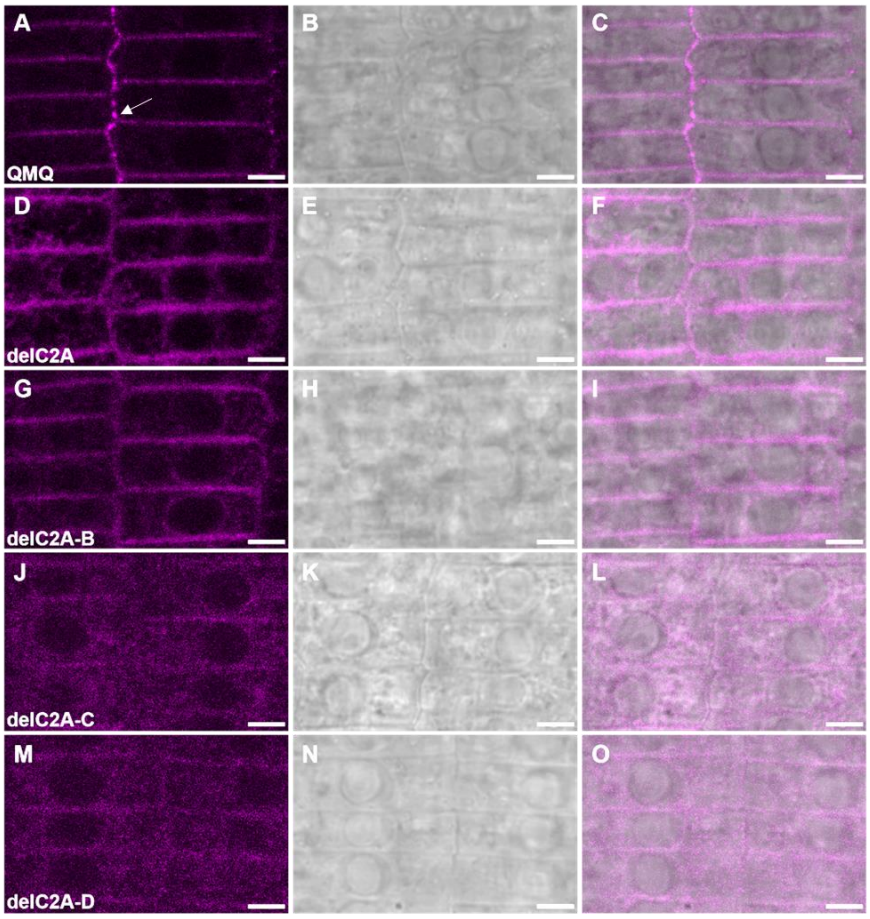

Figure 22 Subcellular localization of different pQKY::mCherry:QKYmut reporters.

Confocal micrographs of root epidermal cells of 6-days-old seedings of pQKY::mCherry:QKY (QMQ) mutant in *qky-9* background. Left panels:mCherry signal. Middle panels: DIC channel. Right panel: merge. (A-C) Note the punctate pattern at the PM in QMQ *qky-9*. (D-I) The punctate pattern was attenuated, but clear PM-like localization is still observable in QMQdelC2A *qky-9* and QMQdelC2A-B *qky-9*. (J-O) Reduced PM-like localization and more diffuse cytoplasmic signal distribution in QMQdelC2A-C *qky-9* and QMQdelC2A-D *qky-9*. Arrow indicate the PD. Scale bars: 5 µm.

Third, I performed the FRET-FLIM experiments in root epidermal cells of 5-days-old seedlings in lines expressing SSG as well as deleted QMQ C2 domain variants. I noticed the SSG mean fluorescence lifetime in QMQdelC2AL and QMQdelC2A-B reporters were not significant different from the level of SSG control in the absence of QMQ (Figure 23). Interestingly, the SSG mean fluorescence lifetime in QMQdelC2A reporter showed a small increase compared to combined with the wild-type QMQ. However, its lifetime was still significantly reduced compared to the SSG control

(Figure 23). The results for the transverse PM, longitudinal PM and longitudinal PD were similar. Taken together, these results indicated that QKY and SUB interact in vivo and that the C2A-B domain of QKY is required for this interaction.

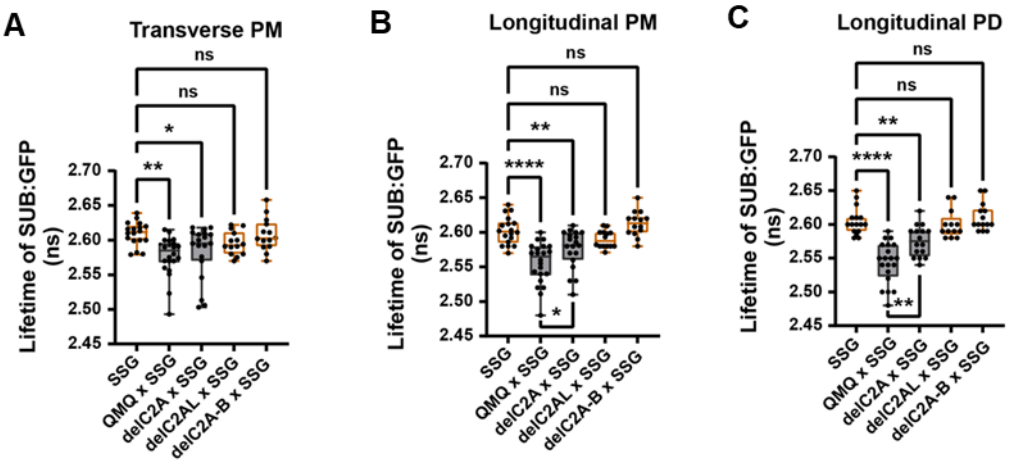

Figure 23 FRET-FLIM detects the interaction of SUB with different regions of QKY.

FRET-FLIM analysis in root epidermal cells of 5-days-old seedlings of stably transgenic Arabidopsis plants carrying SSG combined with different mCherry:QKY variants. All the transgenic plants were in *qky-9* background. 13≤n≤22, each data point represents a mean of at least five cells per root from two independent transgenic lines. *P<0.04, **P<0.01, ****P<0.0001, ns: not significant. One-way ANOVA with Tukey's multiple comparison test. Experiments were repeated at least two times with similar results. Abbreviations: QMQ, pQKY::mCherry:QKY; SSG, pSUB::gSUB:GFP.

3.1.6 Interaction of QKY and SUB is required for SUB stabilization at the PM

Previous studies have reported that QKY-mediated stabilization of SUB at the cell surface counteracts the constitutive endocytosis and degradation of SUB (Gao et al., 2019; Song et al., 2019). However, it still unclear if the physical interaction between QKY and SUB is required for this process. I decided to test whether the C2A-B domain which interact with SUB affect the amount of SUB at the cell surface. To the end, I investigated the effect of the QMQdelC2A, QMQdelC2AL, and QMQdelC2A-B deletion constructs on the level of SSG signal at the PM of root epidermal cells in *qky-9* seedlings. I found that all three constructs were unable to rescue SSG levels (Figure 24). These results suggested that the C2A-B domain is essential for maintain the high

levels SUB at cell surface which required for plant morphogenesis. They also indicated that this process requires the interaction of QKY and SUB.

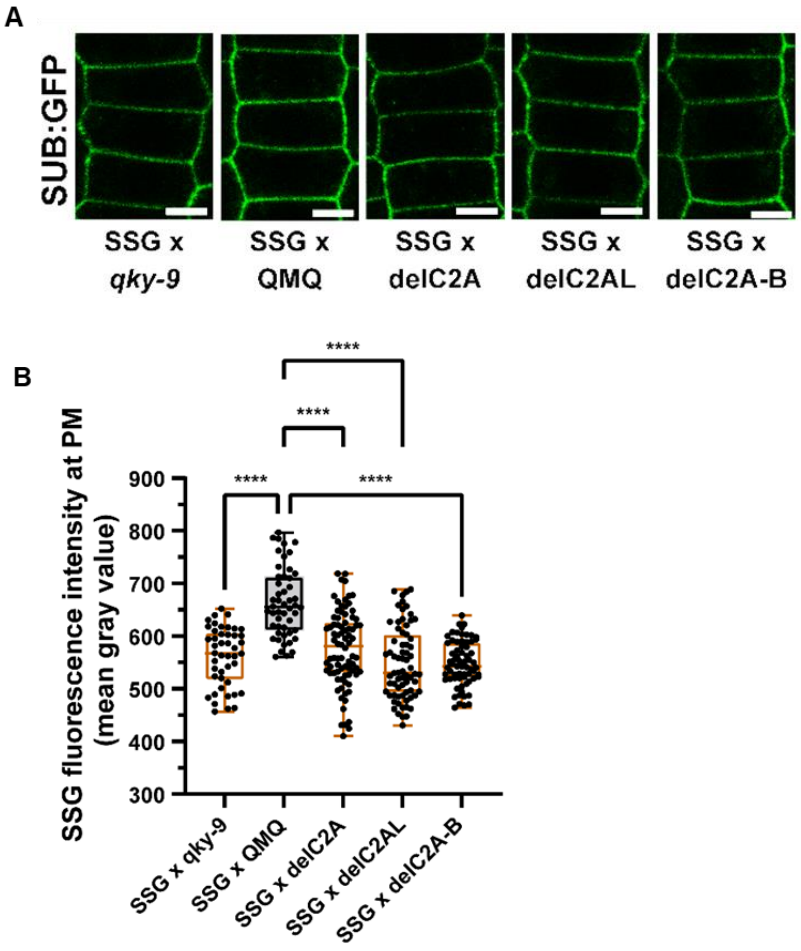

Figure 24 The accumulation of SUB:GFP in QKY mutants.

(A) Confocal micrographs depicting SUB:GFP signal intensity at the PM in root epidermal cells of 6-days-old seedlings of transgenic plants carrying combinations of SSG with different mutant mCherry:QKY variants. All the transgenic plants were in *qky-9* background. (B) Quantification of the data in (A). 31≤n≤70, each data point represents a mean gray value of PM in one cell across 15 different roots from two independent lines. ****P<0.0001. One-way ANOVA with Tukey's multiple comparison test. Experiments were repeated at least two times with similar results. Abbreviation: SSG, pSUB::gSUB:GFP. Scale bars: 5 μm.

3.1.7 SUB undergoes QKY-dependent homo-oligomerization

There is evidence that plant RKs such as BRI1 can form homo-oligomers (Wang et al., 2015a; Russinova et al., 2004). One way QKY could affect the architecture of SUB

complexes at the cell surface is by controlling the clustering of SUB. Therefore, I investigated whether SUB undergoes homo-oligomerization. First I performed Y2H experiments with the ECD or ICD of SUB served as a prey and bait. I could not observe a robust yeast growth on the standard selective medium with 2.5 mM 3-AT when ICD served as bait and prey. Only the weak and variable yeast colonies grown in presence of 1.25 mM 3-AT (Figure 25). In the other hand, a robust yeast growth was observed on the selective medium when the ECD was present as bait and prey (Figure 26A). The results demonstrated that the ECD of SUB can interact with itself in this assay. Second, I performed the FRET-FLIM experiments in the root epidermal cells of 5-days-old seedlings expressing SSE or SSE and pUBQ10::SUB:mCherry (USM) reporters to test the interaction in vivo. Compared to SSE control, the mean fluorescence lifetime of SSE in the presence of USM showed a significant reduction, indicating that SUB forms homo-oligomers in vivo (Figure 26B).

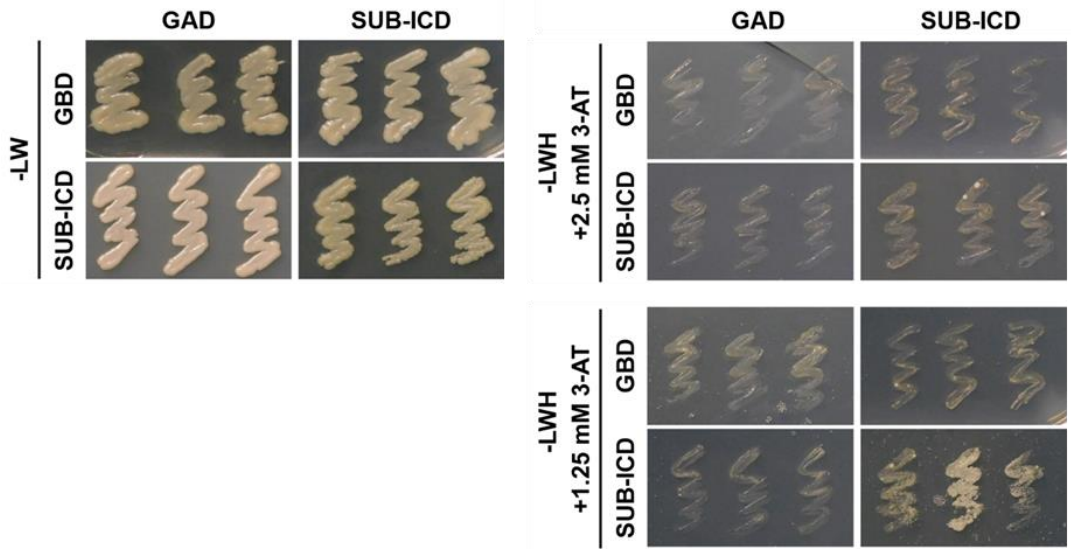

Figure 25 The intracellular domain (ICD) of SUB does not robustly interact with itself in a Y2H assay.

Either standard conditions (2.5 mM 3-AT) or conditions with reduced stringency (1.25 mM 3-AT) were applied. Note the weak and variable growth of yeast colonies carrying BD-ICD and AD-ICD grown in the presence of 1.25 mM 3-AT. First colonies were detected after 5 days. Yeast growth was stopped after 7 days. The experiment was repeated twice with identical results.

In the end, I tested if SUB clustering depended on QKY. For this, I measured the FA value of SSE in root epidermal cells of 5-days wild-type and *qky-9* seedlings. Compared to wild-type, a significant increase of the SSE FA value in *qky-9* was observed (Figure 26C). I also tested the FA values of SSE in wild-type and *sub-1*, and found a modest but statistically nonsignificant increase in *sub-1*, compared to wild-type. This indicated that the SUB concentration at PM has a small, if any, effect on SUB oligomerization (Figure 26C). Furthermore, in order to confirm the effect of QKY on SUB clustering, I measured the FA values of SSG in *qky-9* or SSG in QMQ *qky-9*. I found a significant decrease in the FA value of SSG when QMQ was present (Figure 26D-L). These results suggested that QKY promotes SUB clustering.

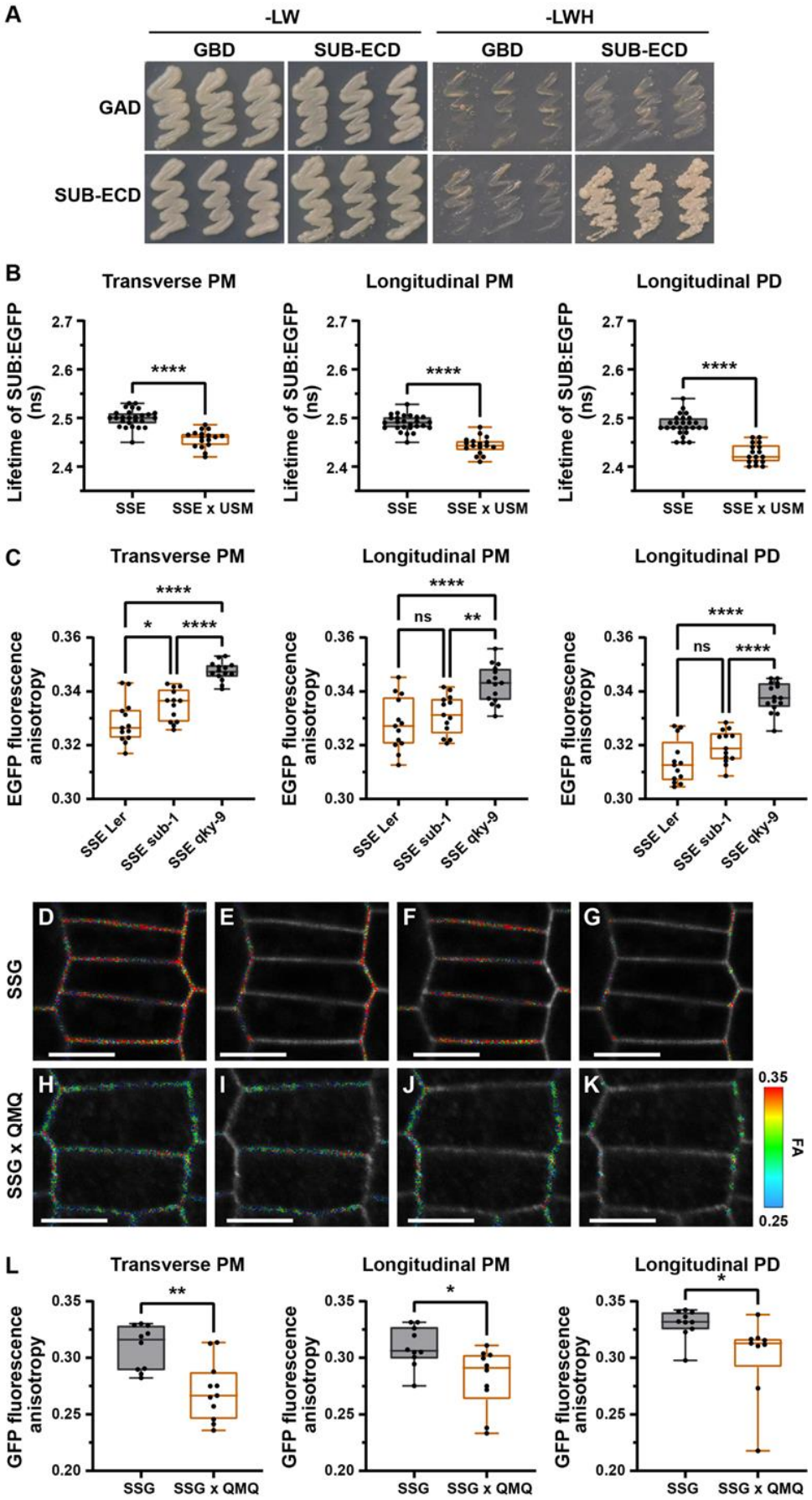
A
-LW
-LWH
GBD
SUB-ECD
GBD
SUB-ECD
GAD
SUB-ECD
B
Transverse PM
Longitudinal PM
Longitudinal PD
Lifetime of SUB:EGFP (ns)
2.7
2.6
2.5
2.4
****
SSE
SSE x USM
C
Transverse PM
Longitudinal PM
Longitudinal PD
EGFP fluorescence anisotropy
0.36
0.34
0.32
0.30
****
*
ns
**
SSE Ler
SSE sub-1
SSE qky-9
D
E
F
G
SSG
H
I
J
K
SSG x QMQ
0.35
FA
0.25
L
Transverse PM
Longitudinal PM
Longitudinal PD
GFP fluorescence anisotropy
0.35
0.30
0.25
0.20
**
*
SSG
SSG x QMQ

Figure 26 SUB undergoes QKY-dependent homo-oligomerization.

(A) Yeast two-hybrid assay involving SUB extracellular domain (SUB-ECD) fused to the GAL4 activating domain (GAD) and SUB-ECD fused to the GAL4 DNA-binding domain (GBD). Growth on -LW panel indicates successful transformation of both plasmids and on -LWH panel indicates presence or absence of interaction. (B) FRET-FLIM analysis in root epidermal cells of 5-days-old seedlings of stably transgenic plants carrying SSE or SSE and USM reporters at the transverse PM, longitudinal PM and longitudinal PD, respectively. $17 \leq n \leq 26$, each data point represents a mean of at least five cells per root. ****$P<0.0001$. Unpaired t test, two-tailed P-values. (C) Quantitative analysis of SUB:EGFP fluorescence anisotropy at the transverse PM, longitudinal PM and longitudinal PD, respectively, in the indicated genetic backgrounds. $10 \leq n \leq 16$, each data point represents a mean of at least five cells per root. *$P<0.03$, **$P<0.01$, ****$P<0.0001$, ns: not significant. One-way ANOVA with Tukey's multiple comparison test. (D-L) Fluorescence anisotropy analysis in root epidermal cells of 5-days-old seedlings. (D-G) Images of transgenic plants carrying SSG. Red areas indicate regions of interest used for signal collection at the transverse and longitudinal PM and at PD located at the longitudinal edges of the cells. (H-K) Images of transgenic plants carrying SSG and QMQ reporters. (L) Analysis of SUB:GFP fluorescence anisotropy (FA) in stably transformed qky-9 plants harboring SSG or SSG combined with QMQ reporters, respectively. SSG fluorescence anisotropy values were assessed at the transverse PM, longitudinal PM and longitudinal PD, respectively. The lower FA values of SSG in qky-9 compared with SSE in qky-9 are explained by weaker expression of the hemizygous SSG reporter (see Materials and Methods). $9 \leq n \leq 11$, each data point represents a mean of at least five cells per root from two independent lines. *$P<0.03$, **$P<0.01$. Unpaired t test, two-tailed P-values. Experiments were repeated at least two times with similar results. Abbreviations: QMQ, pQKY::mCherry:QKY; SSE, pSUB::gSUB:EGFP; SSG, pSUB::gSUB:GFP; USM, pUBQ10::gSUB:mCherry. Scale bars: 7 μm.

3.2 Functional analysis of QKY phosphorylation in vivo

Protein phosphorylation is one of the most common posttranslational modifications (PTMs), acting as an important modulator of intracellular biological processes. It is transient PTM that enables the cell to change the conformation, activity, and interaction of target proteins within a very short timeframe, and is also a reversible modification with complex interplay between specific protein kinases and protein phosphatases, which strict control the temporal and spatial over the phosphorylation and dephosphorylation of target proteins at specific sites (Graves and Krebs, 1999; Li and Liu, 2021). Protein phosphorylation in plants predominantly occurs on serine (Ser, S),

threonine (Thr, T), or tyrosine (Tyr, Y) residues. Protein kinases catalyze the transfer of a phosphoryl group from ATP to the hydroxyl groups of these specific amino acid in the target proteins. Meta-analysis of large-scale phosphoproteomic data revealed that Ser is the most frequently (80-85%) phosphorylated residue in plants (van Wijk et al., 2014).

Phosphorylation events contribute to protein activation, and antagonistic mechanisms often ensure responsiveness to quickly changing conditions by a balanced protein activity. For example, brassinosteroid insensitive 1-associated kinase 1 (BAK1), can directly phosphorylate receptor-like cytoplasmic kinases (RLCK) Botrytis-induced kinase 1 (BIK1) to positively regulates plant immune responses to bacterial flagellin (Lin et al., 2014). Cold-responsive bHLH protein INDUCER of CBF EXPRESSION1 (ICE1) is cold activated by phosphorylation of OPEN STOMATA1 (OST1) (Ding et al., 2015).

A previous Arabidopsis proteomic study based on mass spectrometry has shown that QKY has three phosphorylation sites (P-sites) in vivo of wild-type plants, Ser218 (S218), Ser262 (S262), Ser1075 (S1075) (Mergner et al., 2020). Since the detection of a phosphorylation event does not directly indicate a functional consequence, I decided to use a genetic approach to systematically analyze the function of QKY phosphorylation in vivo.

3.2.1 QKY is phosphorylated in vivo independently of SUB

It is difficult to study the molecular mechanism of QKY phosphorylation in vivo because proving phosphorylation by kinases requires prior knowledge of the concrete interacting protein kinase, but so far only the RK SUB is know to interact with QKY. Therefore, I first decided to test whether the phosphorylation of QKY depends on SUB. In collaboration with Julia Mergner and Nils Rugen from Bavarian Center for

Biomolecular Mass Spectrometry, we observed four phosphorylation sites of QKY at S218, S262, S305, and S1075 in 10-days-old seedlings of wild-type, *sub-1* and *qky-8* by phosphoproteomic analysis based on immunoprecipitation mass spectrometry (Table 6, Figure 27, Supplemental Figure 1). Quantitative comparison of P-site intensity values showed that these P-sites contained peptides of immunoprecipitated EGFP:QKY expressed in *qky-8* and *sub-1* were not significantly different (Figure 27A), revealing that the phosphorylation of QKY in vivo independently of SUB. Sequence comparison showed that S218, S262, and S305 were located on the linker region between C2A and C2B domains of QKY, while only S1075 was located in TMR region (Figure 27B).

Table 6 Two independent mass spectrometry tests of QKY IP samples.

Sample	AGI code	Phosphosites detected	Number of detected events in the first test	Number of detected events in the second test
UBQ::EGFP:QKY /*qky-8*	QKY (AT1G74720)	S218	0/3	2/3
		S262	3/3	3/3
		S305	2/3	3/3
		S1075	3/3	3/3
UBQ::EGFP:QKY /*sub-1*	QKY (AT1G74720)	S218	0/3	3/3
		S262	3/3	3/3
		S305	1/3	3/3
		S1075	3/3	3/3
UBQ::EGFP:QKY /L*er*	QKY (AT1G74720)	S218	-	3/3
		S262	-	3/3
		S305	-	3/3
		S1075	-	3/3

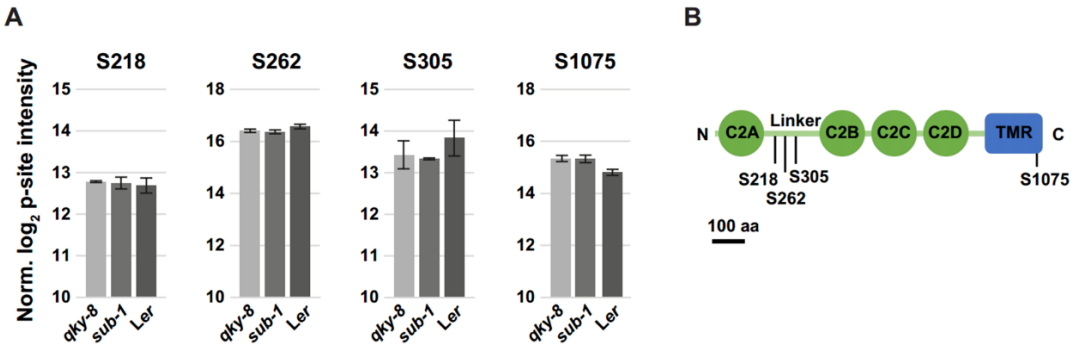

Figure 27 QKY is phosphorylated in a SUB-independent fashion.

(A) Quantitative comparison of QKY phosphorylation sites (P-sites) intensity values for pS218, pS262, pS305, and pS1075 normalized to the total QKY protein intensity for each immunoprecipitation. Bar plots represent the average over three replicates ± standard deviation. EGFP:QKY expressed in *qky-9*, *sub-1*, and L*er* wild-type background. (B) Cartoon depicting the structural features and P-sites of QKY.

3.2.2 Phosphorylation of S1075 is required for efficient PD localization and function of QKY

In order to test the function of these in vivo P-sites, I generated stable transgenic *Arabidopsis* lines expressing non-phosphorylatable (substituting S with A) and phosphomimetic (substituting S with E) variants for these residues with mCherry reporter driven by endogenous promoter (pQKY::mCherry:QKYm/p-site, QMQm/p-site) in the null *qky-9* background and tested for functional complementation by observing floral organ morphogenesis and root hair patterning.

I first focused on the P-site S1075. I analyzed the overview phenotypes of independent T3 homozygous transgenic lines of QMQS1075A and QMQS1075E in *qky-9* background. In particular I scored stem twisting, flower morphology and silique twisting of different lines. The results showed that S1075A transgenic plants could not rescue the phenotype of *qky-9* as wild-type QKY or S1075E transgenic plants (Table 7).

Table 7 Overview phenotype statistics of transgenic lines.

Genotype	Number of different independent T3 homozygous insertion lines		
	Rescue	Partial Rescue	No Rescue
QMQ	15/17 (88.24%)	0/17 (0%)	2/17 (11.76%)
S1075A	3/15 (20%)	3/15 (20%)	9/15 (60%)
S1075E	10/14 (71.43%)	0/14 (0%)	4/14 (28.57%)

As we knew, *qky-9* affects the distribution of root hair in epidermis of seedlings. I also tested the growth of root hair in 6-days-old transgenic plants, and found that S1075A transgenic plants could not rescue the effect of *qky-9* on root hair distribution (Figure 28A-B). Similarly, the analysis of root epidermal cell patterns in combination with pGL2::GUS:GFP reporter which expressed only in non-hair cells also showed that S1075A could not rescue the effect of *qky-9* on root epidermal cell patterns (Figure 28C-D). Each data point in the Figure represents an independent transgenic line. In addition, I also examined the number of wild-type ovules in S1075 mutant lines, and observed that the proportion of wild-type ovules was significantly reduced in S1075A plants compared with wild QMQ or S1075E plants (Figure 28E). These results indicated that phosphorylation of S1075 is required for full QKY activity.

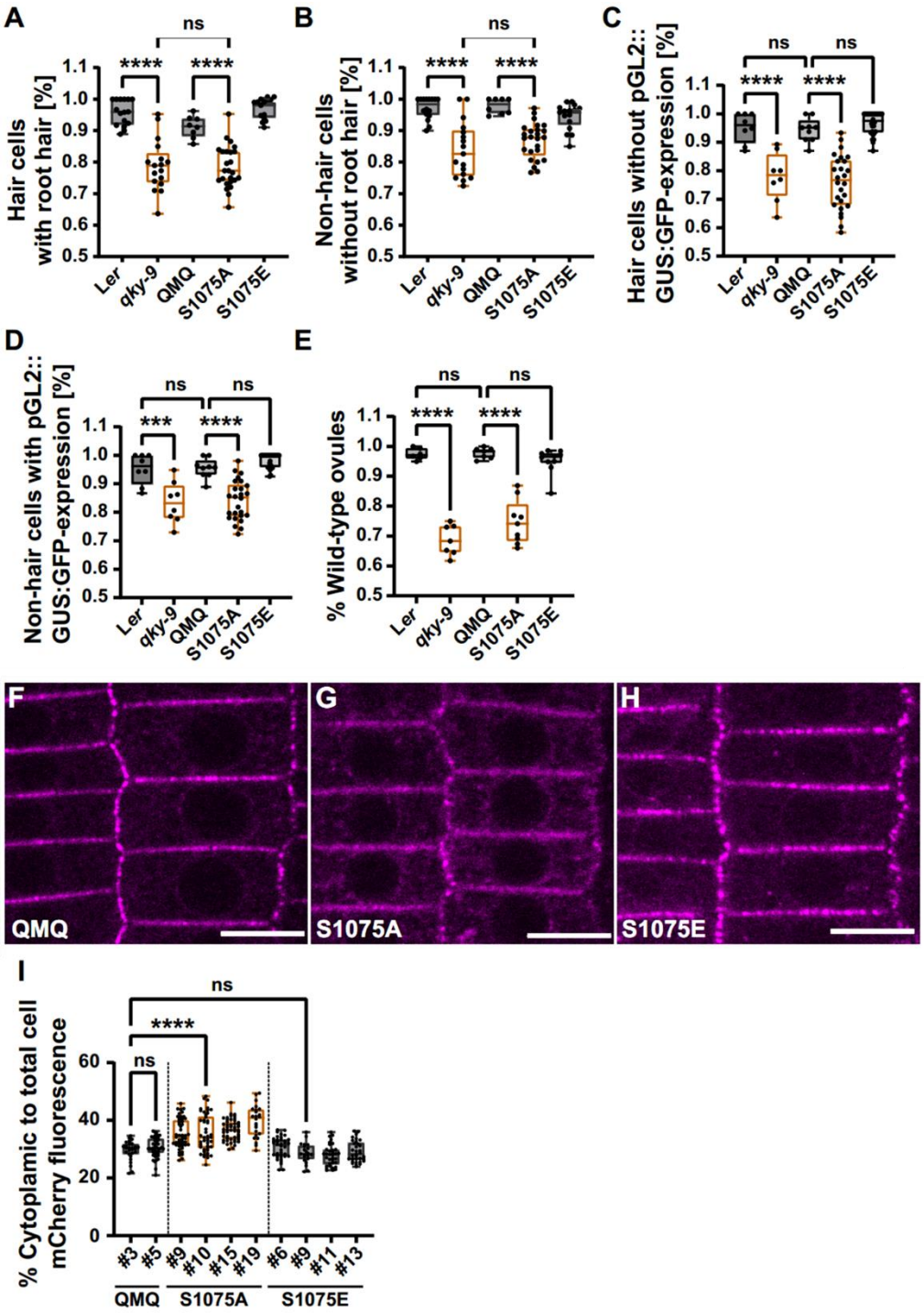

Figure 28 Phosphorylation of S1075 is required for QKY function and controls subcellular localization of QKY.

(A-B) The percentage of H position hair cells with root hair and that of N position hair cells without root hair in independent T3 transgenic lines of each genotype, respectively. $8 \leq n \leq 25$, each data point represents the average percentage of three roots for each independent T3 transgenic lines, which was calculated by at least 15 cells of each cell type in each root. ****P<0.0001, ns: not significant. Unpaired t-test, two-tailed P-values. (C-D) The percentage of H position hair cells without expressing the pGL2::GUS:GFP reporter and that of N position hair cells expressing

pGL2::GUS:GFP reporter in different root combined three independent transgenic lines of each genotype, respectively. 8 ≤ n ≤ 28, each data point represents the percentage in per root from three independent lines, which was calculated by at least 15 cells of each cell type. ***P<0.001, ****P<0.0001, ns: not significant. Unpaired t-test, two-tailed P-values. (E) The proportion of ovules with wild-type appearance in independent T3 transgenic lines of each genotype, respectively. 6 ≤ n ≤ 10, each data point represents the proportion in each independent T3 transgenic lines, which was calculated by 7 to 10 different carpels from at least two different plants in each independent line. ****P<0.0001, ns: not significant. Unpaired t-test, two-tailed P-values. (F-H) Confocal micrographs of root epidermal cells of 6-days-old seedlings of QMQ, QMQS1075A or QMQS1075E transgenic plants. (I) Quantitative analysis of the ratio of mCherry:QKY fluorescence signal intensity in cytoplasm to total cells shown in (F-H). 21 ≤ n ≤ 50 cells from 15 different roots. For each genotype, two independent transgenic lines were quantified, respectively. ****P<0.0001, ns: not significant. Unpaired t-test, two-tailed P-values. All the transgenic plants were in the *qky-9* background. Black boxes represent no significant difference in the data between different transgenic lines of Ler, QMQ and QMQS1075E. Orange boxes represent a significant difference in the data of *qky-9* and QMQS1075A compared to Ler, QMQ or QMQS1075E. Abbreviation: QMQ, pQKY::mCherry:QKY. Scale bars: 10 μm.

Through the analysis of the structural and functional correlation of QKY, we knew that the C2C-D domain of QKY mediates PD localization and that the TMR region is required for QKY anchoring in the ER. I decided to test whether phosphorylation of S1075 was required for QKY localization. I selected four independent S1075 mutant transgenic lines to examine the percentage of mCherry:QKYm in cytoplasmic signal to total cell signal. It was found that compared with the wild QMQ or S1075E, the cytoplasmic signal in S1075A transgenic plants was significantly increased (Figure 28F-I), revealing that the mCherry signal around the cell periphery was decreased in S1075A plants. We hypothesized that S1075 may need to be phosphorylated for the TMR and C2A-D regions of QKY to act together to maintain the proper localization of QKY in PD and ER cortex. Taken together, these data suggested that phosphorylation of S1075 is required for efficient localization and function of QKY.

3.2.3 Phosphorylation of S218 or S262, but not S305, required for QKY-dependent floral organ morphogenesis and specification of hair cell fate

The other three P-sites S218, S262, and S305 are located in the linker between C2A

to C2B domain. Based on previous studies, we knew that the C2A-B domain was required for QKY function and interaction with SUB, so I further examined the function of these three P-sites. Similar, I generated the stable transgenic *qky-9* plants carrying the QMQm/p-site variants and also scored the overview phenotypes specially on stem twisting, flower morphology and silique twisting of different independent T3 lines. The results showed that compared with 60% of S218E and 84% of S262E transgenic lines, only less S218A (33%) and S262A (23%) transgenic lines were counted as wild-type (Table 8). However, there was no significant difference between the phenotypes of S305E and S305A transgenic lines (Table 8).

Table 8 Overview phenotype statistics of transgenic lines.

Genotype	Number of different independent T3 homozygous insertion lines		
	Rescue	Partial Rescue	No Rescue
QMQ	15/17 (88.24%)	0/17 (0%)	2/17 (11.76%)
S218A	4/9 (44.44%)	2/9 (22.22%)	3/9 (33.33%)
S218E	7/10 (70%)	1/10 (10%)	2/10 (20%)
S262A	5/17 (29.41%)	4/17 (23.53%)	8/17 (47.06%)
S262E	11/13 (84.62%)	2/13 (15.38%)	0/13 (0%)
S305A	15/20 (75%)	3/20 (15%)	2/20 (10%)
S305E	14/19 (73.68%)	3/19 (15.79%)	2/19 (10.53%)

In order to count the phenotypes of transgenic lines more objectively, I focused on observing root hair patterns and ovule morphology. To this end, I first observed the growth distribution of root hair in the hair cells and non-hair cells of root epidermis in different independent transgenic lines, and found that neither S218A nor S262A could rescue the defect in hair cell development of *qky-9*, while S305A could rescue it (Figure 29A). Interestingly, all transgenic lines were able to rescue the distribution of non-root hair in non-hair cells in *qky-9* (Figure 29B). Second, the analysis of root epidermal cell patterns in combination with pGL2::GUS:GFP reporter which expressed only in non-hair cells also showed that S305A, but not S218A and S262A, rescued the effect of *qky-9* on root epidermal cell patterns of hair cells (Figure 29C). And all transgenic lines were rescued the effect of *qky-9* on root epidermal cell patterns of non-hair cells (Figure

29D). These results indicated that phosphorylation of S218 or S262, but not S305, is required for QKY-dependent specification of hair cells fate. Third, I also examined the number of wild-type ovules in different transgenic lines, and observed that the proportion of wild-type ovules in S218A and S262A were significantly reduced compared with wild QMQ or S218E, S262E lines, while the proportion of wild-type ovules in S305A and S305E were not significant difference compared with wild QMQ (Figure 29E). Taken together, these results suggested that phosphorylation of S218 or S262, but not S305, is required for QKY-dependent floral organ morphogenesis and specification of root hair cell fate.

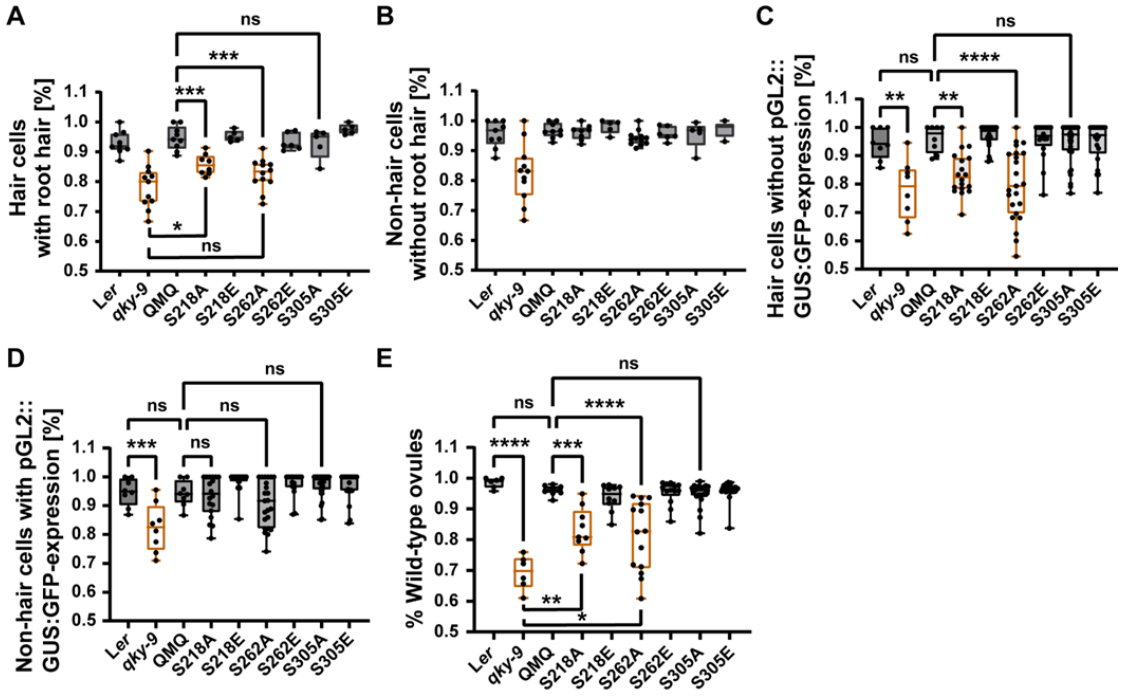

Figure 29 Phosphorylation of S218 and S262 controls QKY function.

(A-B) The percentage of H position hair cells with root hair and that of N position hair cells without root hair in independent T3 transgenic lines of each genotype, respectively. 5≤n≤12, each data point represents the average percentage of five roots for each independent T3 transgenic lines, which was calculated by at least 15 cells of each cell type in each root. *P<0.05, ***P<0.001, ns: no significant. Unpaired t test, two-tailed P-values. (C-D) The percentage of H position hair cells without expressing the pGL2::GUS:GFP reporter and that of N position hair cells expressing pGL2::GUS:GFP reporter in different root combined three independent transgenic lines of each genotype, respectively. 8≤n≤32, each data point represents the percentage in per root from three independent lines, which was calculated by at least 15 cells of each cell type. **P<0.01, ***P<0.001, ****P<0.0001, ns: no significant. Unpaired t test, two-tailed P-values. (E) The proportion of ovules

with wild-type appearance in independent T3 transgenic lines of each genotype, respectively. 6≤n≤20, each data point represents the proportion in each independent T3 transgenic lines, which was calculated by 7 to 10 different carpels from at least two different plants in each independent line. *P<0.05, **P<0.01, ***P<0.001, ****P<0.0001, ns: no significant. Unpaired t test, two-tailed P-values. Black boxes represent no significant difference in the data between Ler, QMQ, and QMQ P-site mutants. Orange boxes represent significant difference in the data of *qky-9* and QMQ P-site mutant compared to Ler or QMQ. Experiments were repeated at least two times with similar results. Abbreviation: QMQ, pQKY::mCherry:QKY.

3.2.4 The expression level of transgenic lines was not correlated with their complementary activities

Furthermore, I also tested whether the phenotypes of different transgenic lines were related to their respective transgenic expression levels. The results of quantitative real-time PCR (qPCR) showed that whether the transgenic plants could rescue the phenotype of *qky-9* was not related to the transcription level of mCherry:QKY in S262 P-site mutant lines (Figure 30A). Fluorescence microscopy imaging also observed similar localization and expression of mCherry:QKY in different transgenic lines (Figure 30B-D).

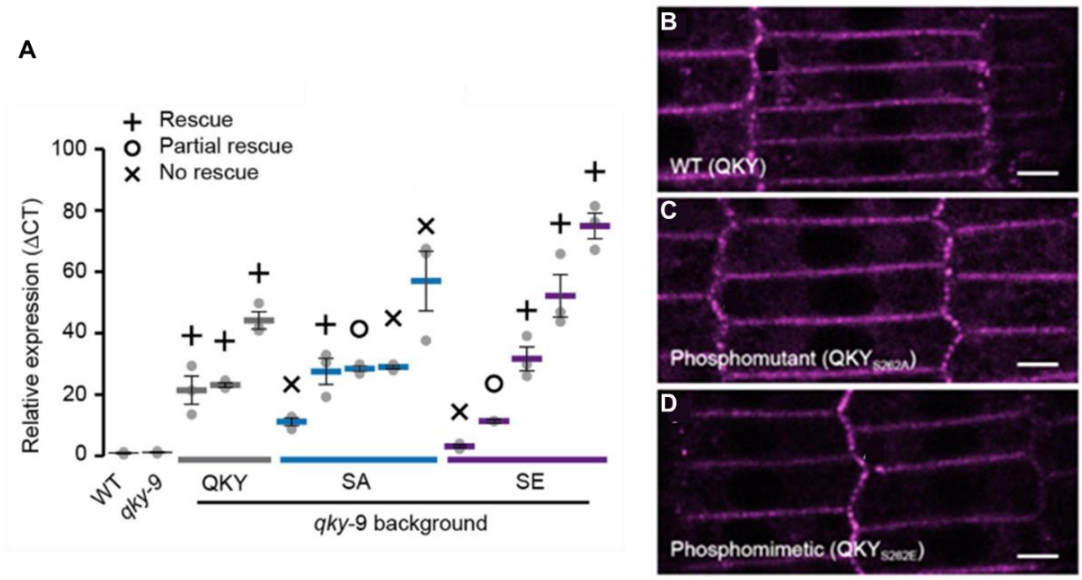

Figure 30 No correlation between transgene expression levels and complementation activity in independent transgenic lines of S262 mutants.

(A) qPCR results (mean ± s.d., n = 3; individual data points as grey dots) show the relative transgene

expression in wild-type, *qky-9* mutant and selected transgenic lines (complete, partial or no rescue lines of S262 phospho-dead mutant (SA), S262 phospho-mimic mutant (SE) and wild-type QKY). (B-D) Representative confocal images of six-day-old transgenic lines in root epidermal cells. Scale bars, 5 μm.

In addition, I also detected the expression level of mCherry:QKY in different QMQ and S218 transgenic plants, and the results showed that the expression level of mCherry:QKY in different lines was not related to whether it could rescue *qky-9* phenotype (Figure 31).

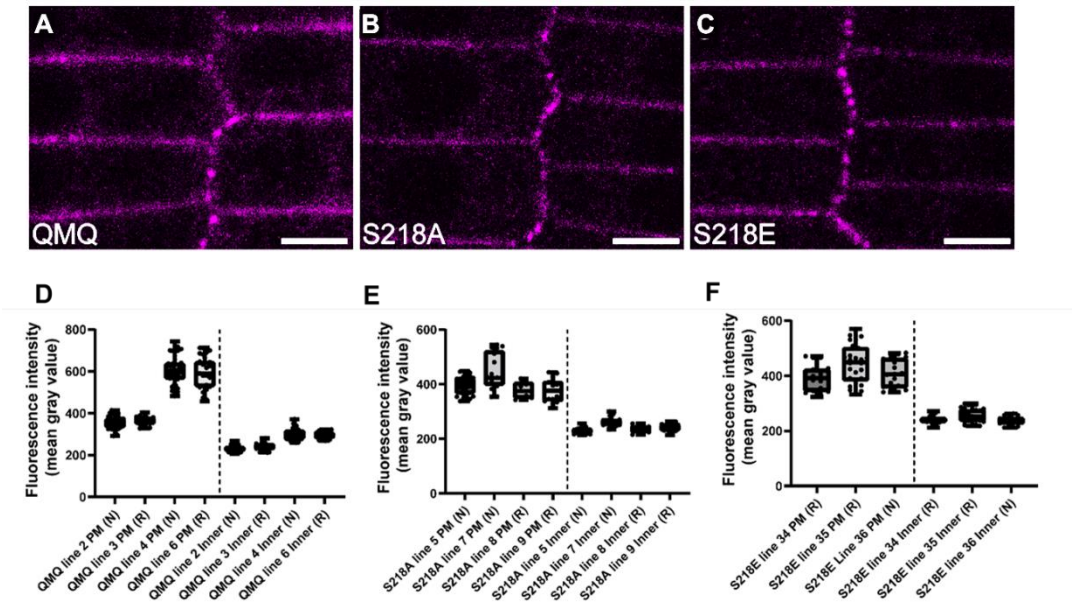

Figure 31 The reduced function of phospho-dead *QKY* constructs does not correlate with their expression levels.

(A-C) Representative confocal images of six-day-old root epidermal cells in transgenic lines of wild-type QKY construct and in S218 phospho-dead or phospho-mimic mutants. Scale bars, 5 μm. (D-F) Quantification of mCherry:QKY fluorescence intensity in different transgenic lines of wild-type QKY or S218 phosphomutants with the phenotype of rescue (R) or no rescue (N) in *qky-9* background.

3.2.5 Phosphorylation of S218 or S262, but not S305, is required for SUB stabilization at the PM

Given that the C2A-B domain is essential for maintain the high levels SUB at cell

surface, it was necessary to examine the role of these P-sites located in the linker region in this process. Using fluorescence confocal microscopy, I monitored the expression level of SUB:GFP on PM in different P-site mutant transgenic plants. The accumulation of SUB:GFP of the PM was significantly decreased in S218A and S262A transgenic plants, compared to the wild-type QMQ transgenic plants (Figure 32). However, the accumulation of SUB:GFP on PM in S305A transgenic plants and different phosphomimetic transgenic lines was not significantly different from that in wild-type QMQ (Figure 32). These results suggested that the phosphorylation of S218 or S262, but not S305, is required for maintaining the high levels of SUB at the PM.

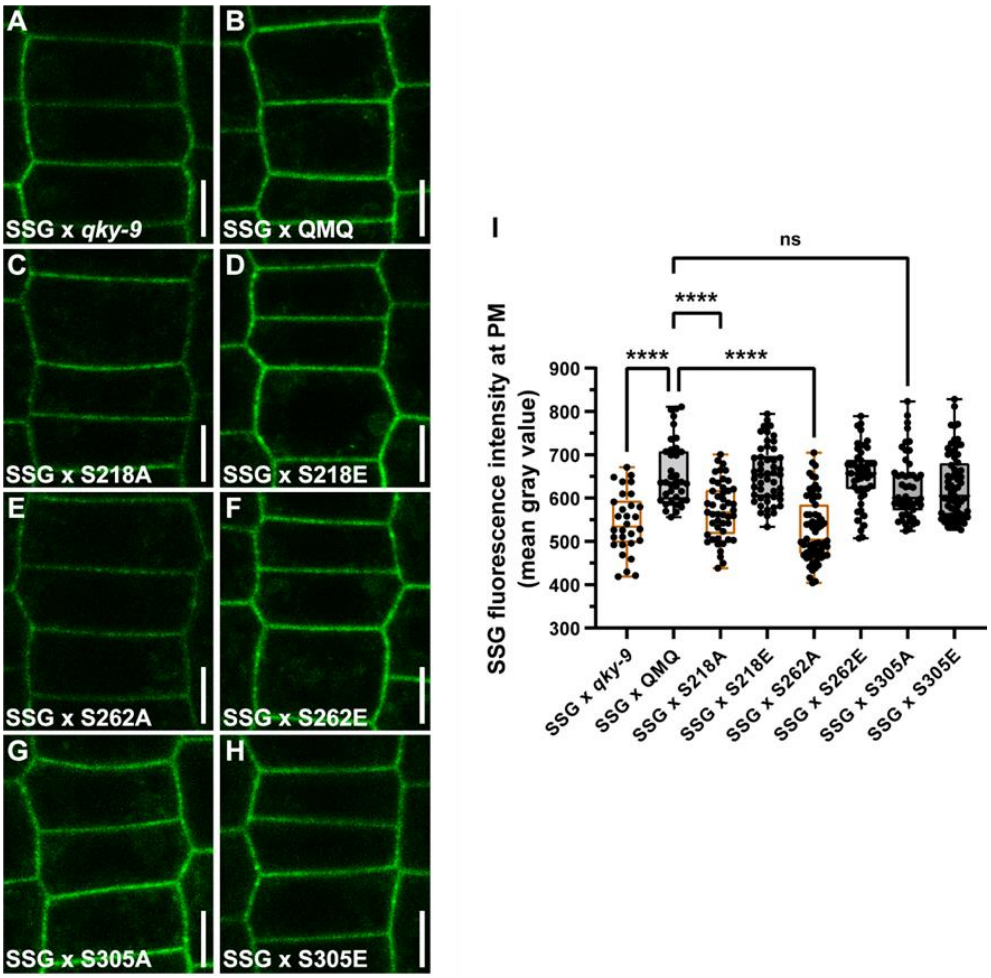

Figure 32 Phosphorylation of S218 and S262 is required for the stabilization of SUB at the PM.

(A-H) Confocal micrographs depicting the SUB:GFP accumulation in root epidermal cells of 6-days-old seedlings of crossed transgenic plants with different QMQ P-site mutants. F1 seedlings

were employed. (I) Quantitative data of the fluorescence intensities in PM from (A-H). 30≤n≤67, each data point represents a mean gray value of PM in one cell across 15 different roots from two independent lines. ****P<0.0001, ns: no significant. Unpaired t test, two-tailed P-values. Black boxes represent no significant difference in the data between SSG x QMQ and SSG x QMQ P-site mutants. Orange boxes represent significant difference in the data of SSG x qky-9 and SSG x QMQ P-site mutants compared to SSG x QMQ. All the transgenic plants were in *qky-9* background. Experiments were repeated at least two times with similar results. Scale bar: 5 μm. Abbreviation: SSG, pSUB::gSUB:GFP; QMQ, pQKY::mCherry:QKY.

3.2.6 Phosphorylation of S218 or S262, but not S305, influences the physical interaction between SUB and QKY in vivo

Since the C2A-B domain is essential for the interaction between QKY and SUB, I also examined the function of these P-sites in it. First, I assessed the effect of phosphorylation on SUB and QKY interactions in the yeast system. I performed a Y2H experiment with C2A-D domain of QKY carrying P-site mutant variants and SUB-ICD served as prey and bait. I observed yeast can growth on all the selective medium with P-site mutant variants and SUB-ICD (Figure 33A). The result suggested that the phosphorylation of P-sites does not affect the interaction between SUB and QKY in yeast.

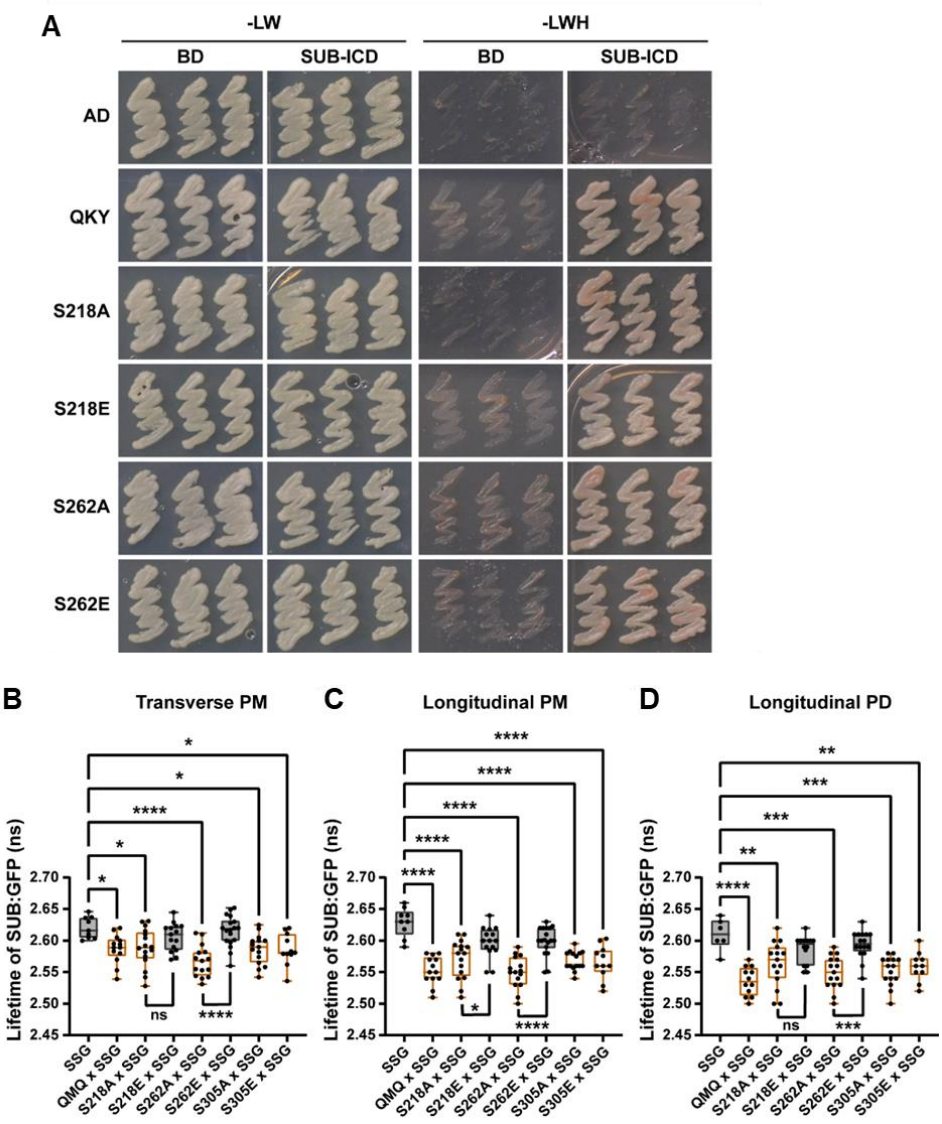

Figure 33 Phosphorylation of S216 or S262 attenuates the physical interaction of QKY and SUB in vivo.

(A) Yeast two-hybrid assay involving different QKY P-site mutants fused to the GAL4 activating domain (GAD) and the SUB intracellular domain (SUB Intra) fused to the GAL4 DNA-binding domain (GBD). Growth on -LW panel indicates successful transformation of both plasmids and on -LWH panel indicates presence or absence of interaction. (B-D) FRET-FLIM analysis in root epidermal cells of 5-days-old seedlings of stably transgenic Arabidopsis plants carrying pSUB::gSUB:GFP combined with different mCherry:QKY P-site mutants. 9≤n≤18, each data point represents a mean of at least five cells per root from two independent transgenic lines. *P<0.05, **P<0.01, ***P<0.001 ****P<0.0001, ns: not significant. Unpaired t test, two-tailed P-values. Black boxes represent no significant difference in the data of SSG x QMQ P-site mutants compared to SSG control. Orange boxes represent significant difference in the data of SSG x QMQ and SSG x QMQ P-site mutants compared to SSG control. All the transgenic plants were in *qky-9* background. Experiments were repeated at least two times with similar results. Abbreviations: QMQ, pQKY::mCherry:QKY; SSG, pSUB::gSUB:GFP.

Second, I examined the effect of phosphorylation on SUB and QKY interaction by FRET-FLIM in vivo. I measured the fluorescence lifetime of SUB:GFP in root epidermal cells of 5-days-old seedlings expressing SSG or SSG and QMQm/p-site variants. Following the previous standard analysis, I distinguished between the transverse PM, the longitudinal PM and longitudinal PD. The results showed that the fluorescence lifetime of SUB:GFP was similar in S218A and S262A while significantly increased in S218E and S262E variants, compared with that in wild-type QMQ (Figure 33B-D), indicating that the interaction between SUB and QKY was attenuated, revealing that the phosphorylation of S218 or S262 attenuates the interaction between SUB and QKY in vivo. Measurements on transverse PM, longitudinal PM and longitudinal PD showed the same results (Figure 33B-D).

3.2.7 Effect of co-phosphorylation of S218 and S262 on QKY function

Since phosphorylation of either S218 or S262 is required for QKY activity, I also examined the role of co-phosphorylation of S218 and S262 in QKY function. I generated stable transgenic *qky-9* plants carrying the QMQS218AS262A or QMQS218ES262E variants and also scored the overview phenotypes of different independent T3 lines. Phenotypic observation showed that both QMQS218AS262A and QMQS218ES262E can rescue the effect of *qky-9* on the morphology of floral, stem, and silique (Table 9). Counts of root hair patterning and ovule morphology also showed that both S218AS262A and S218ES262E can rescue the effect of *qky-9* (Figure 34).

Table 9 Overview phenotype statistics of transgenic lines.

Genotype	Number of different independent T3 homozygous insertion lines		
	Rescue	Partial Rescue	No Rescue
QMQ	15/17 (88.24%)	0/17 (0%)	2/17 (11.76%)
S218AS262A	15/18 (83.33%)	1/18 (5.56%)	2/18 (11.11%)
S218ES262E	11/13 (84.62%)	1/13 (7.69%)	1/13 (7.69%)

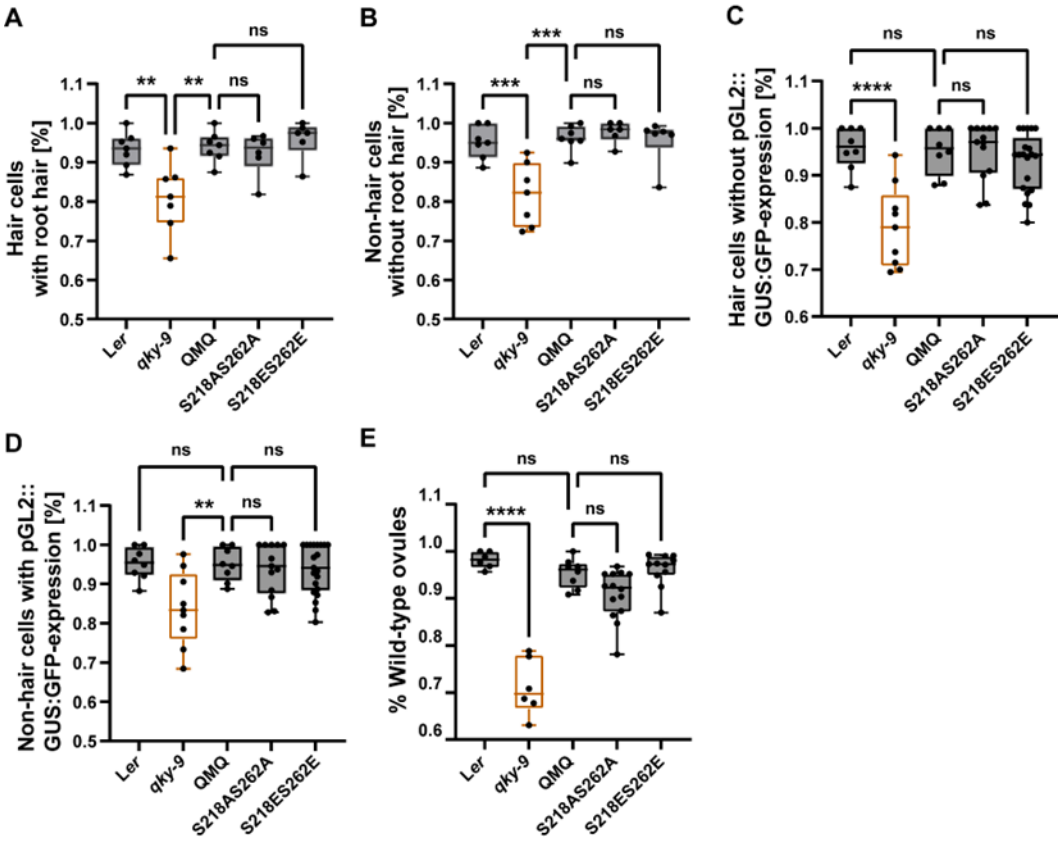

Figure 34 S218AS262A or S218ES262E compensates for QKY function.

(A-B) The percentage of H position hair cells with root hair and that of N position hair cells without root hair in independent T3 transgenic lines of each genotype, respectively. 6≤n≤7, each data point represents the average percentage of five roots for each independent T3 transgenic lines, which was calculated by at least 15 cells of each cell type in each root. **P<0.01, ***P<0.001, ns: no significant. Unpaired t test, two-tailed P-values. (C-D) The percentage of H position hair cells without expressing the pGL2::GUS:GFP reporter and that of N position hair cells expressing pGL2::GUS:GFP reporter in different root combined three independent transgenic lines of each genotype, respectively. 8≤n≤21, each data point represents the percentage in per root from three independent lines, which was calculated by at least 15 cells of each cell type. **P<0.01, ****P<0.0001, ns: no significant. Unpaired t test, two-tailed P-values. (E) The proportion of ovules with wild-type appearance in independent T3 transgenic lines of each genotype, respectively. 6≤n≤14, each data point represents the proportion in each independent T3 transgenic lines, which was calculated by 7 to 10 different carpels from at least two different plants in each independent line. ****P<0.0001, ns: no significant. Unpaired t test, two-tailed P-values. Experiments were repeated at least two times with similar results. All the transgenic plants were in *qky-9* background. Abbreviation: QMQ, pQKY::mCherry:QKY.

In the other hand, I also examined the expression level of SUB:GFP on PM in QMQS218AS262A or QMQS218ES262E transgenic lines to determine the effect of co-phosphorylation of S218 and S262 on SUB. Compared with the SSG control in the absence of mCherry:QKY, the accumulation of SUB:GFP on PM was significantly increased in QMQS218AS262A or QMQS218ES262E transgenic plants (Figure 35). This suggests that localization of SUB on PM is not affected by the co-dephosphorylation of S218 and S262, and perhaps the accumulation of SUB on PM requires the consistency of phosphorylation states of S218 and S262.

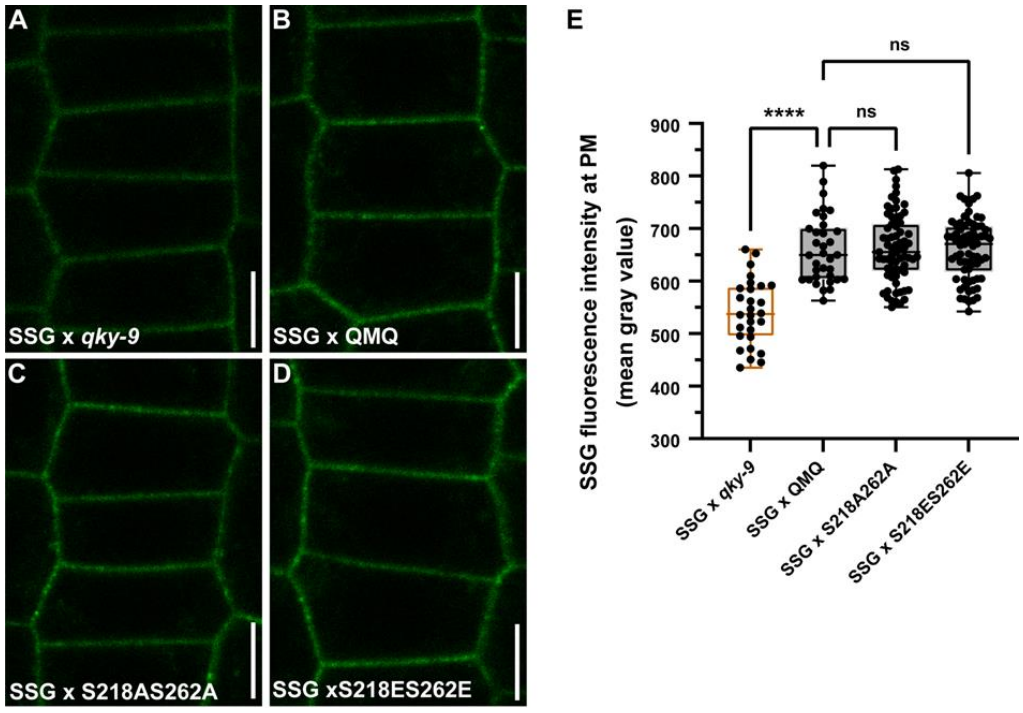

Figure 35 S218AS262A or S218ES262E does not affect the stabilization of SUB at the PM.

(A-D) Confocal micrographs depicting the SUB:GFP accumulation in root epidermal cells of 6-days-old seedlings of crossed transgenic plants with $QMQ_{S218AS262A}$ or $QMQ_{S218ES262E}$ mutants. F1 seedlings were employed. (E) Quantitative data of the fluorescence intensities in PM from (A-D). $28 \leq n \leq 70$, each data point represents a mean gray value of PM in one cell across 15 different roots from two independent lines. ****$P<0.0001$, ns: no significant. Unpaired t test, two-tailed P-values. Black boxes represent no significant difference in the data between SSG x QMQ, SSG x $QMQ_{S218AS262A}$ and SSG x $QMQ_{S218ES262E}$. Orange boxes represent significant difference in the data of SSG x qky-9 compared to SSG x QMQ. All the transgenic plants were in *qky-9* background. Experiments were repeated at least two times with similar results. Scale bar: 5 μm. Abbreviation: SSG, pSUB::gSUB:GFP, QMQ, pQKY::mCherry:QKY.

In the end, I examined the effect of co-phosphorylation of S218 and S262 on the interaction between QKY and SUB. FRET-FLIM results showed that mCherry:QKYS218AS262A and SUB:GFP could still interact with each other in vivo, as indicated by the significantly reduced lifetime of SUB:GFP in QMQS218AS262A transgenic plants compared with SSG control in the absence of mCherry:QKY (Figure 36A-C). However, in QMQS218ES262E transgenic plants, the lifetime of SUB:GFP shows no significant difference compared to SSG control without mCherry:QKY, suggesting that there was no interaction between mCherry:QKYS218ES262E and SUB:GFP in vivo (Figure 36A-C).

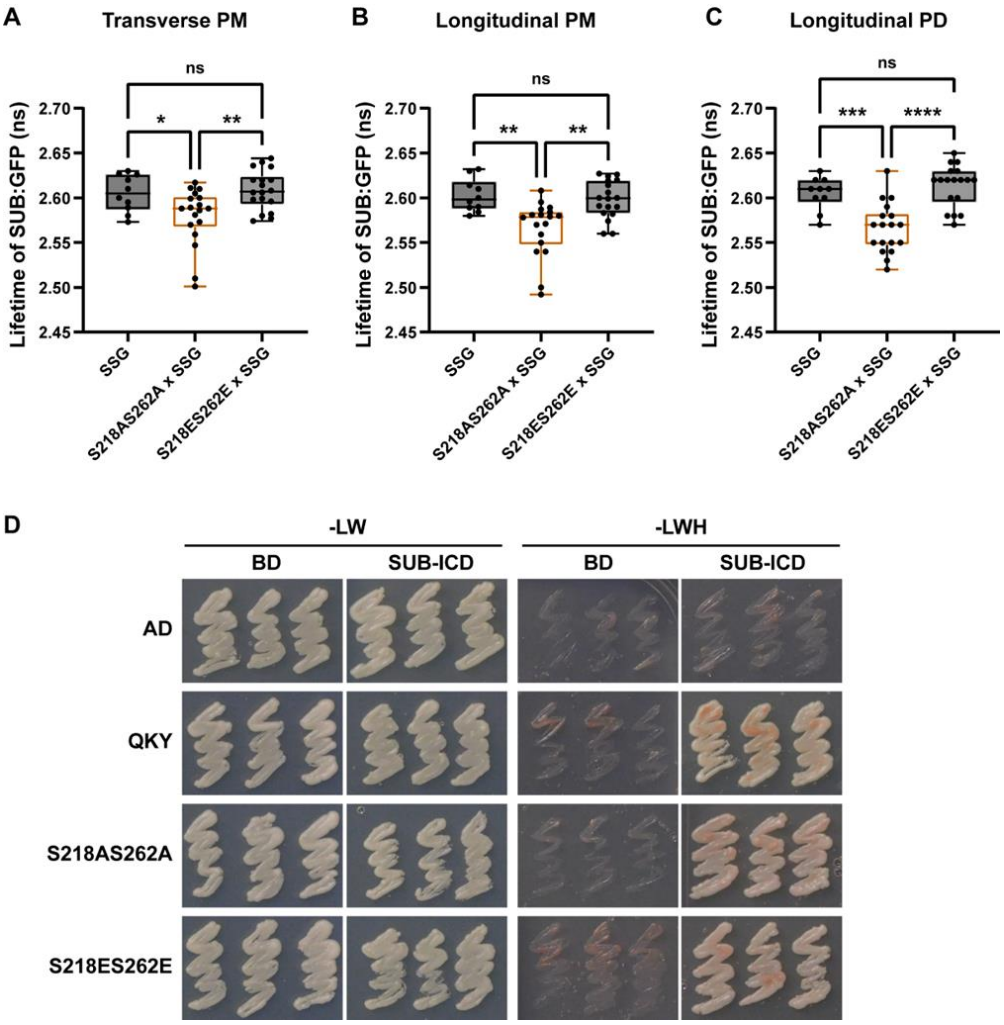

Figure 36 S216ES262E inhibited the physical interaction of QKY and SUB in vivo.

(A-C) FRET-FLIM analysis in root epidermal cells of 5-days-old seedlings of stably transgenic Arabidopsis plants carrying pSUB::gSUB:GFP combined with $QMQ_{S218AS262A}$ or $QMQ_{S218ES262E}$ mutants. $10 \leq n \leq 18$, each data point represents a mean of at least five cells per root from two independent transgenic lines. *P<0.05, **P<0.01, ***P<0.001 ****P<0.0001, ns: not significant. Unpaired t test, two-tailed P-values. Black boxes represent no significant difference in the data of SSG x $QMQ_{S218ES262E}$ compared to SSG control. Orange boxes represent significant difference in the data of SSG x $QMQ_{S218AS262A}$ compared to SSG control. (D) Yeast two-hybrid assay involving $QKY_{S218AS262A}$ or $QKY_{S218ES262E}$ mutants fused to the GAL4 activating domain (GAD) and the SUB intracellular domain (SUB Intra) fused to the GAL4 DNA-binding domain (GBD). Growth on -LW panel indicates successful transformation of both plasmids and on -LWH panel indicates presence or absence of interaction. All the transgenic plants were in *qky-9* background. Experiments were repeated at least two times with similar results. Abbreviations: SSG, pSUB::gSUB:GFP.

Furthermore, the Y2H analysis showed that SUB could interact with both

QKYS218AS262A and QKYS218ES262E in yeast (Figure 36D).

3.3 Role of *QKY* in response to cell wall damage

In previous work, Fourier-transform infrared spectroscopy (FTIR) analysis of cell wall fractions revealed *qky* mutants to be defective in cell wall biochemistry (Vaddepalli et al., 2017). To address if *QKY* plays a role in the seedling responses to cell wall stress, I focused on the possible role of *QKY* in the isoxaben-induced cell wall damage (CWD) response.

3.3.1 *QKY* is not required for isoxaben-induced marker gene induction

I first investigated if *QKY* activity is required for the transcriptional regulation of several marker genes, known to respond to isoxaben-induced CWD within eight hours (Hamann et al., 2009; Van der Does et al., 2017; Engelsdorf et al., 2018). I performed quantitative real-time polymerase chain reaction (qRT-PCR) experiments using RNA isolated from seven days-old liquid-grown seedlings that had been incubated with 600 nM isoxaben for eight hours. I noticed that the transcription of isoxaben-induced genes was not significantly different in *qky-11* compared with Col, indicating that *QKY* did not noticeably effect the transcription levels of the tested marker genes (Figure 37).

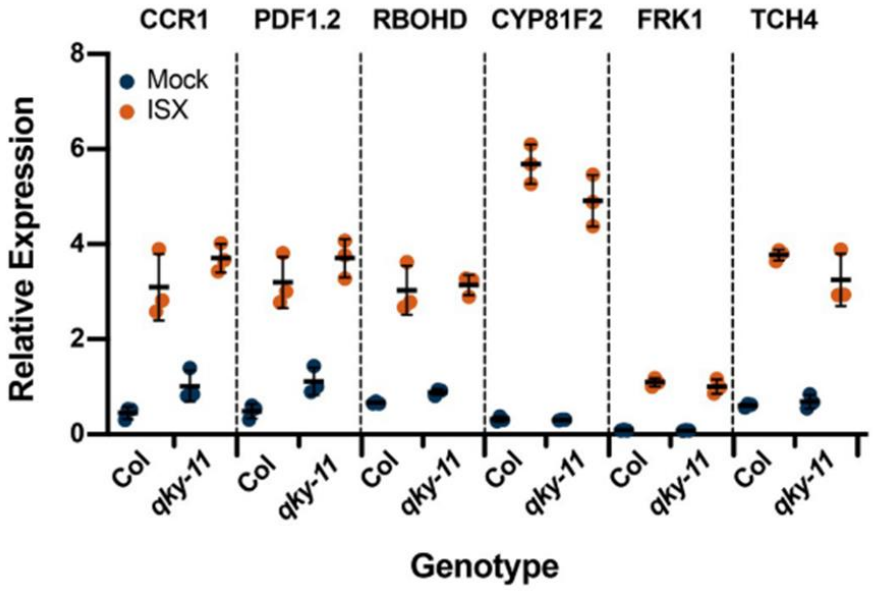

Figure 37 *QKY* is not required for isoxaben-induced marker gene induction.

Gene expression levels of several CBI marker genes by qPCR upon exposure of seven-day-old seedlings to 600 nM isoxaben for eight hours. The results from three biological replicates are shown. Marker genes and genotypes are indicated. Mean ± SD is presented. The experiment was repeated three times with similar results. Abbreviation: ISX, isoxaben.

3.3.2 *QKY* promoted isoxaben-induced ectopic lignin accumulation

Isoxaben-induced cellulose biosynthesis inhibition (CBI) eventually results in the alteration of cell wall biochemistry as evidenced by the ectopic accumulation of lignin and callose (Hamann et al., 2009). To investigate if *QKY* affects lignin biosynthesis, I estimated lignin accumulation in roots of wild-type and *qky* seedlings using phloroglucinol staining after exposing six-days-old liquid-grown seedlings to 600 nM isoxaben for 12 hours. I observed reduced phloroglucinol staining in the root elongation zone of *qky-8* in comparision to wild type L*er*, indicating less ectopic lignin production (Figure 38A-B). I also noticed reduced phloroglucinol signal in *qky-11* seedlings (Col-0 background) although the effect was less prominent.

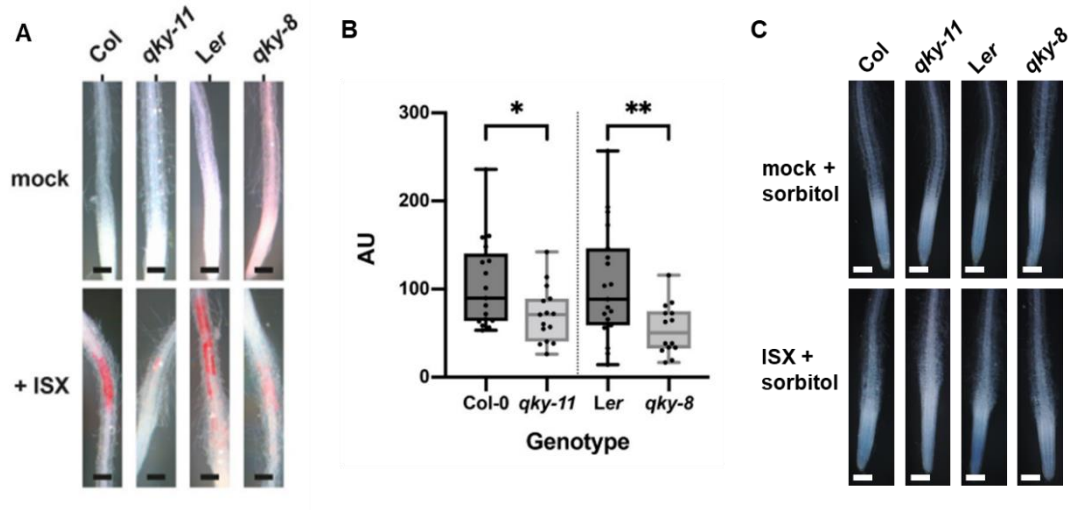

Figure 38 *QKY* affects isoxaben-induced lignin and callose accumulation.

(A) Phloroglucinol signal strength indicating lignin accumulation in roots of six-day-old seedlings exposed to 600 nM isoxaben for 12 hours. (B) Quantification of the results depicted in (A). Genotypes are indicated. $15 \leq n \leq 19$, $^*P < 0.04$, $^{**}P < 0.01$. Unpaired t test, two-tailed P values. (C) Phloroglucinol signal strength indicating lignin accumulation in roots of six-day-old seedlings exposed to mock/300mM sorbitol or to 600 nM isoxaben/300 mM sorbitol for 12 hours. $n \geq 10$. Note absence of detectable signal upon simultaneous application of isoxaben and sorbitol. Genotypes: Col, *qky-11* (Col), Ler, and *qky-8* (Ler). The experiment was performed three times with similar results. Abbreviation: ISX, isoxaben. Scale bars: 0.1 mm.

Furthermore, the isoxaben-induced CWD response is sensitive to turgor pressure, as indicated by the suppression of lignin accumulation in the presence of osmotica, such as sorbitol (Wormit et al., 2012b; Hamann et al., 2009; Engelsdorf et al., 2018). To test if *QKY* affects a turgor-sensitive CBI response, I compared isoxaben-induced accumulation of lignin in six-days-old Col, *qky-11*, Ler, and *qky-8* seedlings in co-treatments with 600 nM isoxaben and 300 mM sorbitol. I noticed that simultaneous application of isoxaben and sorbitol resulted in strongly reduced lignin production in all tested genotypes. I could not observe any phloroglucinol signal in main roots of mock/sorbitol or isoxaben/sorbitol-treated seedlings (Figure 38C). Taken together, these results indicated that *QKY* is required for isoxaben-induced increase in lignin and *QKY* contributes to a turgor-sensitive CBI response.

3.3.3 *QKY* attenuates isoxaben-induced cell swelling

Next, I assessed the biological relevance of *QKY* in the isoxaben-induced CWD response. Exposure of seedlings to isoxaben eventually results in the shortening and swelling of cells of the root epidermis, possibly a result of reduced microfibril formation in the cell wall (Engelsdorf et al., 2018). I transferred six-days-old plate-grown seedlings into a mock solution or a solution containing 600 nM isoxaben for up to seven hours, and then assessed the timing of initial appearance of altered cellular morphology of root epidermal cells and monitored the severity of the phenotype. I focused on cells of the elongation zone that bordered the root meristem. Notably, I did not observe any obvious morphological alterations in mock-treated wild-type or mutant seedling (Figure 39). In Col or L*er* wild-type seedlings cell shortening and swelling first became noticeable during the five to six-hour interval proceeding treatment, as reported previously (Engelsdorf et al., 2018). Upon isoxaben application to *qky-11* or *qky-8* seedlings, however, similar cellular alterations were already detected at the three to four- hour interval post treatment initiation (Figure 39). In addition, *qky* mutants exhibited more pronounced cellular alterations after seven hours of isoxaben treatment in comparison to wild type.

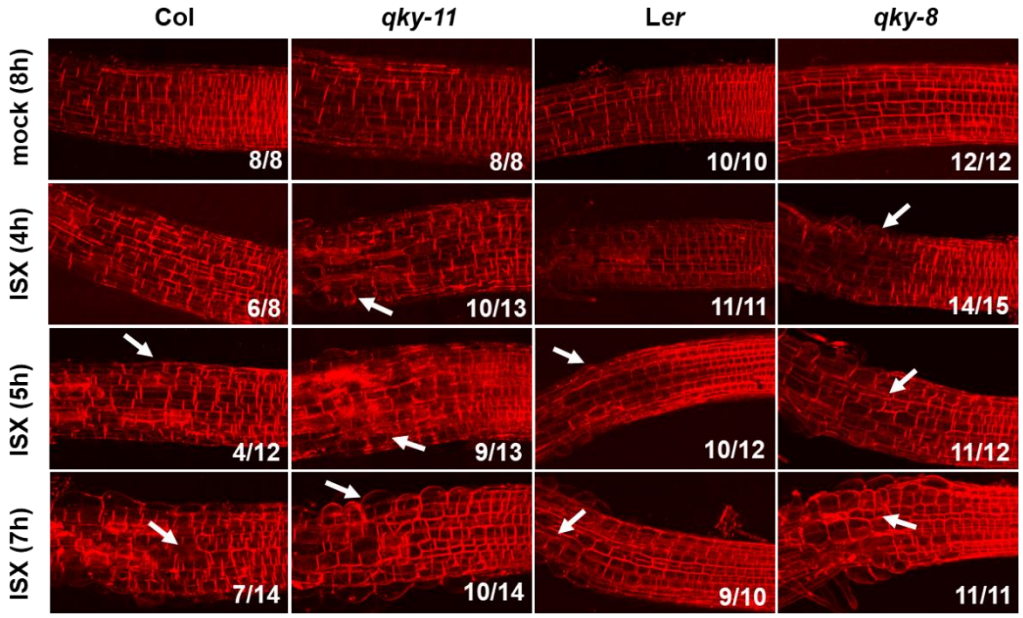

Figure 39 Root epidermal cell shape changes upon isoxaben treatment.

Six-day-old seedlings counter-stained with the membrane stain FM4-64 are shown. Confocal micrographs depict the region where the elongation zone flanks the root meristem. Time of exposure in hours to 600 nM isoxaben (ISX) or mock is indicated as are the genotypes. Numbers of roots showing the phenotype are indicated (n/total number of roots scored). Arrows denote aberrant cell shapes.

3.3.4 Isoxaben treatment reduces *QKY* transcriptionally

In light of the previously discovered role of *QKY* in the CBI-induced CWD response, I investigated whether isoxaben treatment modulates endogenous *QKY* expression. To this end I detected *QKY* transcript expression by qRT-PCR in liquid-grown seedlings exposed to 600 nM isoxaben in comparison with mock-treated seedlings. A slightly significant diminished endogenous *QKY* mRNA levels was detected in seedlings treated with isoxaben for up to 8 hours in three out of six biological replicates (Figure 40A).

In the next step, I tested the effects of prolonged exposure of seedlings to isoxaben on *QKY* levels. *Arabidopsis* seedlings growing in the presence of isoxaben exhibited a response ranging from near normal growth to no growth in the narrow range of 1 to 10

nM isoxaben, with an I_{50} at 4.5 nM (Heim et al., 1989). Thus, I chosed to analyze seven-days-old seedlings that were continuously grown on agar plates containing 3 nM isoxaben. In comparison with mock-treated samples, I observed a significant reduction of *QKY* transcript levels by qRT-PCR in four out of five biological replicates (Figure 40B). Taken together, the results suggested that isoxaben induced a mild reduction in *QKY* transcript.

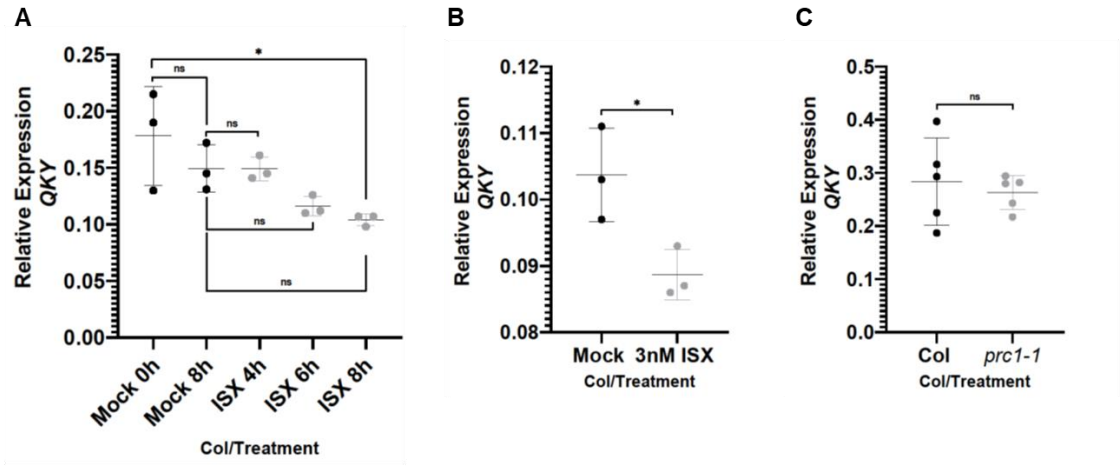

Figure 40 Effect of isoxaben treatment on *QKY* transcript level.

(A) Relative mRNA levels of *QKY* in 7-day-old seedlings exposed to mock or 600 nM isoxaben for different hours. Expression was detected by qPCR. n=3 biological replicates each with mean of three technical replicates. *P<0.05; one-way ANOVA followed by post hoc Tukey's multiple comparison test. (B) Relative expression of *QKY* in 7-day-old seedlings grown on plates containing mock or 3 nM isoxaben. Expression was detected by qPCR. n=3 biological replicates each with mean of three technical replicates. *P<0.05; unpaired t-test, two-tailed P-values. (C) Relative expression of *QKY* in 7-day-old seedlings grown on plates in Col and *prc1-1*. Expression was detected by qPCR. n=3 biological replicates each with mean of three technical replicates. ns, not significant; unpaired t-test, two-tailed P-values. The experiment was performed three times with similar results.

PRC1 encodes the CESA6 subunit of cellulose synthase and the predicted null allele *prc1-1* shows reduced cellulose levels (Fagard et al., 2000). To assess whether *QKY* transcription is also diminished when cellulose biosynthesis is genetically perturbed, I analyzed the endogenous *QKY* transcript levels in wild-type and *prc1-1* seedlings by qPCR, but I could not detect any differences between the two genotypes (Figure 40C).

The results revealing the stronger effect of higher concentrations of isoxaben in comparison with *prc1-1*, may explained by isoxaben affects several primary cell wall CESA subunits and *CESA6* function is buffered by redundantly acting *CESA6*-like genes (Persson et al., 2007; Scheible et al., 2001; Desprez et al., 2007).

3.3.5 Defective in pectin methylation reduces *QKY* on transcription

There is crosstalk between cell wall components (Cosgrove, 2018). For example, plants with a defect in hemicellulose production or in pectin methylation exhibit reduced cellulose content (Du et al., 2020; Xiao et al., 2016). I tested the *QKY* transcript levels upon application of epigallocatechin gallate (EGCG), an inhibitor of pectin methylesterase activity (Lewis et al., 2008), by qRT-PCR in 7-days-old seedlings. I noticed a significant downregulated of QKY mRNA levels upon application of 12.5 uM EGCG (Figure 41). The relative influence of altered pectin architecture and reduced cellulose content on these processes remains to be investigated.

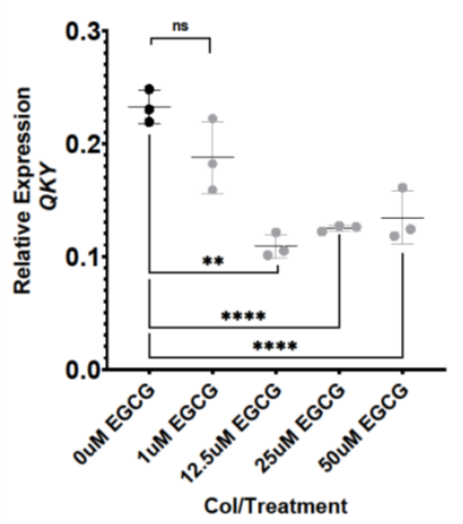

Figure 41 Effects of EGCG treatment on *QKY* transcript level.

Relative transcript levels of *QKY* in seven-day-old seedlings exposed to mock or EGCG for indicated amount and time. Expression was detected by qPCR. n=3 biological replicates each with mean of three technical replicates. **P < 0.01; ****P < 0.0001; one-way ANOVA followed by post hoc Tukey's multiple comparison test.

4 Discussion

Intercellular communication is an essential prerequisite for the growth and development of all multicellular organisms. In plants, due to the presence of cell walls, cytoplasmic bridges called plasmodesmata (PD) have evolved to connect adjacent cells and responsible for this process (Cook et al., 1997; Li et al., 2021). With the development of scientific research, more and more receptor kinases (RKs) has been detected and found to be located on PD (Faulkner et al., 2013; Stahl et al., 2013). Previous work revealed that the RK STRUBBELIG (SUB) is of central importance for the control of tissue morphogenesis and plant architecture and localizes to PM and PD (Chevalier et al., 2005; Vaddepalli et al., 2011). QUIRKY (QKY), the canonical member of the plant MCTP family, was identified to interact with SUB at PD to mediate downstream SUB signal transduction to promote tissue morphogenesis (Vaddepalli et al., 2014; Fulton et al., 2009). SUB/QKY signal transduction represents an excellent model to study the functional cross between RK- and PD-associated intercellular signaling. In the present study, I performed a structure-function analysis of QKY and explored the architecture of QKY/SUB complex in vivo to understand how QKY/SUB mediates its various downstream signaling processes. I also focused on the role of different phosphorylation sites of QKY to gain insight into the molecular mechanisms by which QKY mediates downstream signaling processes. Finally, I examined the important role of QKY in response to cellulose biosynthesis inhibition (CBI)-mediated cell wall damage (CWD).

4.1 Architecture analysis of SUB/QKY complex

4.1.1 Different domains of QKY perform specific functions individually

QKY contains four C2 domains in the N-terminal half and two transmembrane regions (TMR) in the C terminals. Previous studies have suggested that multiple C2

domains either additively or individually act to mediate protein functions (Damer and Creutz, 1994; Cho and Stahelin, 2006). Brault et al (2019) found that members of MCTP family anchor in ER through their transmembrane region and dock to the PM through their C2 domains and act as ER-PM tethers (Brault et al., 2019). Using a genetic approach, I generated stable transgenic *qky-9* plants carrying a set of C2 domain deletion variants of QKY reporters, and noticed that all the C2 domains are necessary for QKY to function correctly in tissue morphogenesis. Y2H and FRET-FLIM assay showed that the N-terminal C2A-B domain is required for the physical interaction of QKY with SUB in vivo and that this process is also required to maintain high levels of SUB at cell surface. Fluorescence microscope observation showed that the combination of C2C-D and TMR domains are required for QKY target to PD, and the TMR domain is necessary to anchor QKY to ER. This is consistent with the case for other MCTP membranes (Liu et al., 2018; Brault et al., 2019).

4.1.2 *qky-9* represents a putative null allele and pQKY:mCherry:QKY can fully complement QKY function

My study found that *qky-9* and *qky-17* represent putative null alleles and that the isolated C2A domain is unlikely to interfere with QKY function, as indicated by the absence of phenotypic differences between *qky-9* and *qky-17*. Phenotypic observation and subcellular localization study of transgenic plants carrying N-terminal fusion of mCherry to QKY driven by endogenous *QKY* promoter (pQKY::mCherry:QMQ) in *qky-9* revealed that it could fully complement QKY function and rescue the phenotype of *qky*. This is in line with previous report that a UBQ10-driven reporter carrying N-terminal fused EGFP can rescue the phenotype of *qky-8* (Vaddepalli et al., 2014). However, this data contrast with a recent study reporting that an N-terminal fusion of GFP to QKY driven by the endogenous promoter fails to complement the *qky-16* phenotype (Song et al., 2019). Further detailed studies are needed to determine the reason for this discrepancy, but it is suspected that *qky-16* is a dominant-negative allele.

4.1.3 QKY may interacts with SUB may not only at PD but also at the cortical ER-PM contact sites

The microscopic images of QKY localization showed that QKY localized on PD and ER, and since the C2A-B domain of QKY interacts with intracellular domain of SUB in the cytoplasm, it raises the possibility that physical interaction between QKY and SUB may occur not only in PD, but also in the sites where the cortical ER and PM are close enough to allow the interaction between QKY which localized on ER and SUB which localized on PM. In addition, my study showed that the physical interaction between QKY and SUB are involved in maintaining a high level of SUB at cell surface, and I also observed the overall reduction in SUB at the cell periphery in *qky* mutants, which includes PD and the sections of the PM between the PD. If we assume that QKY interacts with SUB also at the sites along the cortical ER which are close enough to the PM, it would conveniently explain the phenomenon of the reduced SUB signal at the sites between PD in *qky* mutants. Further exploration should be continued using more advanced and higher resolution microscopy.

4.1.4 The model of QKY and SUB interaction complex

The results of this study indicated that the C2A-B domain of QKY is required for the interaction with SUB and the C2C-D and TMR domains are required for the localization of QKY at PD. Moreover, the TMR domain also is necessary to anchor QKY to ER (Figure 42A). This study also revealed that QKY facilitates the oligomerization of SUB at the cell periphery (Figure 42B). This is one possible may to explain how QKY inhibits the ubiquitination of SUB and maintains the localization of SUB at cell surface. It could be that the ubiquitination site of SUB, or its clathrin binding motif, are masked by SUB homo-oligomers in a QKY-dependent manner. Furthermore, the stoichiometry of SUB/QKY complexes are still unclear. Several different combinations may occur in

vivo (Figure 42C). Further insight may be gained by studying the SUB/QKY complex by X-ray crystallography.

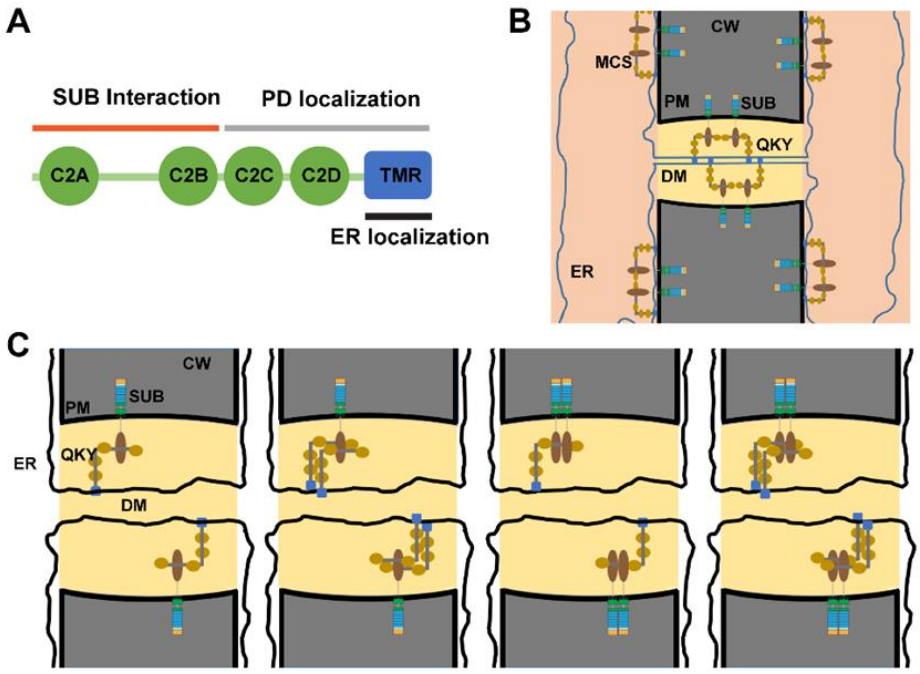

Figure 42 Models of QKY function.

(A) Cartoon depicting the structural and functional modules of QKY. (B) Working model of SUB and QKY complexes located at PD and at sites where the cortical ER is closely associated with the PM. At both sites QKY undergoes SUB-independent homo-oligomerization. The C2A-B domain of QKY interacts with the intracellular domain of SUB thereby maintaining SUB at the PM and facilitating oligomerization of SUB. (C) Cartoon depicting the various possible complexes that could be formed between QKY and SUB. QKY and SUB could interact as monomers or interact in different oligomeric combinations. Abbreviation: CW, cell wall; DM, desmotubule; ER, endoplasmic reticulum; PM, plasma membrane; QKY, QUIRKY; SUB, STRUBBELIG; TMR, transmembrane region.

4.2 Functional analysis of QKY phosphorylation in vivo

4.2.1 Different phosphosites of QKY function differently

My study revealed that QKY is phosphorylated in vivo and the phosphorylation of QKY at these sites is not controlled by SUB signaling. I identified four phosphorylation sites (P-sites) of QKY in young seedlings: S218, S262, S305, and S1075. Among them,

S218, S262, and S305 are located in the C2A-B linker region, and S1075 localized to the TMR region of QKY. Through the structure-function correlation analysis of the P-sites, I found that the P-sites differ in their function.

The phosphorylation of S1075 was found to be required for efficient localization and function of QKY, as the transgenic lines of QMQS1075A showed no rescue of the phenotype of *qky-9* in root hair pattern distribution, ovule development and the subcellular localization. Based on the available analyses, it does not appear that the phosphorylation of S305 is involved in QKY-dependent tissue morphogenesis. It mainly shows that the transgenic lines S305A and S305E exhibit similar phenotypes, and both can basically rescue the phenotype of *qky-9* in terms of root hair pattern distribution and ovule development. Perhaps, the phosphorylation of S305 may be relevant to other QKY-dependent processes that have not yet been discovered, and it may also function in a specific spatial-temporal context, given the temporal sequence of events.

My study suggested that the phosphorylation of S218 or S262 is important for QKY-dependent related function. The transgenic lines carrying QMQS218A or QMQS262A reporter failed to complement *qky-9* defects in the developmental process, whereas the lines carrying S218E or S262E reporter complemented. Interestingly, I observed that while QMQS218A or QMQS262A failed to complement the defects in hair cells in *qky-9*, but it rescued the non-hair cells phenotype. This demonstrates a tissue-specific effects of phosphorylation of S218 or S262 on the function of QKY-dependent root hair patterning phenotype. It has been suggested that QKY regulates the distribution pattern of root hairs by stabilizing the expression of SUB on PM and promoting the PD-mediated transport of root-hair pattern-related transcription factor CPC from non-hair cells to hair cells (Song et al., 2019). I observed that phosphorylation of S218 or S262 is required for the stabilization of SUB at the PM by QKY, so it is speculated that in the transgenic *qky-9* lines carrying S218A or S262A reporter, it maybe unable to develop

into root hairs due to the inability to maintain a sufficient level of SUB expression in hair cells. But the QKY mutant protein present in N cells can still promote the movement of CPC from N to H cells, preventing CPC from interfering with N cell development.

4.2.2 Functional SUB/QKY complexes are required for tissue morphogenesis and SUB threshold

From my data, I noticed that for most of the transgenic reporter lines, if they were able to restore the *qky-9* phenotype, they were usually able to detect the interaction of SUB and QKY in vivo as well, whereas for those who could not restore the phenotype of *qky-9*, the complex of SUB and QKY is usually not easily detected in vivo. For example, when *qky-9* carrying QMQdelC2AL or QMQdelC2A-B transgenic reporter, I observed these reporters could not restore the phenotype of *qky-9*, and I tested there no SUB/QKY complexes in vivo by FRET-FLIM as well, meanwhile the Y2H assay also confirmed SUB and QKY could not interact with each other in these variants (Table 10).

Table 10 Summary of the data in transgenic plants of different QKY variants.

	Phenotype	SUB @ PM	QKY/SUB interaction	
			FRET-FLIM	Y2H
No QKY	no rescue	less	No	No
+ QKY	rescue	more	Yes	Yes
delC2A	no rescue	less	Reduced	Yes
delC2AL	no rescue	less	No	No
delC2A-B	no rescue	less	No	No
S218A	no rescue	less	Yes	Yes
S218E	rescue	more	Yes/modulated	Yes
S262A	no rescue	less	Yes	Yes
S262E	rescue	more	Yes/modulated	Yes
S305A	rescue	more	Yes	Yes
S305E	rescue	more	Yes	Yes

Interestingly, there are some exceptions to this rule, I noticed that when *qky-9* carrying QMQdelC2A reporter, the phenotype of *qky-9* could not be restored, and the FRET-FLIM assay showed SUB and QKY still formed complex in vivo, even though the interaction seems to be reducing (Table 10). It is possible that in QMQdelC2A transgenic lines, the SUB/QKY complexes become non-functional complexes due to changes in the structure and direction of the interaction sites, resulting in the inability of QKY to function normally during plant development. It revealed that the functional SUB/QKY complexes are required for tissue morphogenesis. In addition, the interaction of SUB and QKY have been detected in *qky-9* carrying QMQS218A or QMQS262A reporter, but the phenotype observation showed that the reporters could not restore the defective of *qky-9*. Similarly, I thought SUB/QKY complexes may be in a non-functional state in these transgenic lines. There is a possibility that under normal conditions, the SUB/QKY complex may need the assistance of third partner to perform function or need to function in a certain state, but upon mutation of the phosphosites S218 or S262 to phospho-dead, the third partner cannot bind to the complex to assist in the function or may the specific state of complex is disrupted, resulting in the disability of QKY to control tissue morphogenesis.

4.2.3 S218 and S262 may antagonize each other

QMQ carrying the single mutant of S218A or S262A substitution could not restore the phenotype of *qky-9*, whereas carrying S218E or S262E could fully complement the phenotype. Interestingly, and unexpected, the double phospho-dead (S218AS262A) or phospho-mimic (S218ES262E) mutant reporters, could fully complement the developmental phenotype of *qky-9*. It suggests that keeping S218 and S262 in a dephosphorylated or phosphorylated state enables complete QKY function. It appears that the effect of the first phospho-dead mutation is balanced by the introduction of the second phospho-dead mutation. One possibility is that removing one negative charge

disrupts or changes the structure of the protein, but by also removing a second negative charge, the structure is able to develop again closer to the original structure, becoming more efficient again and allowing the double mutant transgenic lines show more recovery.

The genetic results suggest that phosphorylation of QKY at S218 and S262 leads to complex effects on the structure-function relationship of QKY. Through the observation of the QKY/SUB interaction study in these transgenic lines, I found that the interaction between QKY and SUB can still be detected in the double mutant S218AS262A, and the phospho-dead mutation did not affect the state of the interaction between SUB and QKY, as I discussed earlier, perhaps affecting the relative functionality of the complex.

4.2.4 Phosphorylation of S218 or S262 may alter the architecture of SUB/QKY complex

In my data, the study on the interaction of SUB and QKY are more complex. I found that all the tested mutation of phosphosites still allowed the QKY C2A-D domain to interact with the intracellular domain of SUB in a Y2H assay. The results suggest that none of the mutations eliminates the physical interaction between the two proteins in Y2H system. Interestingly, I tested the interaction of SUB and QKY when QKY carried the S218A or S262A mutation by FRET-FLIM in vivo, but the interaction getting weaker when QKY carried the S218E or S262E mutation, indicated by the observation that the mean fluorescence lifetime of SUB:GFP was significantly higher in QMQS218E or QMQS262E lines than in QMQS218A or QMQS262A lines, although still reduced compared to the absence of mCherry:QKY. Similarly, I could also detect the interaction of SUB and QKY when QKY carried S218AS262A double mutations, but not when carried S218ES262E mutations. It seems that once the phosphorylation site is mutated to E, the interaction state of SUB and QKY is disturbed.

Here are some possibilities to explain this phenomenon. For FRET to occur, the donor/acceptor pair needs to be less than 10 nm apart. In addition, the orientation of the donor's emission transition dipole should be parallel to the orientation of the acceptor's transition absorption dipole for optimal FRET. Deviations from this angle will result in reduced FRET even if the distance between donor and acceptor is less than 10 nm (Lakowicz, 2006). Therefore, when the phosphorylation site was mutated to E, the internal spatial structure of SUB/QKY complex might have changed, resulting in an increase in the mean fluorescence lifetime of SUB:GFP. In another case, the phosphorylation of QKY may lead to a conformational change of the QKY protein, which in turn changes the relative arrangement of the fluorescent markers (GFP and mCherry), so that the distance between them is close to or greater than 10 nm. A more detailed molecular model of SUB/QKY complex and the structural effects triggered by QKY phosphorylation require further studies involving for example X-ray crystallography.

4.3 Role of QKY in response to cell wall damage

SUB signal transduction play an major role in cellulose biosynthesis inhibition (CBI)-induced cell wall damage (CWD) response. SUB is required for promoting isoxaben-induced marker gene expression, and the accumulation of lignin, as well as suppression the alterations in cell morphology in the root epidermis (Chaudhary et al., 2020, 2021). QKY as a central genetic component in SUB signal transduction, I also explored if QKY is required for the isoxaben-induced CWD response. From my results, I noticed that QKY contribute to the isoxaben-mediated induction of lignin accumulation, and also plays a role in the prevention of cell bulging in the root epidermal cells. These are the similar function with SUB. However, unlike SUB, QKY is not required for isoxaben-induced marker gene induction. These data revealed that SUB and QKY contribute differently to the CBI response, and the functions of SUB and QKY only partially overlap.

5 Conclusion

Tissue morphogenesis and organ development in plants relies on the spatiotemporal regulation of cell proliferation, division and growth. Cell-to-cell communication is essential to this regulatory process.

The Arabidopsis multi-functional receptor kinase (RK) STRUBBELIG (SUB) plays the central role to development and stress response in plants. Studies have shown that SUB is involved in regulating root hair patterning, flower morphogenesis, ovule development, and monitoring cell wall integrity (Chevalier et al., 2005; Chaudhary et al., 2021). QUIRKY (QKY), the canonical plant member of the “multiple C2 domains and transmembrane proteins (MCTPs)” family, interacts with SUB and is required for SUB-mediated signal transduction. However, it is still unclear how the structure and function of QKY are related to each other, and what the architecture of the QKY/SUB complex is in vivo. Specifically analyzing the architecture of SUB/QKY complex and exploring the correlation between structure and function, will help to further understand the mechanism of SUB/QKY-mediated intercellular signaling.

In this context, I studied the QKY/SUB complex in vivo using a combination of genetics and fluorescence microspectrometry, including FRET-FLIM and FA. Using new transgenic lines and more advanced microscope set up, I further determined the interaction of SUB and QKY on PM, and found that SUB and QKY preferentially interacted on the longitudinal PM, revealing the subcellular polarity of SUB/QKY complex. In addition, I found that QKY promotes the formation of SUB homo-oligomers in vivo, and also undergoes SUB-independent homomerization in vivo. Furthermore, the data showed that the N-terminal C2A-B region of QKY is essential for the interaction with SUB in vivo, and that this interaction is required to maintain SUB levels at the cell surface.

Conclusion

In order to fully understand how QKY regulates SUB-mediated signal transduction, I also analyzed the functional relevance of QKY phosphorylation in vivo. The data showed that QKY is phosphorylated independently of SUB in vivo. Three phosphorylation sites at S218, S262, S305 and S1075 have been identified. Among these, all S218, S262 and S305 localize to the C2A-B linker region, and S1075 sit on the TMR region in C-terminal of QKY. Combined results from genetics, Y2H assays, confocal and FRET-FLIM indicated that phosphorylation of the S1075 controls the subcellular localization of QKY, whereas the P-sites S218, S262, and S305 revealed a complex picture. It appears that the phosphorylation of S218 or S262, but not S305, is required for QKY-dependent tissue morphogenesis.

Furthermore, the data presented here indicate that QKY plays a role in isoxaben-induced CWD response. Unlike SUB, which plays important role in isoxaben-mediated multiple pathways, QKY mainly contribute to the isoxaben-mediated induction of lignin accumulation, and also plays a role in the prevention of cell bulging in the root epidermal cells, whereas QKY is not required for isoxaben-induced marker gene induction.

6 Supplementary Data

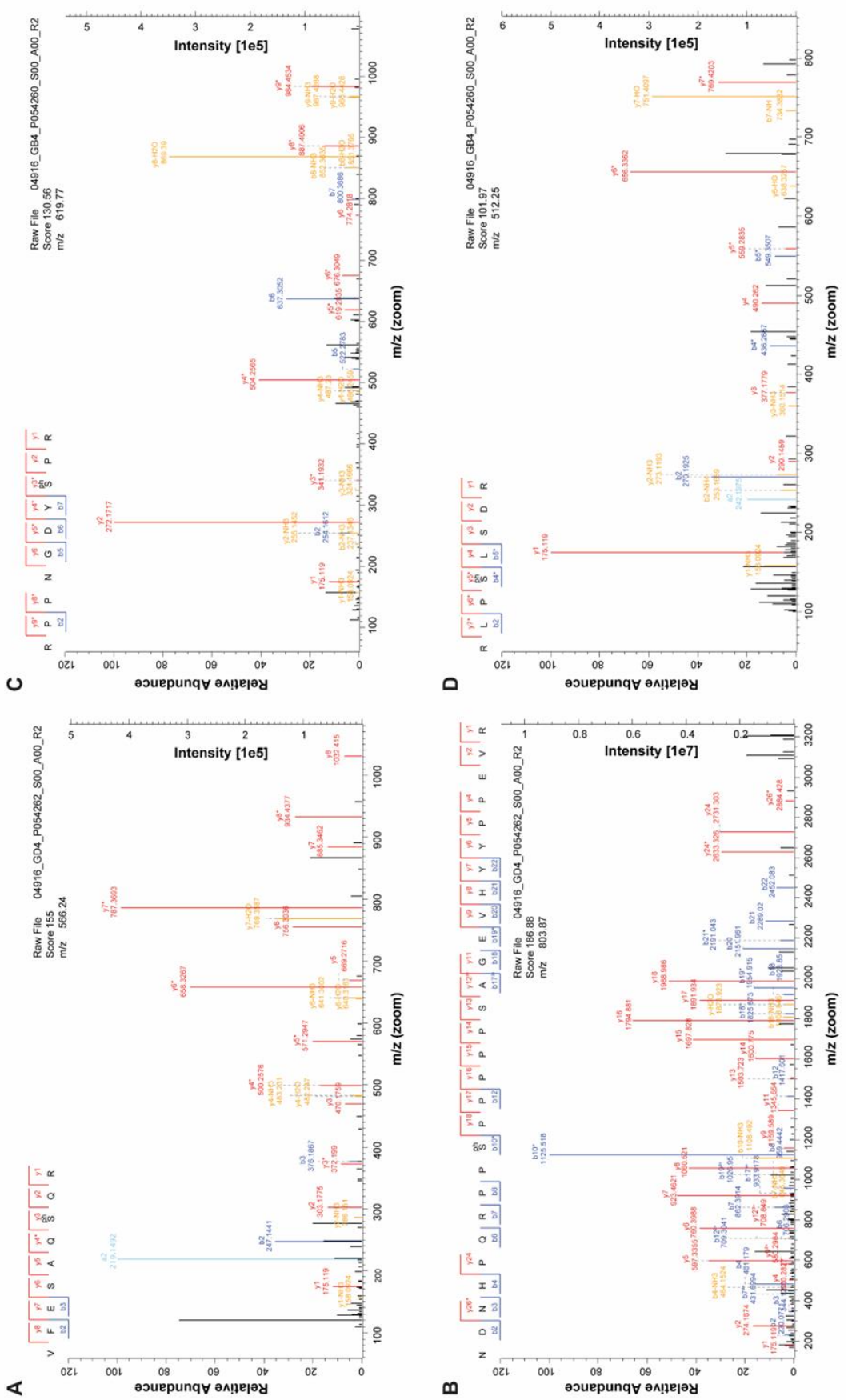

Supplemental Figure 1: Representative MS/MS spectra of QKY phosphorylation sites.

(A) For pS218 (VFESAQpSQR). (B) For pS262 (NDNHPQRPPpSPPPPPSAGEVHYYPPEVR). (C) For pS305 (RPPNGDYpSPR). (D) For pS1075 (RLPpSLSDR). Annotated fragment ion peaks: y-ion series (red), b-ion series (blue), a-ion series (turqois), ammonia and water neutral losses (yellow). Asterisks indicate phosphate group neutral loss.

Table S1. Primers used in this study.

Primer name	**Sequence**
NdeI/QKY(-TM)_F	5’-CGCTCATATGAACACGACGCCGTTTCACTCGGATCCTCCGCCG-3’
QKY(C2A-B)/XmaI_R	5’-TACCCGGGTGAGTACCAATCCAAACAGA-3’
QKY(C2C-D)/NdeI_F	5’-GCTCATATGGGTAGATGAGGCATTTCCGG-3’
QKY(-TM)/XmaI_R	5’-CCCACCCGGGATGGACTAGCACCGTCGT-3’
C2ALinker_XmaI_R	5’-TACCCGGGGATGAGTCTTCTTCTCCATCGTCG-3’
C2A_XmaI_R	5’-TACCCGGGGTAGATTTTGAGTCCAATCTCGCC-3’
C2ALinker_NdeI_F	5’-GCTCATATGTATTACGACGAAGCCGCCGA-3’
sgRNA1	5’-ACTCGGATCCTCCGCCGTCG-3’
sgRNA2	5’-TTACGACGAGCTCGATATCG-3’
Q5SDM S218A_F	5’-ATCGGCTCAGGCTCAGCGCTATAC-3’
Q5SDM S218E_F	5’-ATCGGCTCAGGAACAGCGCTATAC-3’
Q5SDM S218A/E_R	5’-TCGAAAACCCTACCTTCTTC-3’
Q5SDM S262A_F	5’-ACGGCCACCGGCTCCGCCGCCAC-3’
Q5SDM S262A_R	5’-TGAGGATGGTTATCATTTCGGTGAGGATGGTTATCATTTGGACCTTGC-3’

Q5SDM S262E_F	5’-ACGGCCACCGGAACCGCCGCCAC-3’
Q5SDM S262E_R	5’-TGAGGATGGTTATCATTTCGGTGAGGATG-3’
Q5SDM S305A_F	5’-TGGAGATTATGCACCTAGGGTTATC-3’
Q5SDM S305E_F	5’-TGGAGATTATGAACCTAGGGTTATCAATAG-3’
Q5SDM S305A/E_R	5’-TTCGGTGGTCTCTTCGTA-3’
Q5SDM S1075A_F	5’-GCGGTTGCCAGCCTTGTCCGATC-3’
Q5SDM S1075A_R	5’-CGGAAAAAATTGAGACTAGC-3’
Q5SDM S1075E_F	5’-GCGGTTGCCAGAATTGTCCGATC-3’
Q5SDM S1075E_R	5’-CGGAAAAAATTGAGACTAG-3’
sub-1_NdeI_F	5’-CAGGGACAATTCCGCAGGCTTTGCCTTCTTCCATCCGAAACAT-3’
sub-1_NdeI_R	5’-GGAAAAACCGCAGATGCAAGAAACGGTATC-3’
qky-9_XbaI_F	5’-CTAATGTAGTTGTGGTTGAAGAAGGTAGGGTTTTCGAATCGGTC-3’
qky-9_XbaI_R	5’-ATTCTATCTCCGCCGGGAGGTCT-3’

7 References

Aifa, S., Frikha, F., Miled, N., Johansen, K., Lundström, I., and Svensson, S.P.S. (2006). Phosphorylation of Thr654 but not Thr669 within the juxtamembrane domain of the EGF receptor inhibits calmodulin binding. Biochem. Biophys. Res. Commun. **347**: 381–387.

Bader, A.N., Hoetzl, S., Hofman, E.G., Voortman, J., Henegouwen, P.M.P. van B. en, Meer, G. van, and Gerritsen, H.C. (2011). Homo-FRET Imaging as a Tool to Quantify Protein and Lipid Clustering. ChemPhysChem **12**: 475–483.

Bai, Y., Vaddepalli, P., Fulton, L., Bhasin, H., Hülskamp, M., and Schneitz, K. (2013). ANGUSTIFOLIA is a central component of tissue morphogenesis mediated by the atypical receptor-like kinase STRUBBELIG. BMC Plant Biol. **13**: 16.

Balcerowicz, D., Schoenaers, S., and Vissenberg, K. (2015). Cell fate determination and the switch from diffuse growth to planar polarity in arabidopsis root epidermal cells. Front. Plant Sci. **6**: 1–13.

Becker, W., Bergmann, A., Hink, M.A., König, K., Benndorf, K., and Biskup, C. (2004). Fluorescence Lifetime Imaging by Time-Correlated Single-Photon Counting. Microsc. Res. Tech. **63**: 58–66.

Bell, K. and Oparka, K. (2011). Imaging plasmodesmata. Protoplasma **248**: 9–25.

Benavente, J.L., Siliqi, D., Infantes, L., Lagartera, L., Mills, A., Gago, F., Ruiz-López, N., Botella, M.A., Sánchez-Barrena, M.J., and Albert, A. (2021). The structure and flexibility analysis of the Arabidopsis synaptotagmin 1 reveal the basis of its regulation at membrane contact sites. Life Sci. Alliance **4**: 1–17.

Birnbaum, K.D. and Alvarado, A.S. (2008). Slicing across Kingdoms: Regeneration in Plants and Animals. Cell **132**: 697–710.

Blackman, L.M. and Overall, R.L. (2001). Structure and function of plasmodesmata. Aust. J. Plant Physiol. **28**: 709–727.

Bloemendal, S. and Kück, U. (2013). Cell-to-cell communication in plants, animals,

and fungi: A comparative review. Naturwissenschaften **100**: 3–19.

Boller, T. and Felix, G. (2009). A renaissance of elicitors: Perception of microbe-associated molecular patterns and danger signals by pattern-recognition receptors. Annu. Rev. Plant Biol. **60**: 379–407.

Brault, M.L. et al. (2019). Multiple C2 domains and transmembrane region proteins (MCTP s) tether membranes at plasmodesmata . EMBO Rep. **20**: 1–26.

Bücherl, C.A., Bader, A., Westphal, A.H., Laptenok, S.P., and Borst, J.W. (2014). FRET-FLIM applications in plant systems. Protoplasma **251**: 383–394.

Bücherl, C.A., van Esse, G.W., Kruis, A., Luchtenberg, J., Westphal, A.H., Aker, J., van Hoek, A., Albrecht, C., Borst, J.W., and de Vries, S.C. (2013). Visualization of BRI1 and BAK1(SERK3) membrane receptor heterooligomers during Brassinosteroid signaling. Plant Physiol. **162**: 1911–1925.

Burch-Smith, T.M. and Zambryski, P.C. (2012). Plasmodesmata paradigm shift: Regulation from without versus within. Annu. Rev. Plant Biol. **63**: 239–260.

Caño-Delgado, A., Penfield, S., Smith, C., Catley, M., and Bevan, M. (2003). Reduced cellulose synthesis invokes lignification and defense responses in Arabidopsis thaliana. Plant J. **34**: 351–362.

Cantrill, L.C., Overall, R.L., and Goodwin, P.B. (1999). Cell-to-cell communication via plant endomembranes. Cell Biol. Int. **23**: 653–661.

Chaudhary, A., Chen, X., Gao, J., Leśniewska, B., Hammerl, R., Dawid, C., and Schneitz, K. (2020). The Arabidopsis receptor kinase STRUBBELIG regulates the response to cellulose deficiency. PLoS Genet. **16**: e1008433.

Chaudhary, A., Chen, X., Lesniewska, B., Boikine, R., Gao, J., Wolf, S., and Schneitz, K. (2021). Cell wall damage attenuates root hair patterning and tissue morphogenesis mediated by the receptor kinase STRUBBELIG. Dev. **148**.

Chaudhary, A. and Schneitz, K. (2022). Using Steady-State Fluorescence Anisotropy to Study Protein Clustering. Yoselin Benitez-Alfonso Manfred Heinlein (eds.), Plasmodesmata Methods Protoc. Methods Mol. Biol. **2457**: 253–260.

Chen, X.Y. and Kim, J.Y. (2009). Callose synthesis in higher plants. Plant Signal. Behav. **4**: 489–492.

Chevalier, D., Batoux, M., Fulton, L., Pfister, K., Yadav, R.K., Schellenberg, M., and Schneitz, K. (2005). STRUBBELIG defines a receptor kinase-mediated signaling pathway regulating organ development in Arabidopsis. Proc. Natl. Acad. Sci. **102**: 9074–9079.

Cho, W. and Stahelin, R. V. (2006). Membrane binding and subcellular targeting of C2 domains. Biochim. Biophys. Acta - Mol. Cell Biol. Lipids **1761**: 838–849.

Clark, S.E. (1997). The CLAVATA1 Gene Encodes a Putative Receptor Kinase That Controls Shoot and Floral Meristem Size in Arabidopsis. Cell **89**: 575–585.

Clause, S.D. and Sasse, J.M. (1998). Brassinosteroids: Essential Regulators of Plant Growth and Development. Annu. Rev. Plant Biol. **49**: 427–451.

Clough, S.J. and Bent, A.F. (1998). Floral dip: A simplified method for Agrobacterium-mediated transformation of Arabidopsis thaliana. Plant J. **16**: 735–743.

Cock, J.M., Vanoosthuyse, V., and Gaude, T. (2002). Receptor kinase signalling in plants and animals: Distinct molecular systems with mechanistic similarities. Curr. Opin. Cell Biol. **14**: 230–236.

Cook, M.E., Graham, L.E., Botha, C.E.J., and Lavin, C.A. (1997). Comparative ultrastructure of plasmodesmata of Chara and selected bryophytes: Toward an elucidation of the evolutionary origin of plant plasmodesmata. Am. J. Bot. **84**: 1169–1178.

Cosgrove, D.J. (2018). Diffuse growth of plant cell walls. Plant Physiol. **176**: 16–27.

Cosgrove, D.J. (2016). Plant cell wall extensibility: Connecting plant cell growth with cell wall structure, mechanics, and the action of wall-modifying enzymes. J. Exp. Bot. **67**: 463–476.

Cutler, S.R. and Ehrhardt, D.W. (2002). Polarized cytokinesis in vacuolate cells of Arabidopsis. Proc. Natl. Acad. Sci. U. S. A. **99**: 2812–2817.

Cutler, S.R., Ehrhardt, D.W., Griffitts, J.S., and Somerville, C.R. (2000). Random

GFP::cDNA fusions enable visualization of subcellular structures in cells of Arabidopsis at a high frequency. Proc. Natl. Acad. Sci. U. S. A. **97**: 3718–3723.

Damer, C.K. and Creutz, C.E. (1994). Synergistic membrane interactions of the two C2 domains of synaptotagmin. J. Biol. Chem. **269**: 31115–31123.

Desprez, T. et al. (2017). Resistance against Herbicide Isoxaben and Cellulose Deficiency Caused by Distinct Mutations in Same Cellulose Synthase Isoform CESA6 Published by : American Society of Plant Biologists (ASPB) Stable URL : http://www.jstor.org/stable/4280316 Linked refer. **128**: 482–490.

Desprez, T., Juraniec, M., Crowell, E.F., Jouy, H., Pochylova, Z., Parcy, F., Höfte, H., Gonneau, M., and Vernhettes, S. (2007). Organization of cellulose synthase complexes involved in primary cell wall synthesis in Arabidopsis thaliana. Proc. Natl. Acad. Sci. U. S. A. **104**: 15572–15577.

Ding, Y., Li, H., Zhang, X., Xie, Q., Gong, Z., and Yang, S. (2015). OST1 kinase modulates freezing tolerance by enhancing ICE1 stability in arabidopsis. Dev. Cell **32**: 278–289.

Dinneny, J.R. and Benfey, P.N. (2008). Plant Stem Cell Niches: Standing the Test of Time. Cell **132**: 553–557.

Van der Does, D. et al. (2017). The Arabidopsis leucine-rich repeat receptor kinase MIK2/LRR-KISS connects cell wall integrity sensing, root growth and response to abiotic and biotic stresses. PLoS Genet. **13**: 1–27.

Dolan, L., Janmaat, K., Willemsen, V., Linstead, P., Poethig, S., Roberts, K., and Scheres, B. (1993). Cellular organisation of the Arabidopsis thaliana root. Development **119**: 71–84.

Du, J. et al. (2020). Mutations in the Pectin Methyltransferase QUASIMODO2 influence cellulose biosynthesis and wall integrity in arabidopsis. Plant Cell **32**: 3576–3597.

Dünser, K., Gupta, S., Herger, A., Feraru, M.I., Ringli, C., and Kleine-Vehn, J. (2019). Extracellular matrix sensing by FERONIA and Leucine-Rich Repeat Extensins controls vacuolar expansion during cellular elongation in Arabidopsis

thaliana . EMBO J. **38**: 1–12.

Ehlers, K. and Kollmann, R. (2001). Primary and secondary plasmodesmata: Structure, origin, and functioning: Review article. Protoplasma **216**: 1–30.

Ellis, C., Karafyllidis, I., Wasternack, C., and Turner, J.G. (2002). Erratum: The arabidopsis mutant cev1 links cell wall signaling to jasmonate and ethylene responses (Plant Cell (2002) 14 (1557-1566)). Plant Cell **14**: 1981.

Engelsdorf, T., Gigli-Bisceglia, N., Veerabagu, M., McKenna, J.F., Vaahtera, L., Augstein, F., Van der Does, D., Zipfel, C., and Hamann, T. (2018). The plant cell wall integrity maintenance and immune signaling systems cooperate to control stress responses in Arabidopsis thaliana. Sci. Signal. **11**.

Enugutti, B., Kirchhelle, C., Oelschner, M., Ruiz, R.A.T., Schliebner, I., Leister, D., and Schneitz, K. (2012). Regulation of planar growth by the Arabidopsis AGC protein kinase UNICORN. Proc. Natl. Acad. Sci. U. S. A. **109**: 15060–15065.

Eyüboglu, B., Pfister, K., Haberer, G., Chevalier, D., Fuchs, A., Mayer, K.F.X., and Schneitz, K. (2007). Molecular characterisation of the STRUBBELIG-RECEPTOR FAMILY of genes encoding putative leucine-rich repeat receptor-like kinases in Arabidopsis thaliana. BMC Plant Biol. **7**.

Fagard, M. et al. (2016). PROCUSTE1 Encodes a Cellulose Synthase Required for Normal Cell Elongation Specifically in Roots and Dark-Grown Hypocotyls of Arabidopsis Herman Höfte Published by : American Society of Plant Biologists (ASPB) Stable URL : http://www.jstor.org/stable/38.

Fagard, M., Desnos, T., Desprez, T., Goubet, F., Refregier, G., Mouille, G., McCann, M., Rayon, C., Vernhettes, S., and Höfte, H. (2000). Procuste1 encodes a cellulose synthase required for normal cell elongation specifically in roots and dark-grown hypocotyls of arabidopsis. Plant Cell **12**: 2409–2423.

Faulkner, C., Petutschnig, E., Benitez-Alfonso, Y., Beck, M., Robatzek, S., Lipka, V., and Maule, A.J. (2013). LYM2-dependent chitin perception limits molecular flux via plasmodesmata. Proc. Natl. Acad. Sci. U. S. A. **110**: 9166–

9170.

Faulkner, C.R., Blackman, L.M., Collings, D.A., Cordwell, S.J., and Overall, R.L. (2009). Anti-tropomyosin antibodies co-localise with actin microfilaments and label plasmodesmata. Eur. J. Cell Biol. **88**: 357–369.

Feng, W. et al. (2018). The FERONIA Receptor Kinase Maintains Cell-Wall Integrity during Salt Stress through Ca2+ Signaling. Curr. Biol. **28**: 666-675.e5.

Folkers, U., Berger, J., and Hülskamp, M. (1997). Cell morphogenesis of trichomes in Arabidopsis: Differential control of primary and secondary branching by branch initiation regulators and cell growth. Development **124**: 3779–3786.

Franck, C.M., Westermann, J., and Boisson-Dernier, A. (2018). Plant Malectin-Like Receptor Kinases: From Cell Wall Integrity to Immunity and beyond. Annu. Rev. Plant Biol. **69**: 301–328.

Fulton, L., Batoux, M., Vaddepalli, P., Yadav, R.K., Busch, W., Andersen, S.U., Jeong, S., Lohmann, J.U., and Schneitz, K. (2009). DETORQUEO, QUIRKY, and ZERZAUST represent novel components involved in organ development mediated by the receptor-like kinase STRUBBELIG in Arabidopsis thaliana. PLoS Genet. **5**.

Gaillochet, C. and Lohmann, J.U. (2015). The never-ending story: From pluripotency to plant developmental plasticity. Dev. **142**: 2237–2249.

Gao, J., Chaudhary, A., Vaddepalli, P., Nagel, M.K., Isono, E., and Schneitz, K. (2019). The Arabidopsis receptor kinase STRUBBELIG undergoes clathrin-dependent endocytosis. J. Exp. Bot. **70**: 3881–3894.

Glanc, M. et al. (2021). AGC kinases and MAB4/MEL proteins maintain PIN polarity by limiting lateral diffusion in plant cells. Curr. Biol. **31**: 1918-1930.e5.

Gómez-Gómez, L. and Boller, T. (2000). FLS2: An LRR receptor-like kinase involved in the perception of the bacterial elicitor flagellin in Arabidopsis. Mol. Cell **5**: 1003–1011.

Graves, J.D. and Krebs, E.G. (1999). Protein Phosphorylation and Signal Transduction. Pharmacol. Ther **82**: 111–121.

Grebe, M. (2012). The patterning of epidermal hairs in Arabidopsis-updated. Curr. Opin. Plant Biol. **15**: 31–37.

Grierson, C., Nielsen, E., Ketelaarc, T., and Schiefelbein, J. (2014). Root Hairs. Arab. B. **12**: e0172.

Guenoune-Gelbart, D., Elbaum, M., Sagi, G., Levy, A., and Epel, B.L. (2008). Tobacco mosaic virus (TMV) replicase and movement protein function synergistically in facilitating TMV spread by lateral diffusion in the plasmodesmal desmotubule of Nicotiana benthamiana. Mol. Plant-Microbe Interact. **21**: 335–345.

Guimil, S. and Dunand, C. (2006). Patterning of Arabidopsis epidermal cells: epigenetic factors regulate the complex epidermal cell fate pathway. Trends Plant Sci. **11**: 601–609.

Hamann, T. (2012). Plant cell wall integrity maintenance as an essential component of biotic stress response mechanisms. Front. Plant Sci. **3**: 1–5.

Hamann, T. (2015). The plant cell wall integrity maintenance mechanism - A case study of a cell wall plasma membrane signaling network. Phytochemistry **112**: 100–109.

Hamann, T., Bennett, M., Mansfield, J., and Somerville, C. (2009). Identification of cell-wall stress as a hexose-dependent and osmosensitive regulator of plant responses. Plant J. **57**: 1015–1026.

Heim, D.R., Roberts, J.L., Pike, P.D., and Larrinua, I.M. (1989). Mutation of a Locus of Arabidopsis thaliana Confers Resistance to the Herbicide Isoxaben . Plant Physiol. **90**: 146–150.

Heim, D.R., Skomp, J.R., Tschabold, E.E., and Larrinua, I.M. (1990). Isoxaben inhibits the synthesis of acid insoluble cell wall materials in Arabidopsis thaliana. Plant Physiol. **93**: 695–700.

Heiss, E., Masson, K., Sundberg, C., Pedersen, M., Sun, J., Bengtsson, S., and Rönnstrand, L. (2006). Identification of Y589 and Y599 in the juxtamembrane domain of Flt3 as ligand-induced autophosphorylation sites involved in binding

of Src family kinases and the protein tyrosine phosphatase SHP2. Blood **108**: 1542–1550.

Hématy, K., Sado, P.E., Van Tuinen, A., Rochange, S., Desnos, T., Balzergue, S., Pelletier, S., Renou, J.P., and Höfte, H. (2007). A Receptor-like Kinase Mediates the Response of Arabidopsis Cells to the Inhibition of Cellulose Synthesis. Curr. Biol. **17**: 922–931.

Houston, K., Tucker, M.R., Chowdhury, J., Shirley, N., and Little, A. (2016). The plant cell wall: A complex and dynamic structure as revealed by the responses of genes under stress conditions. Front. Plant Sci. **7**: 1–18.

Hu, Q., Zeng, M., Wang, M., Huang, X., Li, J., Feng, C., Xuan, L., Liu, L., and Huang, G. (2021). Family-Wide Evaluation of Multiple C2 Domain and Transmembrane Region Protein in Gossypium hirsutum. Front. Plant Sci. **12**.

Hüttner, S., Veit, C., Vavra, U., Schoberer, J., Dicker, M., Maresch, D., Altmann, F., and Strasser, R. (2014). A context-independent N-glycan signal targets the misfolded extracellular domain of Arabidopsis STRUBBELIG to endoplasmic-reticulum-associated degradation. Biochem. J. **464**: 401–411.

Iglesias, V.A. and Meins, F. (2000). Movement of plant viruses is delayed in a β-1,3-glucanase-deficient mutant showing a reduced plasmodesmatal size exclusion limit and enhanced callose deposition. Plant J. **21**: 157–166.

Jo, Y., Cho, W.K., Rim, Y., Moon, J., Chen, X.Y., Chu, H., Kim, C.Y., Park, Z.Y., Lucas, W.J., and Kim, J.Y. (2011). Plasmodesmal receptor-like kinases identified through analysis of rice cell wall extracted proteins. Protoplasma **248**: 191–203.

Kim, I., Hempel, F.D., Sha, K., Pfluger, J., and Zambryski, P.C. (2002). Identification of a developmental transition in plasmodesmatal function during embryogenesis in Arabidopsis thaliana. Development **129**: 1261–1272.

Kirk, P. and Benitez-Alfonso, Y. (2022). Plasmodesmata Structural Components and Their Role in Signaling and Plant Development. Plasmodesmata Methods Protoc. Methods Mol. Biol. **2457**.

Koncz, C. and Schell, J. (1986). The promoter of TL-DNA gene 5 controls the tissue-specific expression of chimaeric genes carried by a novel type of Agrobacterium binary vector. Mol. Gen. Genet. **204**: 383–396.

Kunze, G., Zipfel, C., Robatzek, S., Niehaus, K., Boller, T., Kunze, G., Zipfel, C., Robatzek, S., Niehaus, K., Boller, T., and Felix, G. (2016). The N Terminus of Bacterial Elongation Factor Tu Elicits Innate Immunity in Arabidopsis Plants Georg Felix Published by : American Society of Plant Biologists (ASPB) Stable URL : http://www.jstor.org/stable/3872365 REFERENCES Linked references are avail. **16**: 3496–3507.

Kurata, T. et al. (2005). Cell-to-cell movement of the CAPRICE protein in Arabidopsis root epidermal cell differentiation. Development **132**: 5387–5398.

Kwak, S.-H., Shen, R., and Schiefelbein, J. (2005). Positional signaling mediated by a receptor-like kinase in Arabidopsis. Science (80-.). **307**: 1111–1113.

Kwak, S.H. and Schiefelbein, J. (2008). A Feedback Mechanism Controlling SCRAMBLED Receptor Accumulation and Cell-Type Pattern in Arabidopsis. Curr. Biol. **18**: 1949–1954.

Lakowicz, J.R. (2006). Principles of fluorescence spectroscopy, 3rd Edition, Joseph R. Lakowicz, editor.

Lampropoulos, A., Sutikovic, Z., Wenzl, C., Maegele, I., Lohmann, J.U., and Forner, J. (2013). GreenGate - A novel, versatile, and efficient cloning system for plant transgenesis. PLoS One **8**.

Lampugnani, E.R., Khan, G.A., Somssich, M., and Persson, S. (2018). Building a plant cell wall at a glance. J. Cell Sci. **131**.

Lee, E., Vanneste, S., Pérez-Sancho, J., Benitez-Fuente, F., Strelau, M., Macho, A.P., Botella, M.A., Friml, J., and Rosado, A. (2019). Ionic stress enhances ER–PM connectivity via phosphoinositide-associated SYT1 contact site expansion in Arabidopsis. Proc. Natl. Acad. Sci. U. S. A. **116**: 1420–1429.

Lefebvre, A., Maizonnier, D., Gaudry, J.C., Clair, D., and Scalla, R. (1987). Some effects of the herbicide EL-107 on cellular growth and metabolism. Weed Res.

27: 125–134.

Lewis, K.C., Selzer, T., Shahar, C., Udi, Y., Tworowski, D., and Sagi, I. (2008). Inhibition of pectin methyl esterase activity by green tea catechins. Phytochemistry **69**: 2586–2592.

Li, L.Y., Shin, O.H., Rhee, J.S., Araç, D., Rah, J.C., Rizo, J., Südhof, T., and Rosenmund, C. (2006). Phosphatidylinositol phosphates as co-activators of Ca2+ binding to C2 domains of synaptotagmin 1. J. Biol. Chem. **281**: 15845–15852.

Li, P. and Liu, J. (2021). Protein Phosphorylation in Plant Cell Signaling. In Plant Phosphoproteomics: Methods and Protocols, X.N. Wu, ed (Methods in Molecular Biology).

Li, Z.P., Paterlini, A., Glavier, M., and Bayer, E.M. (2021). Intercellular trafficking via plasmodesmata: molecular layers of complexity. Cell. Mol. Life Sci. **78**: 799–816.

Lin, L., Zhong, S.H., Cui, X.F., Li, J., and He, Z.H. (2012). Characterization of temperature-sensitive mutants reveals a role for receptor-like kinase SCRAMBLED/STRUBBELIG in coordinating cell proliferation and differentiation during Arabidopsis leaf development. Plant J. **72**: 707–720.

Lin, W., Li, B., Lu, D., Chen, S., Zhu, N., He, P., and Shan, L. (2014). Tyrosine phosphorylation of protein kinase complex BAK1 / BIK1 mediates Arabidopsis innate immunity.: 2–7.

Liu, L., Li, C., Liang, Z., and Yu, H. (2018). Characterization of multiple C2 domain and transmembrane region proteins in arabidopsis. Plant Physiol. **176**: 2119–2132.

Liu, L., Li, C., Teo, Z.W.N., Zhang, B., and Yu, H. (2019). The MCTP-SNARE complex regulates florigen transport in arabidopsis. Plant Cell **31**: 2475–2490.

Liu, L., Liu, C., Hou, X., Xi, W., Shen, L., Tao, Z., Wang, Y., and Yu, H. (2012). FTIP1 is an essential regulator required for florigen transport. PLoS Biol. **10**.

Marty, N.J., Holman, C.L., Abdullah, N., and Johnson, C.P. (2013). The C2

domains of otoferlin, dysferlin, and myoferlin alter the packing of lipid bilayers. Biochemistry **52**: 5585–5592.

Mergner, J. et al. (2020). Mass-spectrometry-based draft of the Arabidopsis proteome. Nature **579**: 409–414.

Mirabet, V., Das, P., Boudaoud, A., and Hamant, O. (2011). The role of mechanical forces in plant morphogenesis. Annu. Rev. Plant Biol. **62**: 365–385.

Mistry, J., Chuguransky, S., Williams, L., Qureshi, M., Salazar, G.A., Sonnhammer, E.L.L., Tosatto, S.C.E., Paladin, L., Raj, S., Richardson, L.J., Finn, R.D., and Bateman, A. (2021). Pfam: The protein families database in 2021. Nucleic Acids Res. **49**: D412–D419.

Musielak, T.J., Schenkel, L., Kolb, M., Henschen, A., and Bayer, M. (2015). A simple and versatile cell wall staining protocol to study plant reproduction. Plant Reprod. **28**: 161–169.

Nissen, K.S., Willats, W.G.T., and Malinovsky, F.G. (2016). Understanding CrRLK1L Function: Cell Walls and Growth Control. Trends Plant Sci. **21**: 516–527.

Noack, L.C., Bayle, V., Armengot, L., Rozier, F., Mamode-Cassim, A., Stevens, F.D., Caillaud, M.C., Munnik, T., Mongrand, S., Pleskot, R., and Jaillais, Y. (2022). A nanodomain-anchored scaffolding complex is required for the function and localization of phosphatidylinositol 4-kinase alpha in plants. Plant Cell **34**: 302–332.

Paredez, A.R., Somerville, C.R., and Ehrhardt, D.W. (2006). Visualization of cellulose synthase demonstrates functional association with microtubules. Science (80-.). **312**: 1491–1495.

Pérez-Sancho, J., Vanneste, S., Lee, E., McFarlane, H.E., del Valle, A.E., Valpuesta, V., Friml, J., Botella, M.A., and Rosado, A. (2015). The arabidopsis synaptotagmin1 is enriched in endoplasmic reticulum-plasma membrane contact sites and confers cellular resistance to mechanical stresses. Plant Physiol. **168**: 132–143.

Persson, S., Paredez, A., Carroll, A., Palsdottir, H., Doblin, M., Poindexter, P., Khitrov, N., Auer, M., and Somerville, C.R. (2007). Genetic evidence for three unique components in primary cell-wall cellulose synthase complexes in Arabidopsis. Proc. Natl. Acad. Sci. U. S. A. **104**: 15566–15571.

de Reuille, P.B. et al. (2015). MorphoGraphX: A platform for quantifying morphogenesis in 4D. Elife **4**: 1–20.

Rio, D.C., Ares, M., Hannon, G.J., and Nilsen, T.W. (2010). Nondenaturing agarose gel electrophoresis of RNA. Cold Spring Harb. Protoc. **5**: 2010–2013.

Rizo, J. and Sudhof, T.C. (1998). C2-domains, structure and function of a universal Ca2+-binding domain. J. Biol. Chem. **273**: 15879–15882.

Roberts, A.G. and Oparka, K.J. (2003). Plasmodesmata and the control of symplastic transport. Plant, Cell Environ. **26**: 103–124.

Rueden, C.T., Schindelin, J., Hiner, M.C., DeZonia, B.E., Walter, A.E., Arena, E.T., and Eliceiri, K.W. (2017). ImageJ2: ImageJ for the next generation of scientific image data. BMC Bioinformatics **18**: 1–26.

Russinova, E., Borst, J.W., Kwaaitaal, M., Caño-Delgado, A., Yin, Y., Chory, J., and De Vries, S.C. (2004). Heterodimerization and endocytosis of Arabidopsis brassinosteroid receptors BRI1 and AtSERK3 (BAK1). Plant Cell **16**: 3216–3229.

Ryu, K.H., Kang, Y.H., Park, Y.H., Hwang, I., Schiefelbein, J., and Lee, M.M. (2005). The WEREWOLF MYB protein directly regulates CAPRICE transcription during cell fate specification in the Arabidopsis root epidermis. Development **132**: 4765–4775.

Salazar-Henao, J.E., Vélez-Bermúdez, I.C., and Schmidt, W. (2016). The regulation and plasticity of root hair patterning and morphogenesis. Dev. **143**: 1848–1858.

Sambrook, J., Fritsch, E.R., and Maniatis, T. (1989). Molecular Cloning: A Laboratory Manual (2nd ed.) (Cold Spring Harbor Laboratory Press.).

Scheible, A.W., Eshed, R., Richmond, T., Delmer, D., Scheible, W., Eshedt, R.,

Delmert, D., and Somerville, C. (2013). Modifications of cellulose synthase confer resistance to isoxaben and thiazolidinoi ie herbicides in Arabidopsis Ixrl mutants.

Scheible, W.R., Eshed, R., Richmond, T., Delmer, D., and Somerville, C. (2001). Modifications of cellulose synthase confer resistance to isoxaben and thiazolidinone herbicides in Arabidopsis Ixr1 mutants. Proc. Natl. Acad. Sci. U. S. A. **98**: 10079–10084.

Scheres, B., Benfey, P., and Dolan, L. (2002). Root Development. Arab. B. **1**: e0101.

Schindelin, J. et al. (2012). Fiji: An open-source platform for biological-image analysis. Nat. Methods **9**: 676–682.

Schlereth, A., Möller, B., Liu, W., Kientz, M., Flipse, J., Rademacher, E.H., Schmid, M., Jürgens, G., and Weijers, D. (2010). MONOPTEROS controls embryonic root initiation by regulating a mobile transcription factor. Nature **464**: 913–916.

Schneitz, K., Hülskamp, M., Kopczak, S.D., and Pruitt, R.E. (1997). Dissection of sexual organ ontogenesis: a genetic analysis of ovule development in Arabidopsis thaliana. Development **124**: 1367–76.

Shin, O.H., Hau, W., Wang, Y., and Südhof, T.C. (2005). Evolutionarily conserved multiple C2 domain proteins with two transmembrane regions (MCTPs) and unusual Ca2+ binding properties. J. Biol. Chem. **280**: 1641–1651.

Shiu, S.H. and Bleecker, A.B. (2001). Receptor-like kinases from Arabidopsis form a monophyletic gene family related to animal receptor kinases. Proc. Natl. Acad. Sci. U. S. A. **98**: 10763–10768.

Shiu, S.H., Karlowski, W.M., Pan, R., Tzeng, Y.H., Mayer, K.F.X., and Li, W.H. (2004). Comparative analysis of the receptor-like kinase family in Arabidopsis and rice. Plant Cell **16**: 1220–1234.

Smet, S. De, Cuypers, A., Vangronsveld, J., and Remans, T. (2015). Gene Networks Involved in Hormonal Control of Root Development in Arabidopsis

thaliana : A Framework for Studying Its Disturbance by Metal Stress.: 19195–19224.

Smyth, D.R., Bowman, J.L., and Meyerowitz, E.M. (1990). Early Flower Development in Arabidopsis. Plant Cell **2**: 755–767.

Somerville, C. (2006). Cellulose synthesis in higher plants. Annu. Rev. Cell Dev. Biol. **22**: 53–78.

Song, J.H., Kwak, S.-H., Nam, K.H., Schiefelbein, J., and Lee, M.M. (2019). QUIRKY regulates root epidermal cell patterning through stabilizing SCRAMBLED to control CAPRICE movement in Arabidopsis. Nat. Commun. **10**: 1744.

Song, S., Chen, Y., Liu, L., Wang, Y., Bao, S., Zhou, X., Teo, Z.W.N., Mao, C., Gan, Y., and Yu, H. (2017). OsFTIP1-mediated regulation of florigen transport in rice is negatively regulated by the ubiquitin-like domain kinase OsUbDKγ4. Plant Cell **29**: 491–507.

Song, S.K., Ryu, K.H., Kang, Y.H., Song, J.H., Cho, Y.H., Yoo, S.D., Schiefelbein, J., and Lee, M.M. (2011). Cell fate in the Arabidopsis root epidermis is determined by competition between WEREWOLF and CAPRICE. Plant Physiol. **157**: 1196–1208.

Stahl, Y. et al. (2013). Moderation of arabidopsis root stemness by CLAVATA1 and ARABIDOPSIS CRINKLY4 receptor kinase complexes. Curr. Biol. **23**: 362–371.

Tofanelli, R., Vijayan, A., Scholz, S., and Schneitz, K. (2019). Protocol for rapid clearing and staining of fixed Arabidopsis ovules for improved imaging by confocal laser scanning microscopy. Plant Methods **15**: 1–13.

Tran, T.M. et al. (2019). Maize Carbohydrate Partitioning Defective33 Encodes an MCTP Protein and Functions in Sucrose Export from Leaves. Mol. Plant **12**: 1278–1293.

Trehin, C., Schrempp, S., Chauvet, A., Berne-Dedieu, A., Thierry, A.-M., Faure, J.-E., Negrutiu, I., and Morel, P. (2013). QUIRKY interacts with

STRUBBELIG and PAL OF QUIRKY to regulate cell growth anisotropy during Arabidopsis gynoecium development. Development **140**: 4807–4817.

Tsuge, T., Tsukaya, H., and Uchimiya, H. (1996). Two independent and polarized processes of cell elongation regulate leaf blade expansion in Arabidopsis thaliana (L) Heynh. Development **122**: 1589–1600.

Ursache, R., Andersen, T.G., Marhavý, P., and Geldner, N. (2018). A protocol for combining fluorescent proteins with histological stains for diverse cell wall components. Plant J. **93**: 399–412.

Vaahtera, L., Schulz, J., and Hamann, T. (2019). Cell wall integrity maintenance during plant development and interaction with the environment. Nat. Plants **5**: 924–932.

Vaddepalli, P., Fulton, L., Batoux, M., Yadav, R.K., and Schneitz, K. (2011). Structure-function analysis of strubbelig, an arabidopsis atypical receptor-like kinase involved in tissue morphogenesis. PLoS One **6**.

Vaddepalli, P., Fulton, L., Wieland, J., Wassmer, K., Schaeffer, M., Ranf, S., and Schneitz, K. (2017). The cell wall-localized atypical β -1 , 3 glucanase ZERZAUST controls tissue morphogenesis in Arabidopsis thaliana. Development **144**: 2259–2269.

Vaddepalli, P., Herrmann, A., Fulton, L., Oelschner, M., Hillmer, S., Stratil, T.F., Fastner, A., Hammes, U.Z., Ott, T., Robinson, D.G., and Schneitz, K. (2014). The C2-domain protein QUIRKY and the receptor-like kinase STRUBBELIG localize to plasmodesmata and mediate tissue morphogenesis in Arabidopsis thaliana. Development **141**: 4139–4148.

Voxeur, A. and Höfte, H. (2016). Cell wall integrity signaling in plants: “To grow or not to grow that’s the question.” Glycobiology **26**: 950–960.

Wang, J.G., Feng, C., Liu, H.H., Ge, F.R., Li, S., Li, H.J., and Zhang, Y. (2016). HAPLESS13-Mediated Trafficking of STRUBBELIG Is Critical for Ovule Development in Arabidopsis. PLoS Genet. **12**: 1–21.

Wang, L., Li, H., Lv, X., Chen, T., Li, R., Xue, Y., Jiang, J., Jin, B., Baluška, F.,

Šamaj, J., Wang, X., and Lin, J. (2015a). Spatiotemporal dynamics of the BRI1 receptor and its regulation by membrane microdomains in living Arabidopsis cells. Mol. Plant **8**: 1334–1349.

Wang, Z.P., Xing, H.L., Dong, L., Zhang, H.Y., Han, C.Y., Wang, X.C., and Chen, Q.J. (2015b). Egg cell-specific promoter-controlled CRISPR/Cas9 efficiently generates homozygous mutants for multiple target genes in Arabidopsis in a single generation. Genome Biol. **16**: 1–12.

van Wijk, K.J., Friso, G., Walther, D., and Schulze, W.X. (2014). Meta-analysis of arabidopsis thaliana phospho-proteomics data reveals compartmentalization of phosphorylation motifs. Plant Cell **26**: 2367–2389.

Wolf, S. (2017). Plant cell wall signalling and receptor-like kinases. Biochem. J. **474**: 471–492.

Wolf, S., Hématy, K., and Höfte, H. (2012). Growth control and cell wall signaling in plants. Annu. Rev. Plant Biol. **63**: 381–407.

Wormit, A., Butt, S.M., Chairam, I., Mckenna, J.F., Nunes-nesi, A., Kjaer, L., Donnelly, K.O., Fernie, A.R., Woscholski, R., Barter, M.C.L., and Hamann, T. (2012a). Osmosensitive changes of carbohydrate metabolism in response to cellulose biosynthesis inhibition. Plant Physiol. **159**: 105–117.

Wormit, A., Butt, S.M., Chairam, I., McKenna, J.F., Nunes-Nesi, A., Kjaer, L., O'Donnelly, K., Fernie, A.R., Woscholski, R., Barter, L.M.C., and Hamann, T. (2012b). Osmosensitive changes of carbohydrate metabolism in response to cellulose biosynthesis inhibition. Plant Physiol. **159**: 105–117.

Xiao, C., Zhang, T., Zheng, Y., Cosgrove, D.J., and Anderson, C.T. (2016). Xyloglucan deficiency disrupts microtubule stability and cellulose biosynthesis in arabidopsis, altering cell growth and morphogenesis1[OPEN]. Plant Physiol. **170**: 234–249.

Xie, K., Zhang, J., and Yang, Y. (2014). Genome-wide prediction of highly specific guide RNA spacers for CRISPR-Cas9-mediated genome editing in model plants and major crops. Mol. Plant **7**: 923–926.

Xu, M., Cho, E., Burch-Smith, T.M., and Zambryski, P.C. (2012). Plasmodesmata formation and cell-to-cell transport are reduced in decreased size exclusion limit 1 during embryogenesis in Arabidopsis. Proc. Natl. Acad. Sci. U. S. A. **109**: 5098–5103.

Yadav, R.K., Fulton, L., Batoux, M., and Schneitz, K. (2008). The Arabidopsis receptor-like kinase STRUBBELIG mediates inter-cell-layer signaling during fl oral development. Dev. Biol. **323**: 261–270.

Yadav, S.R., Yan, D., Sevilem, I., and Helariutta, Y. (2014). Plasmodesmata-mediated intercellular signaling during plant growth and development. Front. Plant Sci. **5**: 1–7.

Yu, F. et al. (2012). FERONIA receptor kinase pathway suppresses abscisic acid signaling in Arabidopsis by activating ABI2 phosphatase. Proc. Natl. Acad. Sci. U. S. A. **109**: 14693–14698.

Zambryski, P. and Crawford, K. (2000). Plasmodesmata: Gatekeepers for cell-to-cell transport of developmental signals in plants. Annu. Rev. Cell Dev. Biol. **16**: 393–421.

8 Acknowledgements

I would like to thank Prof. Dr. Kay Schneitz for providing me the opportunity to work in his lab. I am especially thankful for his excellent guidance, encouragement, support and motivation throughout my thesis journey. He has been instrumental in improving my scientific presentation and writing skills. I consider myself lucky to have had the chance to work with him.

I would like to thank Prof. Dr. Ulrich Hammes for appearing as the second examiner and Prof. Dr. Ralph Hückelhoven for accepting the chairmanship in my doctoral examination.

I would like to thank Prof. Dr. Ramon Angel Torres Ruiz for the introduction to confocal microscopes, scientific suggestions, and teaching of FRET-FLIM and FA techniques. And also thank the Center of Advanced Light Microscopy (CALM) for providing me the chance to make good images with several advanced confocal microscopes.

I would like to thank Dr. Julia Mergner and Dr. Nils Rugen from Chair of Proteomics and Bioanalytics, Technical University of Munich for their help with the phosphoproteomics mass spectrometry experiments and for the analysis of the data.

I also would like to thank the China Scholarship Council (CSC) for their funding towards my PhD.

I would like to thank Jin and Ajeet for introducing me to the lab and their guidance during the early stages of my thesis. I would like to thank Barbara, Rodion and Katrin for the scientific discussion, helping and supporting. I would like to thank Rachele, Athul, Tejasvinee and Ratula for their help with ovule 3D imaging. I would like to thank

Nicole, Annermarie, Regina, and Heidi for the helping with my life and work in Germany. I also would like to thank all of them for the friendly atmosphere and fun moments in lab.

Special thanks go to our administrative secretary Susanna for helping the department to run smoothly and for assisting me in many different ways.

I would like to thank my bachelor student Lena. It has been pleasure guiding and working with you. I would like to thank members of Lehrstuhl für Botanik and Lehrstuhl für Systembiologie der Pflanzen for their support.

I would like to express my sincere gratitude to my husband, Tong. He has given me endless support and encouragement throughout the whole process of my thesis. Thank you for being there with me through these difficult times.

Last but not least, I am grateful to all my family members in China for their encouragement which enable me to complete my thesis work.